Investigation of Thermal Performance of a Solar Assisted Anaerobic Digestion System Integrated With Solar Thermal Energy Storage Packed With Phase Change Material

M.Sc. Thesis

By

Leulseged Tarekegn Kibret

Thermal and Aerospace Engineering Program
School of Mechanical, Chemical and Materials Engineering
Adama Science and Technology University

Adama, Ethiopia
October 2018

Investigation of Thermal Performance of a Solar Assisted Anaerobic Digestion System Integrated With Solar Thermal Energy Storage Packed With Phase Change Material

M.Sc. Thesis

By

Leulseged Tarekegn Kibret

A Thesis Submitted to Thermal and Aerospace Engineering Program of School of Mechanical, Chemical and Materials Engineering, Adama Science and Technology University in partial fulfillment of the requirement of the degree of Master of Science in Thermal Engineering

Advisor:

Dr. Gezahegn Habtamu

Adama, Ethiopia

October 2018

Declaration

I hereby declare that this M.Sc. Thesis entitled “Investigation of Thermal Performance of a Solar Assisted Anaerobic Digestion System Integrated With Solar Thermal Energy Storage Packed With Phase Change Material” in partial fulfillment of the requirement of the degree of Master of Science in Thermal Engineering is an authentic record of my own work carried out from September 2017 to October 2018 under supervision of Dr. Gezahegn Habtamu, Assistant Professor of Thermal Engineering program, Adama Science and Technology University.

The matter embedded in this thesis has not been submitted for the award of a degree or diploma in any other university. All relevant resource information used in this paper has been duly acknowledged.

…….....	……..	…….
Student	Signature	Date

This is to certify that the above statement made by the candidate is correct to the best of our knowledge and belief. This has been submitted for examination with our approval.

…….....	……..	…….
Advisor	Signature	Date

Adama Science and Technology University

School of Mechanical, Chemical and Materials Engineering

Thermal and Aerospace Engineering Program

Approval of Board of Examiners

We, the undersigned, members of the Board of Examiners of the final open defense by Leulseged Tarekegn Kibret have read and evaluated his thesis entitled **"Investigation of Thermal Performance of a Solar Assisted Anaerobic Digestion System Integrated With Solar Thermal Energy Storage Packed With Phase Change Material"** and examined the candidate. This is, therefore, to certify that the thesis has been accepted in partial fulfillment of the requirement of the Degree of Master of science in Thermal Engineering.

…….....	……..	…….
Chair person	Signature	Date
…….....	……..	…….
Internal Examiner	Signature	Date
…….....	……..	…….
External Examiner	Signature	Date

ACKNOWLEDGMENT

Above all, my deepest thanks must go to my shepherd God, for the mercy he has for me in all ticks of my life and for his being with me in every day to day activity of my life. Then, I would like to express my sincere gratitude to Dr. Gezahegn Habtamu, the thesis advisor, for his unlimited support, encouragement, constructive comment and unreserved guidance on the critical issues of the study.

Heartfelt thanks also go to my friends for their encouragement and constructive suggestion on the subject matter of the study.

Last but not least, I would like to thank Adama Science and Technology University for give me the opportunity to join this master's program with full scholarship.

ABSTRACT

Anaerobic digestion is a promising technology for the treatment of organic wastes, since it produces renewable energy (biogas) and valuable digestate as fertilizer. Temperature is an important factor that can affect the performance of anaerobic digestion systems. The amount of gas produced increases with digester temperature. To keep the anaerobic digestion process at higher temperature than ambient air, external source of heating is required. Solar energy can be used as a heating source, but it is intermittent. Solar energy storage system is a key issue to be addressed to allow the intermittence of solar energy.

The objective of this study was to investigate the thermal performance of a solar assisted anaerobic digestion system, which is composed of anaerobic digester, flat plate collector and latent heat thermal energy storage. The digester was used to ferment cow dung and designed to produce 100 peoples average daily energy consumption for their cooking application. Water is used as a heat transfer fluid and spherical capsules of encapsulated paraffin n-Triacontane are used as phase change material. Transient one-dimensional heat transfer models are developed, and solve iteratively using finite difference scheme. Results from a numerical simulation performed with meteorological data from Adama shows that 3 m^3 of phase change material and 31 units of flat plate collectors can satisfy the heat required for the designed digester.

Key words: Anaerobic Digestion, Digester, Solar Energy, Flat Plate Collector, Heat Transfer Fluid, Phase Change Material, Thermal Energy Storage.

TABLE OF CONTENTS

LIST OF FIGURES

LIST OF TABLES

ABBREVIATIONS

PID	Proportional, integral and differential
LCFA	Long chain fatty acids
SCFA	Short chain fatty acids
CSTR	Completely stirred tank reactor
AC	Accumulation system
UASB	Up-flow anaerobic sludge blanket
SHS	Sensible heat storage
LHS	Latent heat storage
PCM	Phase change material
EPDM	Ethylene propylene diene teropolymer
TES	Thermal energy storage
HTF	Heat transfer fluid
NTU	Number of transfer unit

NOMENCLATURE

Q	Heat flow (W)
T	Temperature (K or ^{o}C)
V	Volume (m^3)
C	Specific heat capacity (J/kgK)
h	Convective heat transfer coefficient (W/m^2K)
S	Absorbed solar radiation (W/m^2)
Pr	Panditl number
g	Gravity (m/s^2)
L	Characteristic length (m)
Nu	Nusselt number

k	Thermal conductivity (W/mK)
u	Speed (m/s)
G	Global radiation (W/m^2)
E	Equation of time
n	Day of the year
ST	Solar time (hr)
N	Day time duration
DH	Diffused radiation on horizontal (W/m^2)
BH	Beam radiation on horizontal (W/m^2)
t	Time (s)
R	Radiation factor
I	Incidence solar radiation (W/m^2)
U	Overall heat transfer coefficient (W/m^2K)
A	Area (m^2)
FR	Collector heat removal factor
F	Fin efficiency
e	Porosity
D	Diameter (m)
Re	Reynolds number
H	Enthalpy (J/kg)

GREEK SYMBOLS

ρ	Density (kg/m^3)
ν	Kinematic viscosity (m^2/s)
β‘	Coefficient of thermal expansion (1/K)
Δ	Change

ε	Emissivity
σ	Stefan-Boltzmann constant
δ	Declination angle (^{o})
ω	Solar hour angle (^{o})
θ_i	Incidence angle (^{o})
θ_z	Zenith angle (^{o})
β	Inclination angle (^{o})
α	Thermal absorptivity
ψ_{soil}	Ground albedo
γ	Bond thickness (m)
τ	Transmissivity
μ	Dynamic viscosity (kg/ms)
η	Efficiency
γ'	Melt fraction of phase changing material.

SUBSCRIPTS

At	Atmosphere	min	Minimum
A	Ambient	max	Maximum
Dg	Digestate	pm	Mean plate
Bg	Biogas	T	Tilt
Co	Cover	p	Plate
fd	Feed	g	Glass
ld	Leave from digester	fo	Outlet fluid
eff	Effective	fi	Inlet fluid
c	Convective	ag	Air gap
r	Radiative	ins	Insulation

w	Water	f	Fluid
liq	Liquid	b	Bed
fus	Fusion	m1	Melting starting point
Sr	Sunrise	m2	Melting ending point
Ss	Sunset	Ave	Average
elem	Element		

CHAPTER 1: Introduction

1.1. Background

The continuous depletion of conventional fuel resources, increase in fuel cost and the increasing concern for environmental issues have challenged researchers to develop new techniques to obtain clean and sustainable energy through the utilization of renewable energy sources. There exist many renewable energy sources; such as solar, wind, geothermal, hydropower, and biomass, animal and agricultural wastes are representing an important source of bio-energy. Biogas technology introduces a very attractive way to utilize biomass sources for fulfilling partial energy requirements (Deepanraj et al., 2014). The implementation of biogas technology has a great potential of mitigating several problems related to ecological imbalance, minimize crucial fuel demand, improve hygiene and health, and, therefore, there is an overall improvement in quality of life.

Biogas can be produced from animal or agricultural wastes by anaerobic digestion. Anaerobic digestion is a biological process by which complex organic materials can be transformed, in the absence of oxygen, into biogas (a mixture of methane; carbon dioxide and traces of other gases). The anaerobic digestion of complex organic wastes is a multi-step process of series and parallel reactions, such as hydrolysis, acidogenesis, acetogenesis and methanogenesis. This a multi-step anaerobic digestion process performed under anaerobic digester system. Anaerobic digester is mainly composed of a dome shaped cover, underground buried wall made of concrete and stirring device.

The main objectives of anaerobic digestion are waste stabilization and energy recovery. Biogas can be used for water or space heating, electricity or steam production to meet other thermal energy demands. It is also technically feasible to utilize methane gas as engine fuel. An important additional benefit is the conservation of the fertilizer value, originally present in the waste.

Temperature is an important factor that can affect the performance of anaerobic digestion. The amount of gas produced increases with increase in digester temperature, with retention time and with the percentage of total solid in the slurry. Anaerobic digestion can be achieved under psychrophilic (5 – 25 ^{o}C), mesophilic (25 – 40 ^{o}C) or thermophilic (> 45 ^{o}C) conditions (Hamed

et al., 2003). Digestion under thermophilic conditions has many advantages such as higher metabolic rates and a higher destruction of pathogens and weed seeds (Varel et al., 1980). The major drawbacks of thermophilic treatment compared with mesophilic treatment are less stability and higher energy requirements.

To keep the anaerobic digester operates under desired temperature; external source of heating is used like electricity, oil, or part of the produced biogas, but this lowers the energy efficiency (Kocar and Eryasar., 2007). If another renewable energy resource such as thermal solar energy could be integrated in the process then a high gas production can be achieved with high energy efficiency (Hamed et al., 2003). The combination of solar energy and biogas production represents a kind of solar energy storage in the form of gas. But contrary, incorporation of solar energy in the anaerobic digestion process may affect the process stability, which is resulting from the daily fluctuations of the variable solar energy (El-Mashad., 2003). Solar energy storage is a key issue to be addressed to allow intermittent energy sources, typically renewable sources, to match energy supply with demand (Chopade et al., 2013).

The system considered in this study consisted of flat plate solar collectors, anaerobic digester and phase change material based thermal energy storage device. The flat plate collector is the main component of the heating system and it translates solar energy in to heat. The heat storage device accumulates the surplus heat and supplies heat when there is not sufficient heat-collecting capacity. Furthermore, the storage device reduces the influence of the relatively unstable solar energy heat source and increases the stability of the system. The collected heat is transferred to the heat storage device when the digestion temperature is higher than 55 ^{o}C. When the digestion temperature is lower than 55 ^{o}C, it is used for heating the digestion system.

In this study, the thermal performance of a solar assisted anaerobic digestion system integrated with a packed bed solar thermal energy storage system that uses paraffin n-Triacontane as a phase change material were investigated. The digester is designed to digest cow dung at Adama weather condition. And it is designed to fulfill the energy demand of 100 people for their cooking purpose.

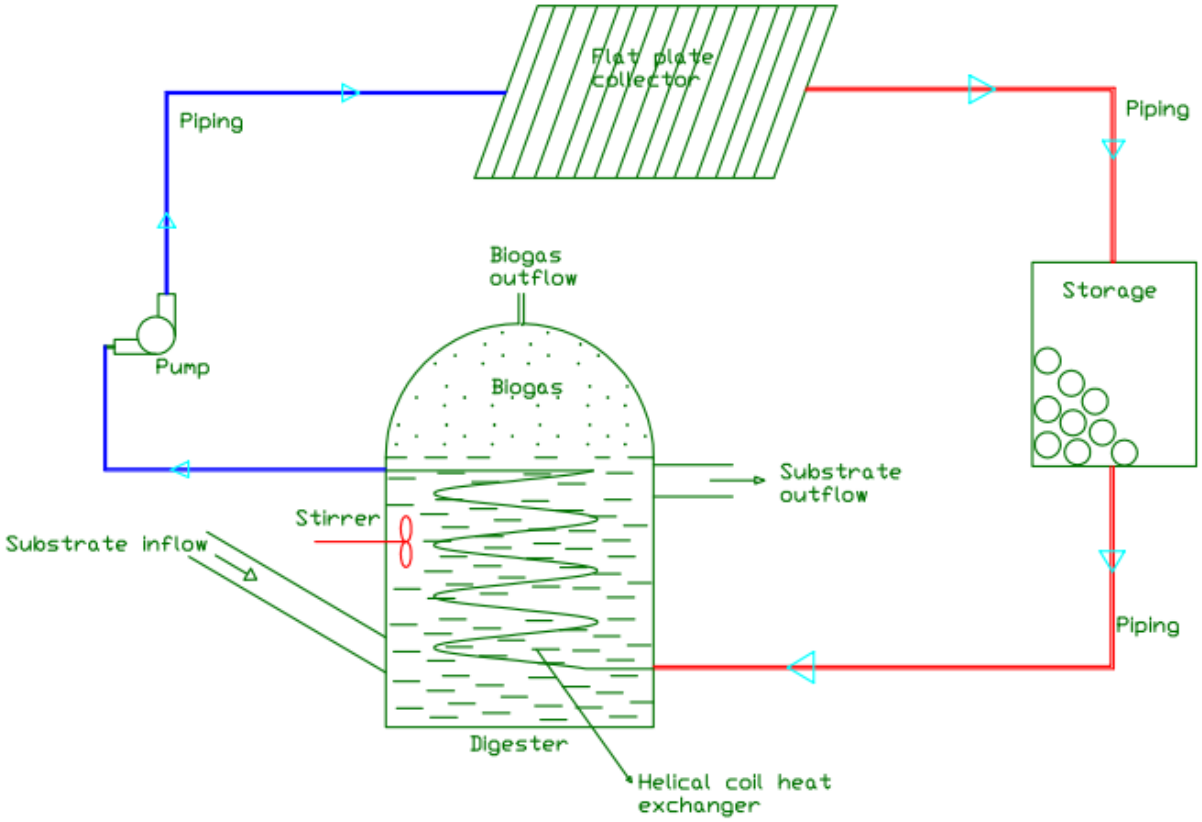

Figure 1.1: System configuration investigated in this study

1.2. Statement of the problem

Temperature is an important factor that can affect the performance of anaerobic digestion system. Digestion under higher temperature conditions has many advantages such as higher metabolic rates and a higher destruction of pathogens and weed seeds. The major drawbacks of higher temperature treatment compared with lower temperatures treatment are less stability and higher energy requirements. To keep the anaerobic digester operates under this higher temperature; external source of heating is used, but this lowers the energy efficiency of digestion system. Solar energy could be integrated in the process then a high gas production rate can be achieved with high energy efficiency of digestion system. But contrary, incorporation of solar energy in the anaerobic digestion process may affect the process stability, which is resulting from the daily fluctuations of the variable solar energy. Solar energy storage is a key issue to be addressed to allow intermittent energy sources, typically renewable sources, to match energy supply with demand.

Some researchers (Yiannopoulos et al., 2008, El-Mashad et al., 2003, Axaopoulos et al., 2001 etc.) have investigated numerically and experimentally the thermal behavior of a solar assisted anaerobic digestion system to specific geographical locations. But there is scarcity on the study of the thermal performance of a solar assisted anaerobic digester theoretically as well as experimentally across seasons in a year specify to a given geographical location in Ethiopia particularly anaerobic digestion system integrated with solar thermal energy storage packed with phase change material.

1.3. Objective of the Study

The general objective of this study is to investigate the thermal performance of a solar assisted anaerobic digestion system, solar water heater and packed bed thermal energy storage system that uses paraffin n-Triacontane as a phase change material, that is designed to digest cow dung at Adama weather condition.

The specific objectives of the study are

- To estimate the anaerobic digester size that fulfills energy demand of 100 people for their cooking application.
- To investigate the transient thermal performance of the anaerobic digester major components using finite difference method i.e.;
    - Transient thermal performance of anaerobic digestion system under Adama weather condition.
    - Transient thermal performance of the flat plate collector system that fulfill the energy demand of the digester.
    - Transient thermal performance of energy storage device packed with phase change material for the digester.

1.4. Scope and Limitations

1.4.1. Scope of the Study

This study mainly focuses on the numerical investigation of thermal performance of a solar assisted anaerobic digester that is designed to treat animal waste (cow dung) and it is designed to work at Adama weather condition. This investigation also includes the analysis of a phase

changing material based thermal energy storage integrated to solar assisted anaerobic digestion system.

1.4.2. Limitations of the Study

This study is delimited to investigate the transient thermal performance of a solar heated anaerobic digester integrated to latent heat thermal energy storage system. The hydrodynamic and cost effectiveness analysis of a system is not included here.

The multi-dimensional heat transfer phenomenon in the digester, solar collector and thermal energy storage system complicates the analysis. Thus in this study, one-dimensional heat flow model is used to investigate the systems.

CHAPTER 2: Literature Review

2.1. Introduction

This chapter concerns some general information on biogas technology, solar energy harnessing technology, and solar thermal energy storage system packed with phase changing material. In addition previous research works on different digesters, solar energy collector and solar thermal energy storage devices are used as input for the current work.

2.2. Anaerobic Digestion Process: A General Overview

2.2.1. Background

Anaerobic digestion is the process of biological degradation of organic matter, in the absence of oxygen, producing biogas, which is a mixture of methane (CH_4), carbon dioxide (CO_2) and traces of other gases. Anaerobic digestion is extensively applied for treatment of waste water and agricultural wastes with relatively high moisture content. Many researchers were carries out on the anaerobic digestion of animal wastes.

The main objectives of digestion of animal slurry can be summarized as follows:

1. Energy production and reduction of CO_2 emission by replacing fossil energy. Anaerobic digesters are attractive as sustainable energy conversion systems. This in fact is the main aim for applying of animal slurries on farm.
2. Reduction of the formation of malodorous compounds.
3. Reduction of emission of greenhouse gases by reduction of CH_4 production and emission during manure storage.
4. Improvement of the fertilizing value of farm manures (e.g. converting a large portion of organic nitrogen to ammonia), thus reducing consumption of the chemical fertilizers.
5. Reduction of pathogens and weed seeds of the effluent. The extent of removal of the pathogens depends on the digestion temperature.
6. Reduction of NH_3 emission in the case of using a combined digestion and storage system (i.e. accumulation system).

7. Enhancement of further processing of the animal slurry. For example, the dewater ability of the digested slurry is easier than that of undigested slurry.

2.2.2. Benefits of Biogas Technology

Biogas technology offers a wide range of benefits which include economic, health, social, and environmental ones.

i. Economic Benefits

Two of the most important outputs of biogas technology are energy and bio-slurry. Biogas energy is utilized commonly for cooking, lighting, refrigeration, and running internal combustion engine. Biogas burns more efficiently as compared to fuel wood and dung. It burns at an efficiency of about 60% whereas fuel wood burns at 5 – 8% efficiency in open fire place and dung burns at 60% of that of fuel wood. Unlike the use of traditional biomass fuel, cooking with biogas is much easier because there is no need to keep the fire burning (Mengistu et al., 2016).

Biogas installations can generate electricity and offer transportation fuel. Electricity generated from biogas could be useful for local pumping, lighting, communication, refrigeration, etc. When methane, the combustible component of biogas, is enriched, it can be used as transportation fuel. With regard to the role of biogas as transportation fuel, after removing carbon dioxide, biogas enriched in methane becomes equivalent to natural gas. Thus, methane enriched biogas can be useful for all applications that natural gas can do.

The slurry from biogas digesters has been attested to be the best organic fertilizer which will lead to increased crop productivity. It can substitute chemical fertilizer and thus reduces the importation of chemical fertilizer and saves foreign currencies.

Biogas technology generates employment opportunities for both skilled and unskilled labor. Specifically, in a well-organized biogas development sector, biogas technology expansion opens employment opportunities for masons, plumbers, civil engineers, and agronomists.

ii. Health and Social Benefits

The use of biogas technology has numerous health and social benefits. The health benefits encompass: reduction in smoke borne diseases such as headache, eye-burning, eye-infection, respiratory organ infection, etc.; improvement in household sanitation via toilet connection with bio-digesters and absence of sooth and ashes in the kitchen; and reduction in burning accidents.

It burns cleanly so that its use minimizes eye illnesses which results from burning of traditional biomass fuels. Besides, it assists maintaining sanitation of areas surrounding households via dung management and hygienic toilets connected to biogas digesters. Thus, it lowers the probability of expansion of contagious diseases. Biogas technology provides health benefits not only to its users but to the whole community in its environs.

Biogas technology has also various social roles. It improves social relations via minimizing bad odors and environmental pollutions of organic wastes which would have been otherwise serve as a source grievance among neighbors and negatively affect social relations.

iii. Environmental Benefits

Biogas technology offers a wide range of environmental benefits.

- It provides sustainable source of energy and soil enriching bio-slurry as a by-product.
- It gives an opportunity to treat and re-utilize variety of organic wastes.
- It minimizes environmental impacts of greenhouse gas emissions, and
- It reduces land use problem associated with disposing organic waste.

Biogas technology is one of the promising solutions to the diverse environmental problems associated with the use of traditional biomass fuels.

2.2.3. The Digestion Process

The anaerobic digestion of complex organic wastes is a multistep process of series and parallel reactions. It consists of four major stages:

1. **Hydrolysis** in which particulate organic matter is converted by extracellular enzymes to monomer or dimeric components, such as amino acids, single sugars and Long Chain Fatty Acids (LCFA). Such compounds can pass the cell membrane.
2. **Acidogenesis** in which the hydrolysis products are fermented or anaerobically oxidized to Short Chain Fatty Acids (SCFA), alcohol and ammonia.
3. **Acetogenesis** in which alcohol and SCFA (other than acetate) are converted to acetic acid or hydrogen and carbon dioxide.

4. **Methanogenesis** in which acetic acid and CO_2 plus H_2 are converted to methane and carbon dioxide.

Generally, hydrolysis is the rate limiting step during the digestion of complex wastewaters and wastes like animal manures.

2.2.4. Anaerobic Digestion Systems for Animal Wastes

Many systems are applied for animal wastes. These systems can be classified as:

1. Batch reactors
2. Continuous systems such as Completely Stirred Tank Reactor (CSTR) and plug flow reactors.
3. Accumulation systems (AC).
4. High rate systems like Up-flow Anaerobic Sludge Blanket (UASB) reactors. This kind is usually used for the liquid fraction of the slurry.

The choice of any of the above systems depends on many factors such as:

1. The characteristics of the slurry (e.g. moisture content).
2. Technical and financial issues.

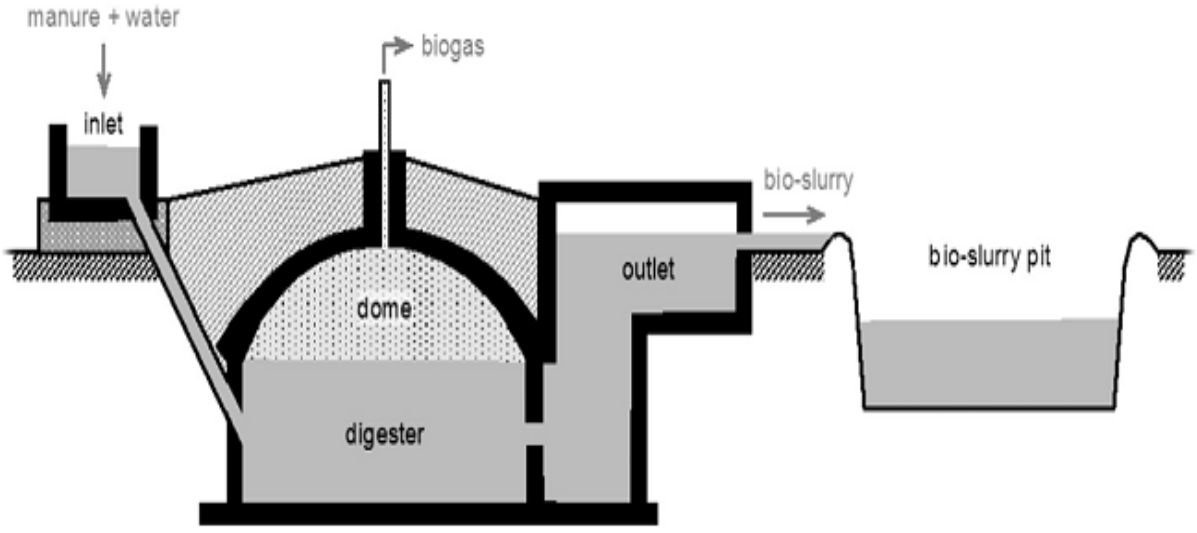

Figure 2.1: Schematic representation of a fixed-dome biogas plant

2.2.5. Parameters Affecting the Net Energy Production

Table 2.1: Parameters affecting the net energy productions

Parameters	Items involved
1. Feed stock characteristics	1. Type of animal from which the manure is collected. 2. The addition of bedding material with the manure. 3. Animal ration feeding. 4. Total solids content. 5. Volatile solids content. 6. Biodegradability of the substrate. 7. First order hydrolysis constant. 8. Ammonia concentration. 9. Viscosity and specific heat. 10. Influent temperature.
2. Reactor design	1. Reactor volume. 2. Reactor type (batch; accumulation; CSTR etc.). 3. The reactor shape. 4. Type and thickness of the insulation. 5. Heating system and its efficiency. 6. Handling system of the manure (e.g. solid separation before digestion).
	1. Digestion or filling time in the case of

3. Operation conditions	batch or accumulation system, respectively. 2. Operation temperature (psychrophilic; mesophilic or thermophilic) 3. Loading rate (at a fixed substrate concentration) in the case of a CSTR. 4. Ambient temperature.

2.2.6. Effect of Temperature on the Process Performance/Stability

Anaerobic digestion can be achieved under psychrophilic (6 – 25 ^{o}C), mesophilic (25 – 40 ^{o}C), and thermophilic (> 45 ^{o}C) conditions (El-Mashad, 2003). Temperature is an important factor affecting the performance of anaerobic digestion. Like many biological process, the digestion rate increases with increasing temperature up to an optimum. Variel et al., (1980) studied the effect of temperature and retention time on the methane production from beef cattle manure using continuously mixed 3–litter working volume of anaerobic fermenters. The temperature ranged from 30 to 65 ^{o}C with 5 ^{o}C increments between the fermenters. The result showed that temperature affects the production rate of methane, but does not increase the amount of CH_4 that can produced from a unit mass of substrate. Digestion under thermophilic conditions has many advantages and disadvantages.

The advantages include:

1. Increased reaction rates as a result of the higher growth rates of thermophilic micro-organisms. But these micro-organisms have lower growth yields.
2. Improved solids-liquid separation.
3. Increased destruction of pathogenic organisms.

Possible disadvantages of the thermophilic process:

1. Higher energy requirement for system operation than at mesophilic conditions.

2. The lower growth yields of thermophilic micro-organisms result in longer start-up times and may make the process more susceptible to toxicity and to changes of temperature or other environmental conditions.
3. Poor process stability especially in the presence of high ammonia concentration.

2.3. Application of Solar Energy for Heating Biogas Plant

A few reports were found concerning the application of solar heating system in the anaerobic digestion of animal wastes. Badra et al., (2017), investigated the feasibility of the integrated solar thermal energy in the anaerobic digestion. In their study a simulation model of the mesophilic digester (35 ± 2 ^{o}C) having a volume of 70 liter coupled with a new design of the solar water thermal system has been developed using TRNSYS. The thermal performance and dynamic behavior of the system under a climatic condition of Kenitra Morocco are investigated. It found that the solar system covers 90% of the energy consumed by the anaerobic digestion during the year. In addition, the result shows integration of solar thermal energy to the anaerobic digester has a feasible benefit. When it integrates with anaerobic digester a daily temperature fluctuation become 0.8 ^{o}C in summer and 2.3 ^{o}C in the winter season.

The heating is carried out by exchanger inside of the digester. Hamed et al., (2003), designed a 10 m^3 Completely Stirred Tank Reactor for anaerobic digestion of liquid cow manure under thermophilic condition (50 ^{o}C), using a solar heating system mounted on the reactor roof. Axaopoulos et al., (2001) developed a mathematical model for simulation of digester treating swine manure heated with solar energy. The model was calibrated with experimental data from a 45 m^3 of digester operated at 6 days hydraulic retention time at an aimed temperature of 35 ^{o}C. The solar heating system consists of four flat plate solar collectors of 8 m^2 each mounted on the reactor roof at a tilt angle of 22^{o}. The model results showed a well agreement with the measured values of the reactor temperature.

The heating load required for the anaerobic digester was performed using a solar collector. A solar collector is a special kind of heat exchanger that transforms solar radiant energy in to heat. A solar collector differs in several respects from more conventional heat exchangers. The latter usually accomplished a fluid to fluid exchange with high heat transfer rates and with radiation as unimportant factor. In solar collector, energy transfer is from a distant source of radiant energy to

a fluid. The flux of incident radiation is at best, approximately 1100 W/m^2 (without optical concentration), and it is variable. The wave length range is from 0.3 to 3 μm, which is considerably shorter than that of the emitted radiation from most energy absorbing surfaces (Duffe and Beckman, 2013).

There are a large number of solar collector designs that have shown to be functional; these designs are classified in to two general types of solar collectors:

- Flat-plate collectors – the absorbing surface is approximately as large as the overall collector area that intercepts the sun's rays.
- Concentrating collectors – large areas of mirrors or lenses focus the sunlight onto a smaller absorber.

Flat-plate collectors are the most common solar collector for solar water-heating systems in homes and solar space heating (Salah, 2012). It can be designed for applications requiring energy delivery at moderate temperatures, up to perhaps 100 ^oC, above ambient temperature. They use both beam and diffuse solar radiation, and do not require tracking of the sun, and require little maintenance (Duffe and Beckman, 2013).

Description of flat plate collector

A typical flat-plate collector, Figure 2.3, consists of an absorber in an insulated box together with transparent cover sheets (glazing). The absorber is usually made of a metal sheet of high thermal conductivity, such as copper or aluminum, with integrated or attached tubes. Its surface is coated with a special selective material to maximize radiant energy absorption while minimizing radiant energy emission. The insulated box reduces heat losses from the back and sides of the collector. The performance and operation of a flat-plate collector is governed by the fundamental laws of thermodynamics and relationships from heat transfer and fluid mechanics (Salah, 2012).

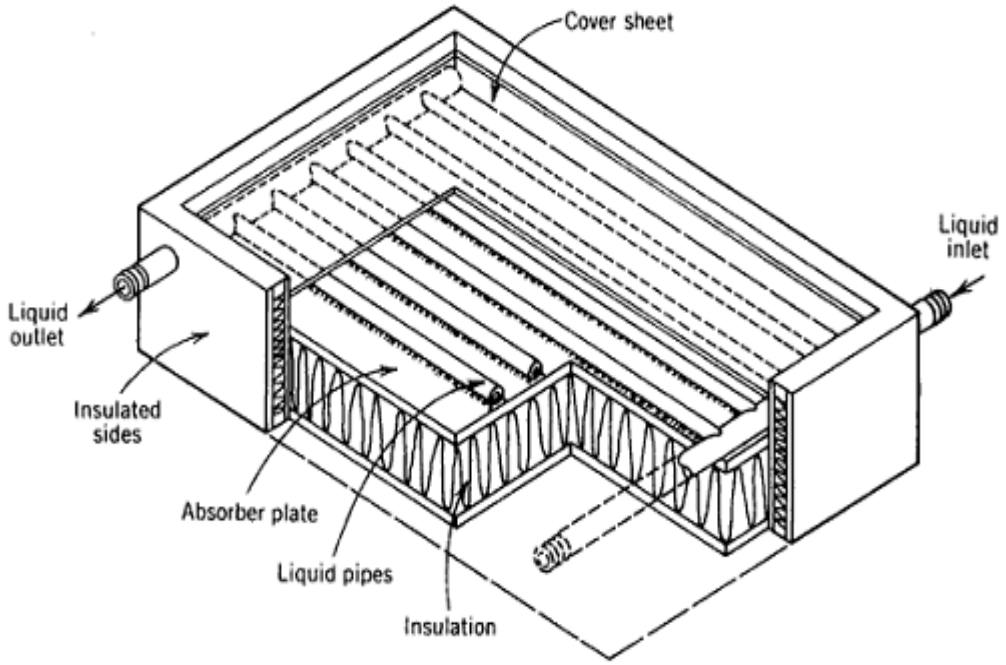

Figure 2.2: Cross-section of a typical liquid flat plate collector (Salah, 2012)

2.4. Types of Thermal Energy Storage Device in Solar Water Heating System

2.4.1. General Overview

The incorporation of solar energy in the anaerobic digestion process may affect the process stability, which is resulting from the daily fluctuation of the variable solar energy (El-Mashad, 2003). Energy storage is a key issue to be addressed to allow intermittent energy sources, typically renewable sources, to match energy supply with demand (Chopade et al., 2013). Thermal energy storage can be stored as a change in internal energy of a material as sensible heat, latent heat and thermochemical or combination of these. The major technique of storage of solar thermal energy is shown below:

1. Sensible heat storage

In sensible heat storage (SHS), thermal energy is stored by raising the temperature of a solid or liquid. SHS system utilizes the heat capacity and the change in temperature of the material during the process of charging and discharging. The amount of heat stored depends on the specific heat of the medium, the temperature change and the amount of storage material.

$$Q = \int_{T_i}^{T_f} mCpdT = mCp_a(T_f - T_i) \quad \text{(2.1)}$$

Where:

- m is the mass of storage material (kg)
- Cp_a is average specific heat between T_i and T_f (J/kg K)
- T_i and T_f are initial and final temperature of a material respectively (^oC)

Water appears to be the best SHS liquid available because it is inexpensive and has a high specific heat capacity. However above 100 ^oC, oils, molten salts and liquid metals, etc. are used. For air heating applications rock bed type storage materials are used (Sharma et al., 2009).

2. Latent heat storage

Latent heat storage (LHS), is based on the heat absorption or release when a storage material undergoes a phase change from solid to liquid or liquid to gas or vice versa. The storage capacity of the LHS system with a PCM medium is given by

$$Q = \int_{T_i}^{T_m} mCp_s dT + ma_m L_{fus} + \int_{T_m}^{T_f} mCp_l dT \quad \text{.....} \quad (2.2)$$

$$Q = m[Cp_s(T_m - T_i) + a_m L_{fus} + Cp_l(T_f - T_m) \text{.....} \quad (2.3)$$

Where:

- m is the mass of the phase change material
- Cps and Cpl are specific heat of material at a solid and liquid state respectively
- T_i, T_m and T_f are the temperature of the material at the initial, molten and final state respectively
- a_m is fraction melted and
- L_{fus} is latent heat of fusion per unit mass.

3. Thermochemical energy storage

Thermochemical systems rely on the energy absorbed and released in breaking and reforming molecular bonds in a completely reversible chemical reaction. In this case, the heat stored depends on the amount of storage material, the endothermic heat of reaction, and the extent of conversion.

$$Q = a_r m \Delta h_r \text{.....} \quad (2.3)$$

Where: a_r is fraction reacted and Δh_r is endothermic heat of reaction.

Amongst above thermal heat storage techniques, latent heat thermal energy storage is particularly attractive due to its ability to provide high-energy storage density and its characteristics to store heat at constant temperature corresponding to the phase transition temperature of phase change material (PCM). Phase change can be in the following form: solid–solid, solid–liquid, solid–gas, and liquid–gas and vice versa.

In solid–solid transitions, heat is stored as the material is transformed from one crystalline to another. These transitions generally have small latent heat and small volume changes than solid–liquid transitions.

Solid–gas and liquid–gas transition through have higher latent heat of phase transition but their large volume changes on phase transition are associated with the containment problems and rule out their potential utility in thermal-storage systems. Large changes in volume make the system complex and impractical. Solid–liquid transformations have comparatively smaller latent heat than liquid–gas. However, these transformations involve only a small change (of order of 10% or less) in volume. Solid–liquid transitions have proved to be economically attractive for use in thermal energy storage systems.

Phase change materials themselves cannot be used as heat transfer medium. A separate heat transfer medium must me employed with heat exchanger in between to transfer energy from the source to the PCM and from PCM to the load (Sharma et al., 2009).

Any latent heat energy storage system therefore, possess at least following three components:

- A suitable PCM with its melting point in the desired temperature range,
- A suitable heat exchange surface, and
- A suitable container compatible with the PCM.

2.4.2. Latent Heat Thermal Energy Storage Materials

Phase change materials (PCM) are ‘‘Latent’’ heat storage materials. The thermal energy transfer occurs when a material changes from solid to liquid, or liquid to solid. This is called a change in state, or ‘‘Phase.’’ Initially, these solid–liquid PCMs perform like conventional storage materials; their temperature rises as they absorb heat. Unlike conventional (sensible) storage materials, PCM absorbs and release heat at a nearly constant temperature (Sharma et al., 2009).

They store 5 – 14 times more heat per unit volume than sensible storage materials such as water, masonry, or rock (Sharma et al., 2009). A large number of PCMs are known to melt with a heat of fusion in any required range. However, for their employment as latent heat storage materials these materials must exhibit certain desirable thermodynamic, kinetic and chemical properties. Moreover, economic considerations and easy availability of these materials has to be kept in mind.

The PCM to be used in the design of thermal-storage systems should passes desirable thermos-physical, kinetics and chemical properties which are as follows:

1. Thermal properties
    - Suitable phase-transition temperature.
    - High latent heat of transition.
    - Good heat transfer.

Selecting a PCM for a particular application, the operating temperature of the heating or cooling should be matched to the transition temperature of the PCM. The latent heat should be as high as possible, especially on a volumetric basis, to minimize the physical size of the heat store. High thermal conductivity would assist the charging and discharging of the energy storage.

2. Physical properties
    - Favorable phase equilibrium.
    - High density.
    - Small volume change.
    - Low vapor pressure.

Phase stability during freezing melting would help towards setting heat storage and high density is desirable to allow a smaller size of storage container. Small volume changes on phase transformation and small vapor pressure at operating temperatures to reduce the containment problem.

3. Kinetic properties
    - No super cooling.

- Sufficient crystallization rate.

Super cooling has been a troublesome aspect of PCM development, particularly for salt hydrates. Super cooling of more than a few degrees will interfere with proper heat extraction from the store, and 5 – 10 ^{o}C super cooling can prevent it entirely.

4. Chemical properties

    - Long-term chemical stability.
    - Compatibility with materials of construction.
    - No toxicity.
    - No fire hazard.

PCM can suffer from degradation by loss of water of hydration, chemical decomposition or incompatibility with materials of construction. PCMs should be non-toxic, nonflammable and non-explosive for safety.

5. Economics

    - Abundant.
    - Available.
    - Cost effective.

Low cost and large-scale availability of the phase change materials is also very important.

2.4.3. Classification of Phase Change Materials

A large number of phase change materials (organic, inorganic and eutectic) are available in any required temperature range.

There are a large number of organic and inorganic chemical materials, which can be identified as PCM from the point of view melting temperature and latent heat of fusion. However, except for the melting point in the operating range, majority of phase change materials does not satisfy the criteria required for an adequate storage media as discussed earlier. As no single material can have all the required properties for an ideal thermal-storage media, one has to use the available materials and try to make up for the poor physical property by an adequate system design. For

example metallic fins can be used to increase the thermal conductivity of PCMs, super cooling may be suppressed by introducing a nucleating agent or a 'cold finger' in the storage material and incongruent melting can be inhibited by use of suitable thickness.

In general inorganic compounds have almost double volumetric latent heat storage capacity (0.25 – 0.4 kg/m^3) than the organic compounds (0.128 – 0.2 kg/m^3). For their very different thermal and chemical behavior, the properties of each subgroup which affects the design of latent heat thermal energy storage systems using PCMs of that subgroup are discussed in detail below (Sharma et al., 2009).

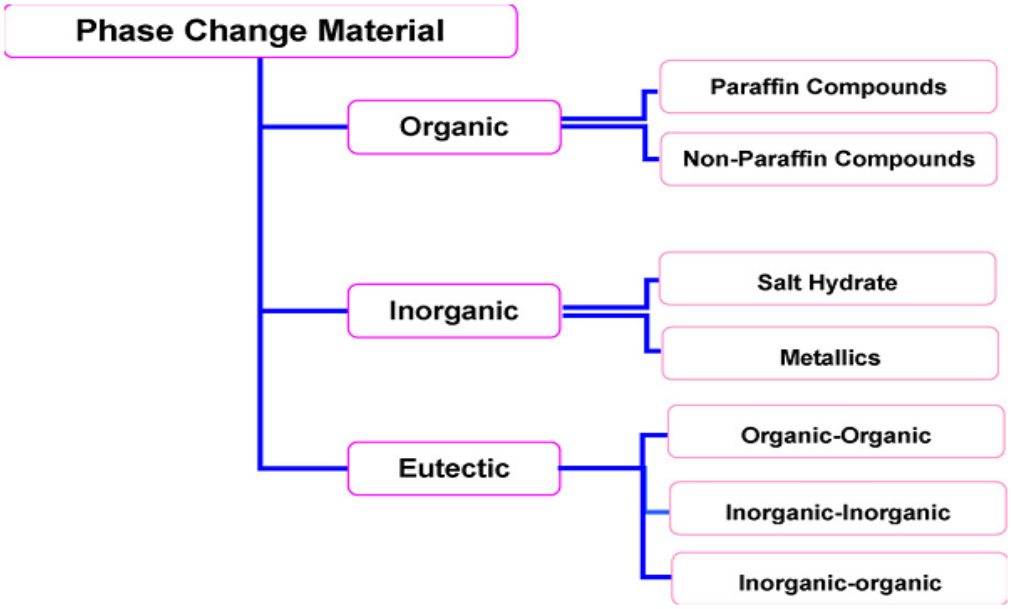

Figure 2. 3: Classification of phase change materials (Sharma et al., 2009)

2.4.3.1. Organic Phase Change Materials

Organic materials are further described as paraffin and non-paraffin. Organic materials include congruent melting means melt and freeze repeatedly without phase segregation and consequent degradation of their latent heat of fusion, self-nucleation means they crystallize with little or no super cooling and usually non-corrosiveness.

i. Paraffin

Paraffin wax consists of a mixture of mostly straight chain alkanes CH_3–(CH_2)–CH_3. The crystallization of the (CH_3)-chain release a large amount of latent heat. Both the melting point

and latent heat of fusion increase with chain length. Paraffin qualifies as heat of fusion storage materials due to their availability in a large temperature range. Due to cost consideration, however, only technical grade paraffin's may be used as PCMs in latent heat storage systems. Paraffin is safe, reliable, predictable, less expensive and non-corrosive. They are chemically inert and stable below 500 ^{o}C, show little volume changes on melting and have low vapor pressure in the melt form. For these properties of the paraffin's, system-using paraffin's usually have very long freeze–melt cycle. They show some undesirable properties such as: (i) low thermal conductivity, (ii) non compatible with the plastic container and (iii) moderately flammable.

ii. Non-Paraffin

The non-paraffin organic are the most numerous of the phase change materials with highly varied properties. Each of these materials will have its own properties unlike the paraffin's, which have very similar properties. This is the largest category of candidate's materials for phase change storage. These organic materials are further subgroups as fatty acids and other non-paraffin organic. These materials are flammable and should not be exposed to excessively high temperature, flames or oxidizing agents.

Some of the features of these organic materials are as follows: (i) high heat of fusion, (ii) inflammability, (iii) low thermal conductivity, (iv) low flash points, (v) varying level of toxicity, and (vi) instability at high temperatures.

2.4.3.2. Inorganic Phase Change Materials

Inorganic materials are further classified as salt hydrate and metallics. These phase change materials do not supercool appreciably and their heats of fusion do not degrade with cycling.

i. Salt Hydrates

Salt hydrates may be regarded as alloys of inorganic salts and water forming a typical crystalline solid of general formula AB • nH_2O. The solid–liquid transformation of salt hydrates is actually a dehydration of hydration of the salt, although this process resembles melting or freezing thermodynamically. A salt hydrates usually melts to either to a salt hydrate with fewer moles of water, i.e.

$$AB \bullet nH_2O \rightarrow AB \bullet mH_2O + (n - m)H_2O$$

At the melting point the hydrate crystals breakup in to anhydrous salt and water, or into a lower hydrate and water. One problem with most salt hydrates is that of incongruent melting caused by the fact that the released water of crystallization is not sufficient to dissolve all the solid phase present. Due to density difference, the lower hydrate (or anhydrous salt) settles down at the bottom of the container.

Most salt hydrates also have poor nucleating properties resulting in super cooling of the liquid before crystallization beings. One solution to this problem is to add a nucleating agent, which provides the nucleon which crystal formation is initiated. Another possibility is to retain some crystals, in a small cold region, to serve as nuclei.

Salt hydrates are the most important group of PCMs, which have been extensively studied for their use in latent heat thermal energy storage systems. The most attractive properties of salt hydrates are: (i) high latent heat of fusion per unit volume, (ii) relatively high thermal conductivity (almost double of the paraffin's), and (iii) small volume changes on melting. They are not very corrosive, compatible with plastics and only slightly toxic. Many salt hydrates are sufficiently inexpensive for the use in storage.

ii. Metallics

This category includes the low melting metals and metal eutectics. These metallics have not yet been seriously considered for PCM technology because of weight penalties. However, when volume is a consideration, they are likely candidates because of the high heat of fusion per unit volume. They have high thermal conductivities, so fillers with added weight penalties are not required. The use of metallics poses a number of unusual engineering problems. A major difference between the metallics and other PCMs is their high thermal conductivity. Some of the features of these materials are as follows: (i) low heat of fusion per unit weight (ii) high heat of fusion per unit volume, (iii) high thermal conductivity, (iv) low specific heat, and (v) relatively low vapor pressure.

2.4.4. Configuration of Capsules in Storage Devices

There are two types of capsule configurations in the packed bed latent heat thermal energy storage devices:

1. Spherical

2. Cylindrical

Spherical capsule configurations have the advantage of large surface to volume ratio of the packed beds and of higher storage density for the phase change materials compared to the cylindrical configuration of packing (Regin et al., 2009).

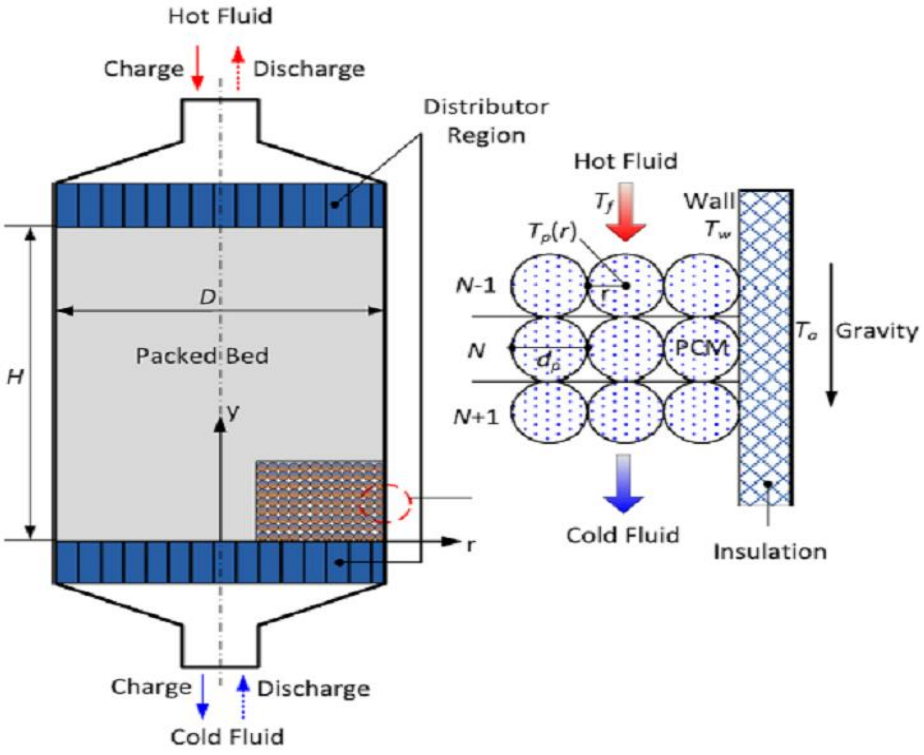

Figure 2. 4: Schematic diagram of a packed bed latent heat thermal energy storage system with spherical capsules (Regin et al., 2009)

2.5. Related Works Done by Previous Researchers

Variel et al., (1980), studied the effect of temperature and retention time on the methane production from beef cattle manure using continuously mixed 3 litres working volume of anaerobic fermenters. The temperature ranged from 30 to 65 ^{o}C with 5 ^{o}C increments between the fermenters. The result showed that temperature affects the production rate of methane, but does not increase the amount of CH_4 that can produced from a unit mass of substrate.

Kablan et al., (2000), experimentally investigated the utilization of solar energy for heating a bioreactor. For the purpose of their study, a solar collector combined with a heat exchanger are designed, manufactured, and installed to provide the necessary heating requirements for a water

jacket around the bioreactor. In addition, an inexpensive PID (proportional. integral, and differential) controller was also designed, installed, and tested to maintain a constant temperature of 40 ^{o}C in the water-jacket around the bioreactor. They also analyzed the cost of the system. The result showed the internal rate of return of the investment in such solar heating system was found to be 32.7%, which indicates that the system is very attractive.

Zupancic and Ros, (2003), studied the heating requirements of the thermophilic anaerobic digestion process and experimentally investigate the biogas production in the laboratory at a retention times from 1 to 10 days. The data gathered in the experiments was then used to perform a heat and energy analysis. The source of heat was a conventional combined heat and power unit system. The results showed that thermophilic digestion is much faster than mesophilic digestion and therefore produces more biogas in a shorter time or at smaller digester volumes. The major part of the heating requirements consisted of sludge heating. The heat losses of the digester were only 2 – 8% of the sludge heating requirements. The heating requirements in thermophilic digestion are about twice those of mesophilic digestion.

El-Mashad et al., (2004), they perform simulation model of a 10 m^3 completely stirred tank reactor, under thermophilic conditions (50 ^{o}C), using a solar heating system mounted on the reactor roof. The simulation results show that the temperature fluctuation of the reactor during the night is less than 1^{o}C, which is too small to harm the microbial activity. The results show that an annual net thermal energy production and overall annual energy efficiency of 100% and 95% respectively.

Chen and Qin, (2014), experimentally investigated a solar-assisted biogas system. The initiative was to combine popularly-available house biogas plant with solar-collector at a reasonable cost, therefore to maintain year-round operation of biogas plant and to produce enough amount of biogas in winter for daily use. The recorded data in a pilot project revealed that additional electricity consumed accounted to only 7.2% of biogas produced, suggesting an economically feasible approach.

Axaopoulos et al., (2001), developed a mathematical model for simulating an innovative design of a solar-heated anaerobic digester. They construct 45 m^3 of digester for swine manure below ground level and fix cover is made of flat-plate solar collectors, which are an integral part of the roof structure. The solar collectors are coupled to a heat exchanger immersed in the digester

manure. The upper part of the digester, under the tilted cover, forms an airtight enclosure that is used to collect and store the daily produced biogas. They experimentally investigated the performance of the system and the results indicate that the use of solar collectors as a cover reduces the digester thermal losses and positively affects the heat balance of the digester.

Heriz et al., (2017), developed a transient thermal model for predicting temperature variation in semi-buried anaerobic digester as a function of climatic conditions (ambient temperature, solar radiation, rain intensity etc.). The simulation results help in identifying causes that leads to major energy losses from the reactor. They presented a model that constitutes a powerful predictive tool for assisting engineers in determining the optimal design of digesters, as well as in the investigation of the influence of materials type on the reactor heating requirements.

Yiannopoulos et al., (2008), designed a solar heated reactor system to enhance the anaerobic treatment of wastewater or biological sludge at a temperature of 35 ^{o}C. Furthermore, they developed a mathematical model for the prediction of temperature distribution within the reactor under steady state conditions. Preliminary results obtained based on model simulations performed using meteorological data from various geographical regions of the world suggested that the solar reactor system proposed by them could be a promising and environmentally friendly approach for anaerobic treatment of wastewater and biological sludge.

Kokar and Eryasar, (2007), in their study, solar heated biogas plants were reviewed. Furthermore, the optimization of insulation thicknesses and solar energy systems for 5 m^3 biogas reactor were carried out for two different cities under three different climatic zones in Turkey. Based on the obtained results, the ratio of annually produced biogas required for reactor heating was calculated for each city, with and without solar heating system. The obtained results indicate that the biogas consumption for reactor heating is decreased by approximately 19 % for average of six cities when solar heating system is used. This means that available biogas potential would be increased.

Badra et al., (2017), investigated the feasibility of integration of solar thermal energy in the anaerobic digestion. In their study, a simulation model of the mesophilic digester (35 ± 2 ^{o}C) having a volume of 70 litres coupled with a new design of the solar water thermal system has been developed using TRNSYS. The heating is carried out by exchanger inside of the digester. The thermal performance and dynamic behavior of the system under a climatic condition of

Kenitra Morocco are investigated. It was found that the solar system covers 90 % of the energy consumed by the anaerobic digestion during the year. In addition, their results showed a daily temperature fluctuation of 0.8 ^{o}C in the summer and 2.3 ^{o}C in the winter.

Yuan et al., (2011), designed a solar heating biogas fermentation system, its volume is 6 m^3, and then calculates digester's heat load based on Hohhot's weather data. They uses October experimental data and looking for the heat matching relationship between the solar collector system and biogas fermentation system. They can concluded that, at Hohhot, in October, the heat was absorbed by 2 m^2 solar collectors that was run for 8 hours can meet the 6 m^3 digester's fermentation heat demand.

El-Mashad et al., (2003), evaluated the consequence of the use of solar energy under Egyptian weather conditions. In their study, they did experiments and compared the result with numerical model. In the experimental part, anaerobic digestion on laboratory scale is studied in two continuously stirred tank reactors at 50 and 60 ^{o}C. Daily temperature fluctuations in the tank caused a decrease in methane production rate of only 12 and 20% at 50 and 60 ^{o}C, respectively. These results are used in a model for the thermal energy demand. In the model the net thermal energy production as a function of reactor volumes, thermal insulation and additional pre-heating of the influent was evaluated. The model results show that for continuously stirred tank reactors, additional pre-heater is not recommended since it decreases the efficiency. The results also show that a maximum overall heat transfer coefficient of 1 W $m^{-2}K^{-1}$ is needed for reaching at least 50% of energy efficiency. Furthermore, adding a solar energy system improves the efficiency for large reactors only slightly, while for small reactors a large improvement is achieved.

A new technique of solar heating biogas fermentation system integrated with a phase change thermal storage device is introduced for improving the low efficiency of the traditional biogas fermentation devices.

Lu et al., (2015), investigated the optimum relative proportion between the heat supplied by solar and that stored in phase change heat storage device. And for a designed solar heated biogas system, its performance of anaerobic fermentation process under different natural cooling conditions has been assessed by varying the thickness of the insulation materials.

Shobo and Mawire, (2015), have presented a numerical investigation of the transient behavior of a packed bed latent heat thermal energy storage system, using encapsulated Erythritol as the

phase change material and sunflower oil as the heat transfer fluid. The investigated thermal energy system is used for domestic cooking needs, using dual phase mathematical model. From the result they concluded that, an increase in the inlet temperature and flow velocity of the heat transfer fluid in to the packed bed has shown to significantly decrease the charging time of the thermal energy storage unit.

Gonzalez-Aguilar et al., (2017), analyzed a latent thermal energy storage system for concentrating solar power plant applications, which consists of sodium nitrate filled spherical capsules in a cylindrical tank. The high temperature synthetic oil, Therminol 66, is used as heat transfer fluid. They developed a numerical model to investigate the behavior of the system. They also studied the influence of capsule size and the flow rate of heat transfer fluid on the temperature distribution, fluid flow, melting and solidification of the system. The results indicated that the heat transfer rate is increased and eventually the charging/discharging time is decreased when the capsule size is decreased, or the heat transfer fluid flow rate is increased.

Romero et al., (2015), developed a numerical model to obtain the detailed heat transfer characteristics of lab-scale latent thermal energy storage system, which consists of molten salt encapsulated spherical capsules and air. They predicted the melting process and the corresponding temperature and velocity distributions in every capsule of the system. They validated their model with the reported experimental results. They also predicted the influence of initial condition on the thermal performance of the thermal energy storage system.

Bellan et al., (2017), numerically and experimentally analyzed the dynamic thermal performance of high temperature latent thermal energy storage system packed with spherical capsules. The spherical capsules are encapsulated by sodium nitrate and air is used as heat transfer fluid. Transient two-dimensional continuous solid phase and effective packed bed models are developed and validated by comparing to the experimental results. Based on those models, they analyzed the detailed characteristics of the heat transfer between the capsules and heat transfer fluid. Parametric analyses are conducted to study the influence of mass flow rate, Stefan number, thickness and the thermal conductivity of the shell. The results indicate that the Stefan number plays a vital role on the total heat storage capacity due to sensible heat, and the shell properties of the capsule significantly influence the thermal performance of the system; the influence of the shell thickness increases (decreases) when the thermal conductivity of the shell is low or high.

From literature can conclude that, temperature affect the production rate of biogas. Biogas yield rate increases with increasing the operating temperature of anaerobic digestion system. To increase the operating temperature of digester external source of energy is required. Solar energy for heating a biogas reactor could be a promising and environmentally friendly approach for anaerobic digester. The combination of solar energy and biogas production represents a kind of solar energy storage in the form of fuel gas. But contrary, incorporation of solar energy in the anaerobic digestion process may affect the process stability, which results from the daily fluctuations of the variable energy. Solar energy storage is a key issue to be addressed the intermittence of solar energy. Packed bed solar thermal energy storage with phase change material have a higher energy storage density and energy storage at constant temperature or with in small temperature range. Therefore, integrating a solar assisted anaerobic digestion system with packed bed solar thermal energy storage with phase change material have a higher advantage in biogas technology.

Some researchers (Yiannopoulos et al., 2008, El-Mashad et al., 2003, Axaopoulos et al., 2001 etc.) have investigated numerically and experimentally the thermal behavior of a solar assisted anaerobic digestion system to specific geographical locations. But there is scarcity on the study of the thermal performance of a solar assisted anaerobic digester theoretically as well as experimentally across seasons in a year specify to a given geographical location in Ethiopia particularly anaerobic digestion system integrated with solar thermal energy storage packed with phase change material.

In this study, the thermal performance of a solar assisted anaerobic digestion system integrated with a packed bed solar thermal energy storage system that uses paraffin n-Triacontane as a phase change material were investigated. The digester is designed to digest cow dung at Adama weather condition. And it is designed to fulfill the energy demand of 100 people for their cooking purpose.

CHAPTER 3: Thermal Modeling of Anaerobic Digester

3.1. Anaerobic Digester

The present investigation considers an underground anaerobic digester. It designed to digest cow dung. Its walls are made of reinforced concrete and having a 20 cm thickness, it has similar construction design used by Hreiz et al., (2017). The reactor cover is a deformable black EPDM (Ethylene Propylene Diene Terpolymer) membrane, whose thickness is about 3 mm. The operating pressure is maintained approximately equal to atmospheric pressure. The digester is equipped with a mechanical mixing system, powered by electrical motor. Indeed, an efficient stirring of the digestate is required for homogenization (i.e. temperature, species and biomass concentrations etc.), minimizing heavy solids sedimentation and reducing the formation of floating scum or straw blankets.

Hot water coming from the solar collector is used to heat the digesate through an immersed helical-coil heat exchanger. The digestate temperature is designed to maintain at 55 ^{o}C.

To perform a heat requirement analysis, the biogas production rates have to be determined. The reactor is designed to produce biogas that can fulfill the energy demand of 100 peoples for their cooking application. The average amount of biogas required to fulfill the energy demand of a person per day for cooking application is 0.225 m^3 of biogas (Otim et al., 2010). The designed biogas reactor is responsible to produce 22.5 m^3 of biogas per day for 100 people.

Abubakar et al., (2012), observed that the biogas yield from anaerobic digestion of cow dung at 53 ^{o}C is 0.15 liter of biogas per gram of volatile solid added, so daily 150 kg of volatile solid is required to feed in to the reactor to produce 22.5 m^3 of biogas per day. Varel et al., (1981) utilizes beef cattle waste with 6% of volatile solid content, in this study the concentration of volatile solid within cow dung that is added in to the reactor is the same as utilized by Varel et al., (1981).

To produce 22.5 m^3 of biogas per day, daily 2500 kg of cow dung should feed in to the reactor. Cow dung diluted by tap water at the ratio of 1:1 Varel et al., (1981) and Abubakar et al., (2012). The total daily substrate feed in to the reactor is 5000 kg. In this analysis, the density of water and cow dung mixture has been calculated as the weight average of water and cow dung densities and has been evaluated to be 952.5 kg/m^3.

The digester volume can be calculated using the following formula:

$Vd = SR * RT$ ……...… (3.1)

Where: Vd is digester volume, SR is substrate feeding rate, and RT is the retention time of a substrate with in a digester.

Abubakar et al., (2012), from the results of experimental investigation of a thermophilic anaerobic digestion of cow dung, the maximum biogas yield rate was achieved at a retention time of 10 days. The digester volume can be calculated from the Equation 3.1, and found to be 50 m^3. Digester volume can only cover 70% of the total volume of anaerobic digester. The total volume of digester can be calculated as:

$VT = Vd/0.7 = 71.43\ m^3$ ……. (3.2)

30% of the total volume of digester is left for holding produced biogas, and it cover 21.43 m^3. The gas holder has a hemispherical shape and its diameter is equal to the diameter of digester:

Volume of gas holder = $\frac{1}{12}\pi d^3 = 21.43\ m^3$…… (3.3)

Where d is the diameter of a gas holder, solving Equation (3.3) to get the diameter of gas holder, gives to be 4.34 m.

Digester volume = $\frac{1}{4}\pi d^2 h = 50\ m^3$…….... (3.4)

Where h is the digester height, solving for h results h = 3.38 m.

3.2. Climatic Condition

Adama region is characterized by a climatic condition of tropical; it has high intensity of solar radiation. The monthly average temperature of Adama ranges between 18.2 ^oC (December) and 22.5 ^oC (April). Thirty year average monthly average temperatures and wind speed in Adama are presented in Table 3.1.

Table 3.1: Monthly average annual climatic condition of Adama (Ethiopia national meteorology agence)

Temperature	MONTH											
	Jan	Feb	Mar	Apri	May	Jun	July	Aug	Sep	Oct	Nov	Dec
Average(^{o}C)	19.5	20.5	21.8	22.5	22.4	22.3	18.4	20.6	21	20.1	18.6	18.2
Min(^{o}C)	11.4	12.9	14.2	15.1	14.5	15.2	12.4	15.1	14.7	12.3	10.7	10.7
Max(^{o}C)	27	28.1	29.5	30	30.4	29.5	24.4	26.1	27.4	27.9	26.6	25.7
Wind speed (m/s)	3.5	2.7	3.5	3.5	3.5	2.8	2.8	2.7	2.8	3.4	4.3	3.4

Meteorological data are required for evaluating heat transfer between the digester and its surroundings. In this paper, thirty years average climatic conditions of Adama are used to analyze different parameters.

3.3. The Governing Heat Balance Equations for the Digester

The heat requirements of cow dung digesters generally consist of three parts; first, that required for raising the temperature of incoming sludge for digestion; second, for compensating heat losses through the boundaries of the digester: and third, for compensating losses that might occur in the piping between the heat source and the digester. By appropriate construction the heat losses in the piping (the third part) can be minimized to the point where such losses can be neglected (Zupancic and Ros, 2003).

The energy requirements of anaerobic cow dung digestion consist of mixing and pumping. But, solar water heating system is not responsible to generate this required energy, because both mixing and pumping processes are performed by the action of electrical energy.

The heat requirements considered were the heat losses of the digester and the heat necessary for raising the incoming sludge temperature.

$$\dot{Q}_u = \dot{Q}_s + \dot{Q}_l \quad \text{(3.5)}$$

Where - $\dot{Q}_u$ is the required heat energy to maintain the temperature of digester at constant value, $\dot{Q}_l$ is heat losses from the digester to the soil and ambient air, and $\dot{Q}_s$ is the heat needed to raise the influent temperature to the operating temperature (in this study it is 55 ^oC).

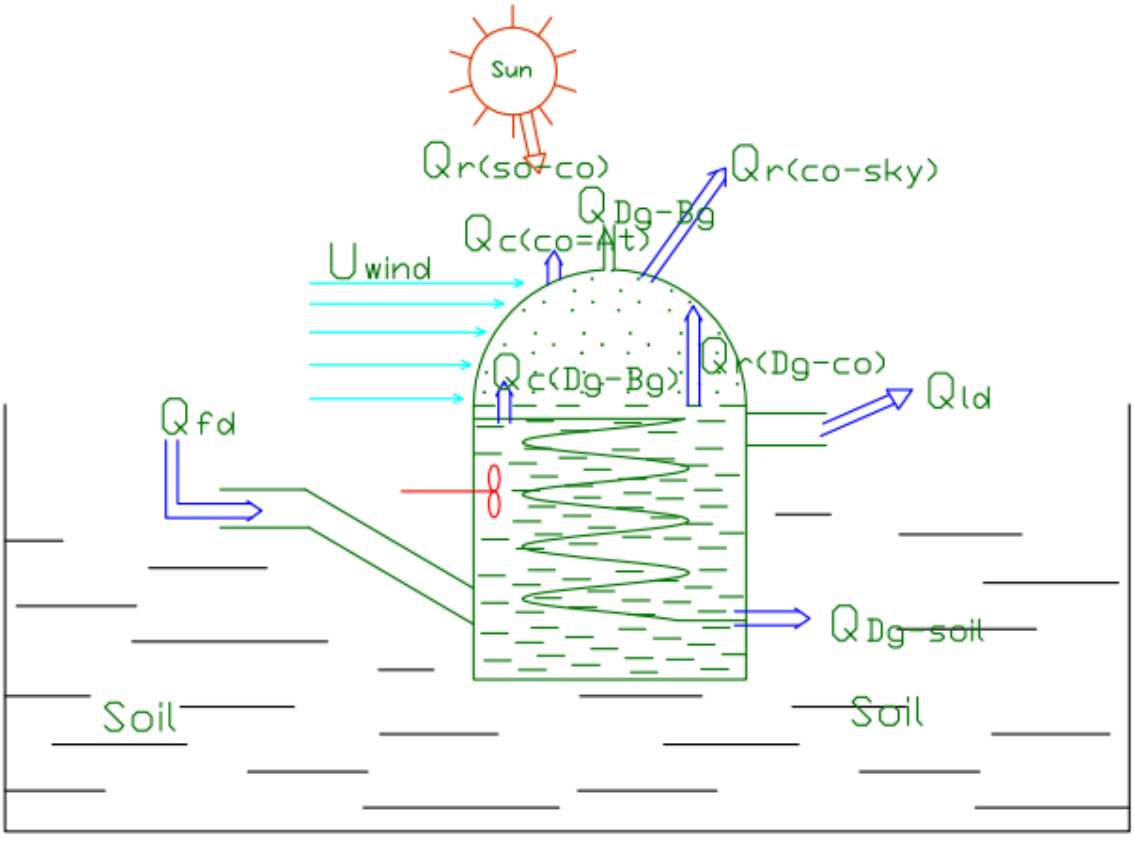

Figure 3. 1: Simplified schematic diagram and heat transfer phenomenon's of anaerobic digester

To investigate the heat requirement of the digester, transient one dimensional thermal model that include three governing heat balance equations were written over the digestate, the biogas and the cover (the temperature of each of these elements is supposed uniform). The thermal model equations are presented in the following sections.

i. The Digestate Phase

To investigate the heat transfer between digetate and its surrounding it is important applying the conservation of energy principle to the digestate contained in the digester and it gives (Hreiz et al., 2017):

$$\rho_{Dg} V_{Dg} C_{Dg} \frac{dT_{Dg}}{dt} = (Q_{fd} - Q_{ld}) - Q_{Dg\_Bg} - Q_{c_{(Dg\_Bg)}} - Q_{Dg\_soil} - Q_{r_{(Dg\_co)}} \quad \text{(3.6)}$$

Where :

- ρ is the represents density
- V is the volume
- C the constant pressure heat capacity,
- T the temperature and t the time.
- Subscript Dg refers to the digestate, fd to the feed, Bg to the biogas, Co to the cover and ld to the leaving the digester.

The right hand sides of Equation (3.6) are heat transfer in and out of the digestate and the left hand side of Equation (3.6) is energy stored in the digestate.

Where in Equation (3.6) the heat transfer terms are

- Q_{fd} -represents the heat carried by the feed.
- Q_{ld} - denotes the heat lost due to the digestate leaving the reactor by overflow.
- Thus, the term $(Q_{fd} - Q_{ld})$ corresponds to the heat required to warm the inputs up to the digestate temperature.
- Q_{Dg_Bg} - represents heat loss by mass transfer from the digestate to the biogas.
- $Q_{c(Dg\_Bg)}$ - is the convective heat transfer from the digestate to the biogas.
- Q_{Dg_soil} - represents heat transfer from the digestate to the soil across the walls.
- $Q_{r(Dg\_co)}$ - represents the net radiative heat transfer from the digestate to the cover.

All radiative heat transfer phenomena from/with the biogas are neglected. Indeed, gases have very low thermal emissivity, and are almost transparent to infrared rays.

ii. The Biogas Phase

Similarly for biogas phase, applying the energy balance around the biogas phase and it gives (Hreiz et al., 2017):

$$\rho_{Bg} V_{Bg} C_{Bg} \frac{dT_{Bg}}{dt} = Q_{Dg\_Bg} - Q_{Bg} + Qc_{(Dg\_Bg)} - Qc_{(Bg\_co)} \quad \text{..... (3.7)}$$

- Q_{Bg} - Denotes the heat carried by the outgoing biogas.

- $Qc_{(Dg\_Bg)}$ - Is the convective heat transfer from the biogas to the cover

The heat carried by the outgoing biogas is small compared to the other heat transfer terms, because the mass flow rate of the outgoing biogas is small.

iii. The Cover

Similarly to the cover, applying the energy balance over the cover and it gives (Hreiz et al., 2017):

$$\rho_{co}V_{co}C_{co}\frac{dT_{co}}{dt} = Q_{c_{(Bg\_co)}} - Q_{c(co_{\mathrm{At}})} + Q_{r_{(Dg\_co)}} - Q_{r_{(co\_At)}} + Q_{r_{(so\_co)}} \quad \text{(3.8)}$$

Where the subscript At refers to the atmosphere (and the ambient air) and So to solar irradiation.

- $Q_{c(co\_At)}$ - Represents convective heat transfer from the cover to the ambient air.
- $Q_{r(co\_At)}$- Corresponds to long-wave radiations emitted by the cover to the atmosphere.
- $Q_{r(co\_So)}$- Denotes the cover heat gain from solar irradiation.

The cover is exposed to atmosphere and solar radiation, at day time solar energy is absorbed by cover and heat is lost from cover to atmosphere by convective heat transfer because of wind.

3.4. Modeling of the Heat Transfer Phenomena's

3.4.1. Modeling of the Heat Carried by the Feed, and the Heat Lost Due to the Digestate Leaving the Digester

The digester is mainly fed with a daily average of 5000 kg of feed (manure) and water mixture. As the mass flow rates of the generated biogas is small compared to that of the feed, the mass flow rate of the feed and the outgoing digestate may be considered equal.

$$Q_{fd} = \dot{m}_{fd}C_wT_{At} \quad \text{(3.9)}$$

$$Q_{ld} = \dot{m}_{fd}C_wT_{Dg} \quad \text{(3.10)}$$

Where :

- $\dot{m}_{fd}$ is the feed mass flow rate
- C_w the water heat capacity at constant pressure and temperature and
- T_{At} is the ambient air temperature.

3.4.2. Modeling of the Heat Loss by Mass Transfer from the Digestate to the Biogas and the Heat Carried by the Outgoing Biogas

The heat loss by mass transfer from the digestate to the biogas and heat carried by the outgoing biogas are calculated as follows (Hreiz et al., 2017):

$$Q_{Dg\_Bg} = \dot{m}_{Bg} C_{Bg} T_{Dg} \quad \text{(3.11)}$$

$$Q_{Bg} = \dot{m}_{Bg} C_{Bg} T_{Bg} \quad \text{(3.12)}$$

Where :

- $\dot{m}_{Bg}$ represents the mass flow rate of biogas,
- C_{Bg} the specific heat capacity of biogas and
- T_{Dg} the temperature of digestate and T_{Bg} the temperature of biogas.

Axaopoulose et al. (2001), experimentally investigated a medium size digester (45m^3), under mild weather conditions, the temperature difference between the biogas and the digestate can exceed 10^{o}C.

Biogas composition was taken as 50% CH_4 by volume, 46% CO_2 and 4% water vapor. The operating pressure being nearly atmospheric, the biogas density was estimated as 1.06 kg/m^3. Its heat capacity was taken as the mass weighted average of the CO_2, CH_4 and water vapor heat capacities and hence, was estimated at 1374 J/kgK, at the biogas temperature of 45 ^{o}C.

3.4.3. Modeling of the Convective Heat Transfer from the Digestate to the Biogas

The convective heat flux from the digestate to the biogas is given by (Hreiz et al., 2017):

$$Q_{c_{(Dg\_Bg)}} = h_{Dg\_Bg} S_{Dg\_Bg} (T_{Dg} - T_{Bg}) \quad \text{(3.13)}$$

Where - $S_{(Dg\_Bg)}$ is the digestate free surface area (equals the digester's cross-section area, 9.35 m^3) and $h_{(Dg\_Bg)}$ the convective heat transfer coefficient between the digestate surface and the biogas.

Considering the biogas phase, given the low gas velocities, forced convection effects may be neglected. Thus, it is assumed that $h_{(Dg\_Bg)}$ is due to free convection in the biogas phase.

Thermally-driven natural convection flows occur if the thermal gradients lead to unstable density stratification and the Rayleigh number, Ra, exceeds a critical value. Ra is defined as follows:

$$Ra = \frac{g\beta'_{Bg}|\Delta T|L^3}{v_{Bg}^2} Pr \quad \text{(3.14)}$$

Where :

- g is the constant of gravity
- |ΔT| the absolute value of a characteristic temperature difference
- β'_{Bg} the fluid coefficient of thermal expansion
- L a characteristic length scale and is taken as $D_{Dg}/4$ (the ratio of the area over the perimeter of the digester cross surface)
- v the fluid kinematic viscosity and
- Pr the Prandtl number

In the current study, Pr_{Bg} has been taken as 0.75 which is a typical value for gases, and β_{Bg} as $1/T_{Bg}$ (ideal gas assumption given the moderate biogas pressure). Note that T_{Bg} should be expressed in K and not in ^{o}C, v_{Bg} was calculated as the volume weighted average of the CH_4 and CO_2 kinematic viscosities, and thus, has been estimated to 1.5×10^{-5} m^2s^{-1} (evaluated at 45 ^{o}C).

The convective heat transfer coefficient between the digestate surface and the biogas h_{Dg_Bg} is calculated using the correlations presented below (Hreiz et al., 2017):

$$Nu = \frac{h_{Dg\_Bg}L}{k_{Bg}} = 0.54 \times \mathrm{Ra}^{0.25} \text{ if } 2 \times 10^4 \leq \mathrm{Ra} \leq 8 \times 10^6 \quad \text{(3.15)}$$

$$Nu = \frac{h_{Dg\_Bg}L}{k_{Bg}} = 0.15 \times \mathrm{Ra}^{0.33} \text{ if } 8 \times 10^6 \leq \mathrm{Ra} \leq 10^{11} \quad \text{(3.16)}$$

Where, Nu is the Nusselt number, and k_{Bg} is the biogas thermal conductivity.

In the current study, this free convection flow type is encountered in three situations: (1) Heat transfer between the biogas and the digestate if T_{Dg} is higher than T_{Bg}. (2) Heat transfer between the biogas and the cover if T_{Bg} is greater than T_{co}. (3) Heat transfer between the ambient air and the cover if T_{co} is greater than T_{At}.

k_{Bg} has been calculated as the volume weighted average of the CH_4 and CO_2 thermal conductivities, and has been estimated to be 27×10^{-3} W/mK (evaluated at 45 ^{o}C). k_{At} has been taken as 25×10^{-3} W/mK (evaluated at 20 ^{o}C).

3.4.4. Modeling of the Convective Heat Transfer from the Biogas to the Cover

The convective heat flux from the biogas to the cover is given by (Hreiz et al., 2017):

$$Qc_{(Bg\_Bg)} = h_{Bg\_co} S_{co} (T_{Bg} - T_{co}) \quad \text{(3.17)}$$

Where - S_{co} is the cover single-sided surface and h_{Dg_co} the associated heat transfer coefficient. S_{co} equals 18.7 m^2: this value has been calculated by assuming that the cover has a spherical cap shape.

If T_{Bg} is higher than T_{co} and the associated Ra greater than 2×10^4, a 'free convection on the lower surface of a cold plate' flow type occurs in the gas in the vicinity of the cover. In this case, h_{Dg_co} is calculated using correlation used to calculate h_{Dg_Bg}.

3.4.5. Modeling of the Net Radiative Heat Transfer from the Digestate to the Cover

The cover's internal surface and the digestate free surface delimit a closed domain. Considering that both surfaces behave as gray bodies, and since the digestate free surface is planar, $Q_{r(Dg\_co)}$, the net radiative heat transfer between the digestate and the cover is given by (Hreiz et al., 2017):

$$Q_{r(Dg\_co)} = \sigma \frac{T_{Dg}^4 - T_{co}^4}{\frac{1-\varepsilon_{Dg}}{\varepsilon_{Dg} S_{Dg\_Bg}} + \frac{1}{S_{Dg\_Bg}} + \frac{1-\varepsilon_{co}}{\varepsilon_{co} S_{co}}} \quad \text{(3.18)}$$

Where :

- σ is the Stefan–Boltzmann constant and
- ε designates thermal emissivity

The emissivities of both the EPDM cover and the digestate have been taken as 0.9. Note that temperatures values should be expressed in K and not in ^{o}C.

3.4.6. Modeling of the Long-Wave Radiations Emitted by the Cover to the Atmosphere

The cover loses heat to the atmosphere by long-wave radiations through its external surface. This heat loss, $Q_{r(co\_At)}$, is calculated as follows:

$$Q_{r(co\_At)} = \varepsilon_{co} \sigma S_{co} (T_{co}^4 - T_{sky}^4) \quad \text{(3.19)}$$

Where: T_{sky} the equivalent sky temperature is evaluated according to Swinbank (1963) correlation (as reported by Hreiz et al., 2017):

$T_{sky} = 0.0552 T_{At}^{1.5}$…….. (3.20)

Note that temperatures values should be expressed in K.

3.4.7. Modeling of the Convective Heat Transfer from the Cover to the Ambient Air

The convective heat transfer from the cover to the ambient air is given by (Hreiz et al., 2017):

$Qc_{(co\_At)} = h_{co\_At} S_{co} (T_{co} - T_{At})$……... (3.21)

In the presence of wind, forced convection is assumed when u_{wind} greater than 0.5 m/s, correlations used to estimate h_{co_At} are given below:

In the presence of wind, for wind speeds, u_{wind}, lower than 0.5 m/s, mixed convection occurs and h_{co_At} is evaluated using the correlation proposed by Okada and Kusaka (2013) (as reported by Hriez et al., 2017):

$h_{co\_At} = 0.0065 \rho_{At} C_{At} (T_{co} - T_{At})\, u_{wind}$…….. (3.22)

For greater wind speeds, forced convection is assumed. The heat transfer coefficient is calculated using the correlation of Rao (2004) (as reported by Hriez et al., 2017) for u_{wind} lower than 7 m/s, and using the correlation of McAdams (1954) (as reported by Hriez et al., 2017) for larger wind speeds:

$h_{co\_At} = 0.025 \rho_{At} C_{At} {u_{wind}}^{0.3}$, if 0.5 m/s $\leq u_{wind} \leq$ 7 m/s……... (3.23)

$h_{co\_At} = 7.2\, {u_{wind}}^{0.78}$, if $u_{wind} \geq$ 7 m/s…….. (3.24)

For simplification, air properties are considered constant. ρ_{At} is taken as 1.1924 kg/m^3, and C_{At} as 1006 J/kgK (evaluated at 20 ^{o}C, the average annual temperature in Adama).

In the absence of wind, if Ra is sufficiently important, free convection occurs whether T_{co} is greater or lower thanT_{At}.

3.4.8. Modeling of the Cover Heat Gain from Solar Irradiation

Solar radiation reaching the digester's cover consists of: (1) Beam–or direct–radiation coming on a straight path from the sun, i.e. its trajectory is not deviated during its passage through the atmosphere. (2) Diffuse radiation, which is the fraction of solar radiation that reaches the earth after being scattered by the atmosphere (Rayleigh and aerosols scattering, reflections and

scattering by the cloud cover, multiple-reflections between the ground and the atmosphere, etc.). This radiation component has no preferential path, i.e. is isotropic. (3) Albedo radiation, which is the fraction of solar radiation reaching the cover after diffuse reflection on the ground (thus it can be considered isotropic).

Several steps are performed by the thermal model for calculating the cover's heat gain from solar radiation:

1. **Calculation of the global daily solar irradiation at the upper limit of the earth atmosphere**

An astronomical model is used for determining the sun's position in the sky (as seen from Adama) as a function of the day of the year and of the time of the day. This model allows calculating for each day of the year, the day time duration, and, $G_{0,H}$, the global daily solar irradiation (J/m^{2}day) received by a horizontal surface located at the upper limit of the earth atmosphere.

The first step for modeling the incident solar irradiation is to determine the sun's position and path in the sky, as seen from the digester geographic position, as a function of the day of the year and time of the day. Solar time is a time based on the apparent angular motion of the sun across the sky with solar noon the time the sun crosses the meridian of the observer and it is given by:

$$solar\ time = standard\ time + 4(L_{st} - L_{loc}) + E \quad \text{(3.25)}$$

Where, L_{st} is the standard meridian for the local time zone, L_{loc} is the longitude of the location in question, and longitudes are in degrees west, that is, 0^o < L <360^o.The parameter E is the equation of time (in minutes), and is given by (Duffie and Beckman, 2013):

$$E = 229.2(0.000075 + 0.001868\ cosB - 0.032077\ sinB - 0.014615\ cos\ 2B - 0.04089\ sin\ 2B) \quad \text{(3.26)}$$

$$B = (n-1)\frac{360}{365} \quad \text{(3.27)}$$

Where, n is the day of the year, thus $1 \leq n \leq 365$.

The sun declination angle, δ (^{o}), the angular position of the sun at solar noon (i.e., when the sun is on the local meridian) with respect to the plane of the equator, north positive; $-23.45^o \leq \delta \leq 23.45^o$ and is given by (Duffie and Beckman, 2013):

$$\delta = 23.45 \sin(\frac{360}{365}(284 + n)) \ldots\ldots (3.28)$$

The solar hour angle ω (^{o}), the angular displacement of the sun east or west of the local meridian due to rotation of the earth on its axis at 15^o per hour; morning negative, afternoon positive. And it is given by (Duffie and Beckman, 2013):

$$\omega = 15(solar\ time - 12) \ldots\ldots (3.29)$$

The zenith angle θ_z, the angle between the vertical and the line to the sun, that is the angle of incidence of beam radiation on a horizontal surface.

$$cos\theta_z = cos\varphi cos\delta cos\omega + sin\varphi sin\delta \ldots\ldots (3.30)$$

Where: φ refers to the latitude and is equal to 8.54^o.

At sunrise, the hour angle magnitude, ω_{sr}, and the local solar time, ST_{sr}, are calculated as follows:

$$cos(\omega_{sr}) = -tan(\varphi)tan(\delta) \ldots\ldots (3.31)$$

$$ST_{sr} = 12 - \frac{\omega_{sr}}{15} \ldots\ldots (3.32)$$

The local solar time at sunset, ST_{ss}, is given by:

$$ST_{ss} = 12 + \frac{\omega_{sr}}{15} \ldots\ldots (3.33)$$

Thus, the day time duration, N (h), equals:

$$N = \frac{2}{15}\omega_{sr} \ldots\ldots (3.34)$$

$G_{0,H}$, the global daily solar irradiance received by a horizontal surface at the upper limit of earth atmosphere, is calculated as follows (expressed in J/m^{2}day) (Duffie and Beckman, 2013):

$$G_{0,H} = \frac{24*3600}{\pi} Gsc \left[1 + 0.033 \cos\left(\frac{360n}{365}\right)\right] * \left[cos\varphi cos\delta sin\omega_{sr} + \pi\frac{\omega_{sr}}{180} sin\varphi sin\delta\right] \ldots\ldots (3.35)$$

Where Gsc is the solar constant, is 1367 W/m^2.

2. Calculation of the global daily solar irradiation on a surface at ground level

Solar energy reaching the earth surface is attenuated while crossing the atmosphere because of absorption, reflection and scattering by liquid and solid aerosols, etc., especially in the case

where a cloud cover is present. This attenuation factor is estimated based on the daily sunshine duration experimental data, which allows calculating G_H (J/m^{2}day), the global daily solar irradiation received by a horizontal surface at ground level, and is given by (Duffie and Beckman, 2013):

$$\frac{G_H}{G_{0,H}} = a + b(\frac{n_s}{N_s}) \quad \text{(3.36)}$$

Where G_H global daily solar radiation on horizontal surface, $G_{0,H}$ is the global daily solar radiation outside of the atmosphere for the same location, a and b are empirical constants, (values are evaluated by regression), n_s is the daily hours of bright sun shine and N_s is the maximum possible daily hours of bright sunshine.

The regression parameters a and b can be determined from:

$$a = -0.110 + 0.235cos\varphi + 0.323(\frac{n_s}{N_s}) \quad \text{(3.37)}$$

$$b = 1.449 - 0.533cos\varphi - 0.694(\frac{n_s}{N_s}) \quad \text{(3.38)}$$

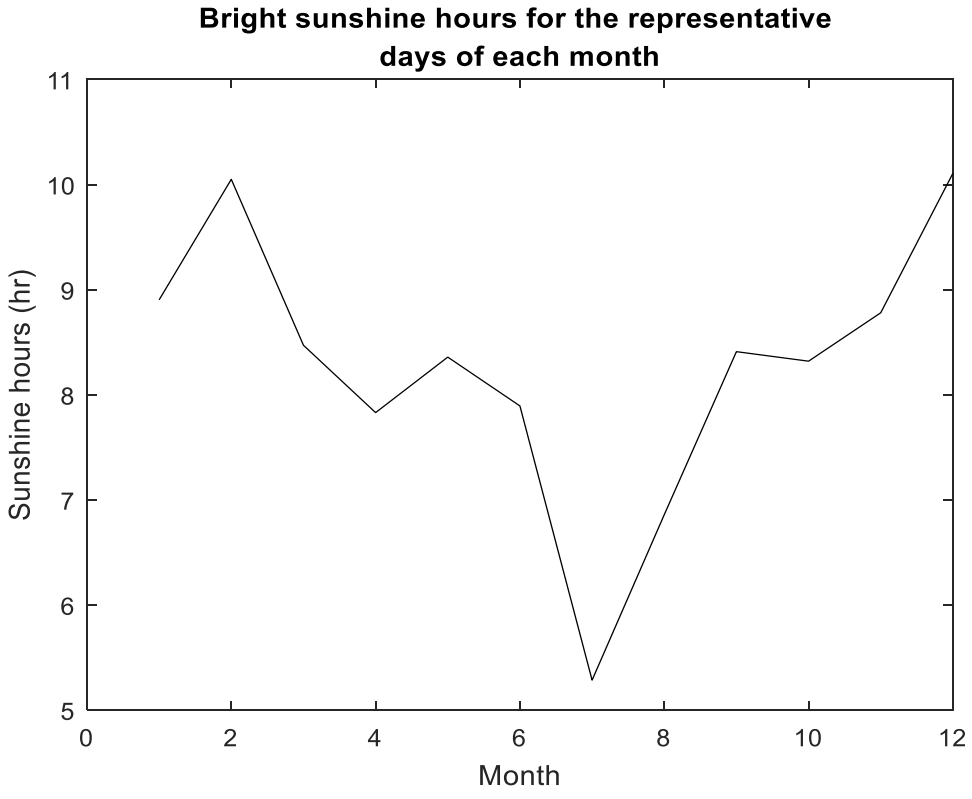

Figure 3. 2: Bright sunshine hours for the representative days of each month

3. Calculation of the beam and diffuse daily solar irradiation on a surface at ground level

B_H and D_H (J/m^2 day), the beam and diffuse components of G_H. The average daily diffuse radiation on a horizontal surface can be determined from the average daily global radiation on a horizontal surface and the number of bright sunshine hours (Duffie and Beckman, 2013):

$$\frac{D_H}{G_H} = 0.931 - 0.814\left(\frac{n_s}{N_s}\right) \quad \text{(3.39)}$$

The daily beam solar radiation hitting a horizontal surface at ground level, B_H (J/m^{2}day), is simple deduced using:

$$B_H = G_H - D_H \quad \text{(3.40)}$$

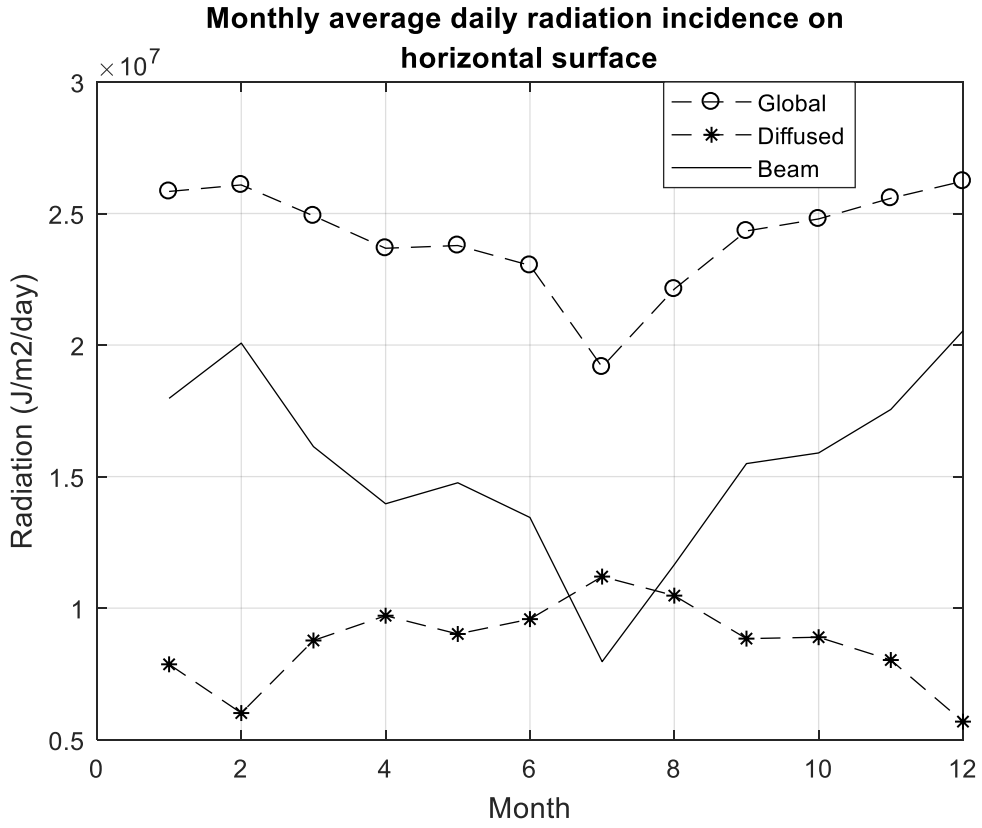

Figure 3.3: Monthly average daily global, beam and diffused radiation on a horizontal surface

4. Calculation of the beam and diffuse solar irradiances on a horizontal surface at ground level

B_H and D_H are daily average quantities. However, the knowledge of the instantaneous solar heat flux is required for the transient thermal model. Therefore, the Collares-Pereira and Rable, (1978) model is used to calculate B_H^* and D_H^*, the beam and diffused solar irradiances (W/m^2) on a horizontal surface at ground level, as a function of the time of the day. During day time (i.e.$ST_{sr} \leq ST \leq ST_{SS}$), B_H^* and D_H^* are given by (they are nil the remainder of the day) (Hriez et al., 2017):

$$D_H^* = \frac{\pi}{24*3600}[a + bcos\omega] * \frac{cos\omega - cos\omega_{sr}}{sin\omega_{sr} - \frac{\pi\omega_{sr}}{180}cos\omega_{sr}} * D_H \quad \text{(3.41)}$$

$$B_H^* = \frac{\pi}{24*3600}[a + bcos\omega] * \frac{cos\omega - cos\omega_{sr}}{sin\omega_{sr} - \frac{\pi\omega_{sr}}{180}cos\omega_{sr}} * B_H \quad \text{(3.42)}$$

Where $a = 0.409 + 0.502\sin(\omega_{sr} - 60)$ (3.43)

$b = 0.661 - 0.477\sin(\omega_{sr} - 60)$ (3.44)

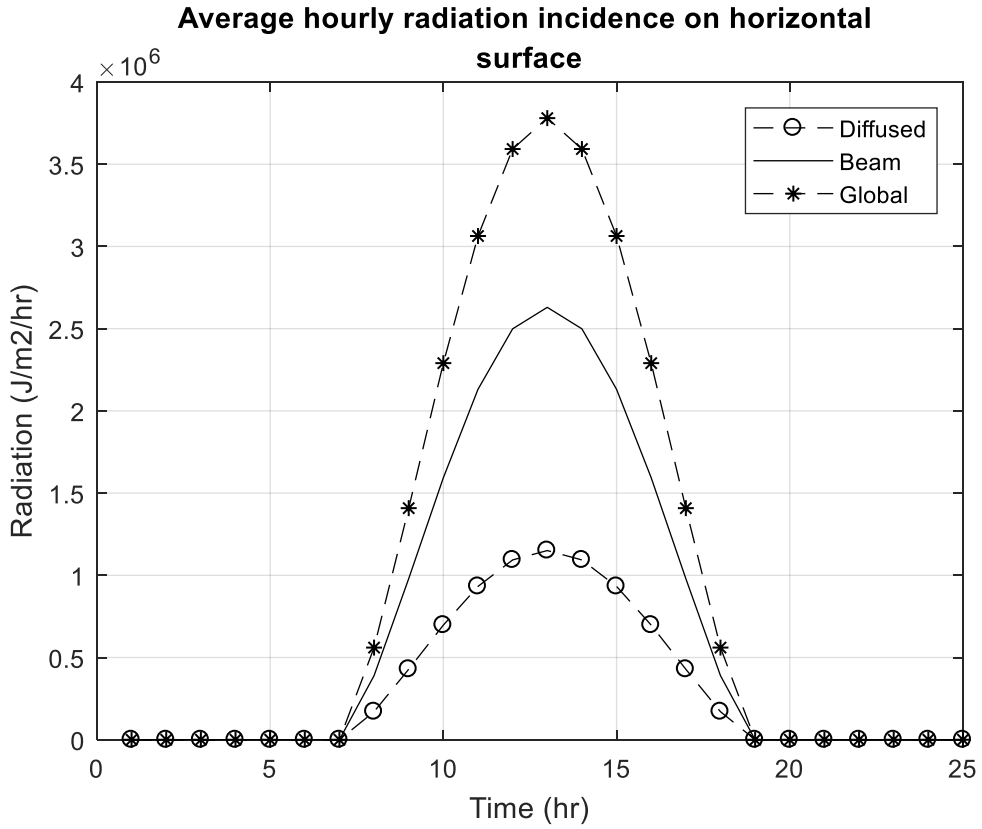

Figure 3. 4: Hourly global, beam and diffused radiation on a horizontal surface in January 17

5. Calculation of the solar heat flux absorbed by the cover

The diffuse solar irradiance on a tilted plan, D_I^* (W / m^2), is given by:

$$D_I^* = \frac{D_H^*}{2}[1 + cos\beta] \quad (3.45)$$

Where, β the inclination angle from the horizontal. Thus, assuming no shading effects since there is no buildings, trees or other obstacles nearby the digester, the diffuse solar heat flux absorbed by the digester cover, D_{Co}^*(W), is calculated as follows (Hriez et al.,2017):

$$D_{Co}^* = \alpha_{co} \frac{D_H^*}{2} \iint [1 + cos\beta] d^2S \quad (3.46)$$

Where, α_{co} is the cover thermal absorptivity taken as 0.9 in the current study (integration is performed on the cover's external surface). Considering that the cover has a spherical cap shape, solving the above equation in spherical coordinates gives (the azimuthal angle γ being equal to the inclination angle (β):

$$D_{Co}^* = 0.626\pi r_{co}^2 \alpha_{co} D_H^* \quad (3.47)$$

Where, r_{co} the cover's radius of curvature equals 1.725m.

The reflected solar irradiance on a tilted plan, R_I^* (W/m^2), is given by:

$$R_I^* = \Psi_{soil} \left(\frac{D_H^* + B_H^*}{2}\right) * [1 - cos\beta] \quad (3.48)$$

Where, Ψ_{soil} is the ground albedo, taken as 0.4 in the current study. Thus, the ground-reflected solar flux that is absorbed by the cover, R_{Co}^* (W), equals:

$$R_{Co}^* = \Psi_{soil}\alpha_{co} \left(\frac{D_H^* + B_H^*}{2}\right) \iint [1 - cos\beta] d^2 = 0.0586\, \Psi_{soil}\pi r_{co}^2 \alpha_{co}(D_H^* + B_H^*) \quad (3.49)$$

Contrary to diffuse and albedo solar radiations, beam radiation is anisotropic: the part of the cover surface that is exposed to beam radiation depends on the solar elevation angle. Thus, it is difficult to derive an analytical relationship between the beam solar heat flux absorbed by the digester cover, B_{Co}^* (W), and B_H^* (W). Instead, a simpler approach has been adopted for estimating B_{Co}^* (W).

Considering that the cover has a spherical cap shape, when θ_z equals 0^o, the projection of the cover surface on a plane perpendicular to the direct rays (i.e. a vertical plane) is a circular

segment which area is 4.67 m^2. For θ_z equal to 90°, the projection of the cover surface on a plane perpendicular to the direct rays (i.e. on a horizontal plane) is a disk which surface is 9.35 m^2 (equal to the digester cross-section). For simplicity, assuming a linear relationship between θ_z and B^*_{Co} gives (Hriez et al., 2017):

$$B^*_{Co} = \alpha_{co} B^*_H (4.67 + \frac{\theta_z}{1.185}) \quad \text{(3.50)}$$

Finally, $Q_{r(co\_So)}$ (W), the cover total heat flux gain from solar irradiation is given by:

$$Q_{r(co\_So)} = B^*_{Co} + D^*_{Co} + R^*_{Co} \quad \text{(3.51)}$$

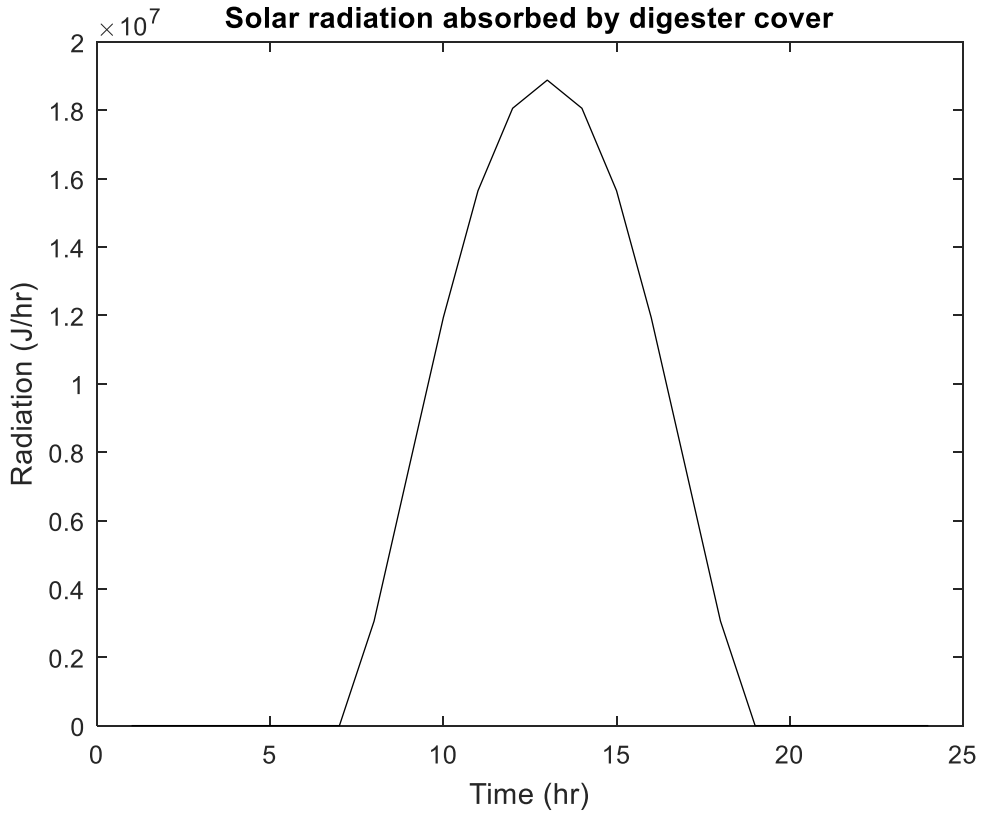

Figure 3.5: Solar heat flux absorbed by the cover in January 17

3.4.9. Modeling of the Heat Transfer from the Digestate to the Soil across the Walls

The heat transfer from the digestate to the soil across the walls can be expressed as (Hreiz et al., 2017):

$$Q_{Dg\_soil} = U_{Dg\_soil} A_{Dg} (T_{Dg} - T_{soil}) \quad \text{(3.52)}$$

Where, $\boldsymbol{U_{Dg\_soil}}$ is the overall heat transfer coefficient for each walls and can be calculated as:

$$\frac{1}{\boldsymbol{U_{Dg\_soil}}} = \frac{1}{h_{Dg}} + \frac{L_{wall}}{k_{wall}} \quad \text{(3.53)}$$

Where, h_{Dg} is the interior surface heat transfer coefficient (i.e. the convective heat transfer coefficient of the digestate), L_{wall} is the thickness of the concrete wall, A_{Dg} is the surface area of digester and k_{wall} is the thermal conductivity of the soil.

The soil temperature is affected by the long term operation of the digester: it increases with time due to heat transfer from the digester (and thus Q_{Dg_soil} decreases), until equilibrium state is reached. So it becomes more complicated to analyze. A pseudo-steady state analysis is used, using annual monthly average weather conditions. Based on this assumption the undisturbed soil temperature can be calculated as follows (Ouzzan et al., (2015), as reported by Hreiz et al., 2017):

$$T_{soil} = 17.898 + 0.951 T_{At} \quad \text{(3.54)}$$

Where, T_{At} [K] is atmospheric temperature in Adama.

3.5. Estimation of Hourly Variation of Atmospheric Temperature

The hourly temperature variation is described by a cosine wave model. It was initially presented by De Wit et al., (1978) and was obtained from the subroutine WAVE in ROOTSIMU V4.0 by Hoogenboom and Huck, (1986). This method requires T_{min} of the next day and divides the day in to two segments, from sunrise to 14:00 h and from 14:00 to sunrise of the next day. The method assumes T_{max} at 14:00 h and T_{min} at sunrise, and the intervening temperatures are calculated from the following equations.

From 0 ≤ H ≤ sunrise hour or 14:00 h ≤ H ≤ 24:00 h

$$T(H) = T_{ave} + AMP\left(\cos\left(\frac{\pi H'}{(10+rise)}\right)\right) \quad \text{(3.55)}$$

For rise ≤ H ≤ 14:00 h

$$T(H) = T_{ave} - AMP\left(\cos\left(\frac{\pi(H-rise)}{(14-rise)}\right)\right) \quad \text{(3.56)}$$

Where rise is the time of sunrise in hours and T (H) is the temperature at any hour, H is time in hours, H' = H + 10 if H ≤ rise, H' = 14 if H > 14:00 h and Tave and AMP are defined as T_{ave} = (T_{min} + T_{max})/2 and AMP = (T_{max} - T_{min})/2, respectively (Baker et al., 1989).

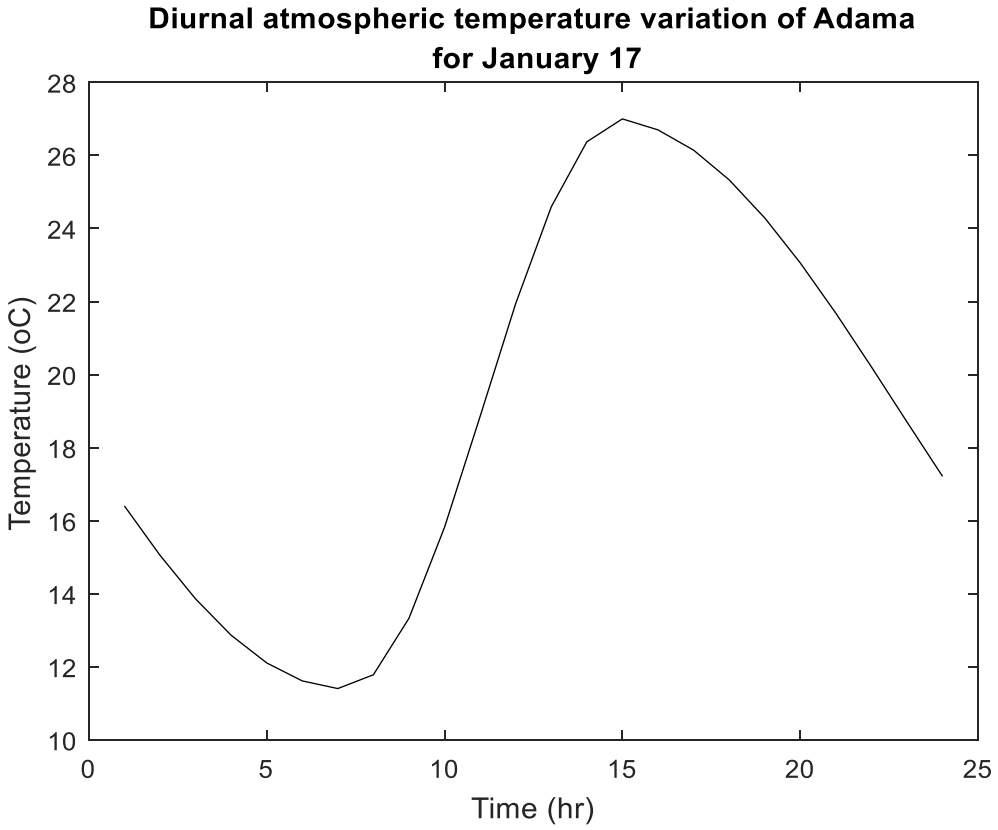

Figure 3.6: Diurnal temperature variation of Adama in January 17

3.6. Transient Thermal Analysis of a Digester Using Finite Difference Method

The derived differential equations, those represents the energy balance for the digestate phase, biogas phase and cover phase are solved using the explicit finite difference method. The time derivative is replaced by the forward difference scheme. The transient temperatures are evaluated iteratively, using relations derived for the equation of energy balance.

$$\frac{dT_{Dg}}{dt} = \frac{{T_{Dg}}^{t+\Delta t} - {T_{Dg}}^{t}}{\Delta t} \quad \text{(3.57)}$$

$$\frac{dT_{Bg}}{dt} = \frac{{T_{Bg}}^{t+\Delta t} - {T_{Bg}}^{t}}{\Delta t} \quad \text{(3.58)}$$

$$\frac{dT_{co}}{dt} = \frac{{T_{co}}^{t+\Delta t} - {T_{co}}^{t}}{\Delta t} \quad \text{(3.59)}$$

For the digestate phase:

$${T_{Dg}}^{t+\Delta t} = {T_{Dg}}^{t} * (1 - A * B - A * C - D * A - E * A) - A * F * ({T_{Dg}}^{t})^{4} + A * B * {T_{a}}^{t} + A * C * {T_{Bg}}^{t} + A * F * \left({T_{co}}^{t}\right)^{4} + A * D * {T_{soil}}^{t} \quad \text{(3.60)}$$

For the biogas phase:

$${T_{Bg}}^{t+\Delta t} = {T_{Bg}}^{t} * (1 - H * E - H * C - H * G) + {T_{Dg}}^{t} * (H * E + H * C) + {T_{co}}^{t} * H * G \quad \text{(3.61)}$$

For the cover phase:

$${T_{co}}^{t+\Delta t} = {T_{co}}^{t} * (1 - I * G - I * J) - (F * I + K * I) * \left({T_{co}}^{t}\right)^{4} + I * J * {T_{a}}^{t} + I * F * \left({T_{Dg}}^{t}\right)^{4} + I * K * \left({T_{sky}}^{t}\right)^{4} + Q_{r(so\_co)} * I \quad \text{(3.62)}$$

Only considering the heat loss, that required for raising the temperature of incoming sludge for digestion. Applying the energy conservation principle to the digestate gives:

$$\rho_{Dg} V_{Dg} C_{Dg} \frac{dT_{Dg}}{dt} = Q_{fd} - Q_{ld} \quad \text{(3.63)}$$

$$\rho_{Dg} V_{Dg} C_{Dg} \frac{dT_{Dg}}{dt} = \dot{m}_{fd} C_{w} (T_{a} - T_{Dg}) \quad \text{(3.64)}$$

$${T_{Dg}}^{t+\Delta t} = A * B * T_{a} + {T_{Dg}}^{t} * (1 - A * B) \quad \text{(3.65)}$$

Where, T is for temperature, the abbreviations Dg, Bg and co are for the digestate, biogas and the cover respectively. In the above equations:

$$A = \frac{\Delta t}{\rho_{Dg} V_{Dg} C_{Dg}} \quad \text{(3.66)}$$

$$B = \dot{m}_{fd} C_{w} \quad \text{(3.67)}$$

$$C = h_{Dg\_Bg} S_{Dg\_Bg} \quad \text{(3.68)}$$

$$D = U_{Dg\_soil} A_{Dg} \quad \text{(3.69)}$$

$$E = \dot{m}_{Bg} C_{Bg} \quad \text{(3.70)}$$

$$F = \frac{\sigma}{\frac{1-\varepsilon_{Dg}}{\varepsilon_{Dg}S_{Dg\_Bg}} + \frac{1}{S_{Dg\_Bg}} + \frac{1-\varepsilon_{co}}{\varepsilon_{co}S_{co}}} \quad \text{(3.71)}$$

$$G = h_{Bg\_co}S_{co} \quad \text{(3.72)}$$

$$H = \frac{\Delta t}{\rho_{Bg}V_{Bg}C_{Bg}} \quad \text{(3.73)}$$

$$I = \frac{\Delta t}{\rho_{co}V_{co}C_{co}} \quad \text{(3.74)}$$

$$J = h_{co\_At}S_{co} \quad \text{(3.75)}$$

$$K = \varepsilon_{co}\sigma S_{co} \quad \text{(3.76)}$$

3.7. Thermal Performance of a Solar Assisted Anaerobic Digestion System

The thermal performance of a solar assisted anaerobic digestion system can be expressed in terms of the specific net thermal energy production of digestion system. Specific net thermal energy production is defined as the net daily energy production per unit volume of anaerobic digester; it is the caloric value of the produced biogas minus the total energy required for heating the anaerobic digestion system. The daily net thermal energy production can be calculated using a biogas calorific value. To calculate specific net thermal energy production after applying the solar energy (E_T), the following equation can be used (El-Mashad et al., 2003).

$$E_T = \frac{E-(1-P)Q_{req}}{E} \quad \text{(3.77)}$$

Where: P is the percentage of daily heat requirements which can be covered by solar energy; Q_{req} is the daily heat requirements to heat the digester at the desired digester temperature level; and E is the potential energy production based on daily biogas production in the anaerobic digestion system.

CHAPTER 4: Thermal Performance Analysis of Flat Plate Solar Collector for the Digestion System

4.1. Introduction

Solar water heating devices are very common systems that are used in many countries which have higher solar radiation. Exploiting solar energy for heating requires the use of flat-plate collector systems which receive the incoming solar radiation and then delivers a large fraction of the thermal energy to the working fluids. Solar flat plate collector with metal absorber plate and covers are the most successful devices that convert solar energy in to heat at reasonable price without affecting environment (Robi et al., 2017).

Flat Plate Collector

The designed flat plate collector used for the present study consists of brazed riser and header pipes, plate material, a single glass cover, and insulated casing. The brazed riser and header pipe assembly is illustrated in Figure 4.1.

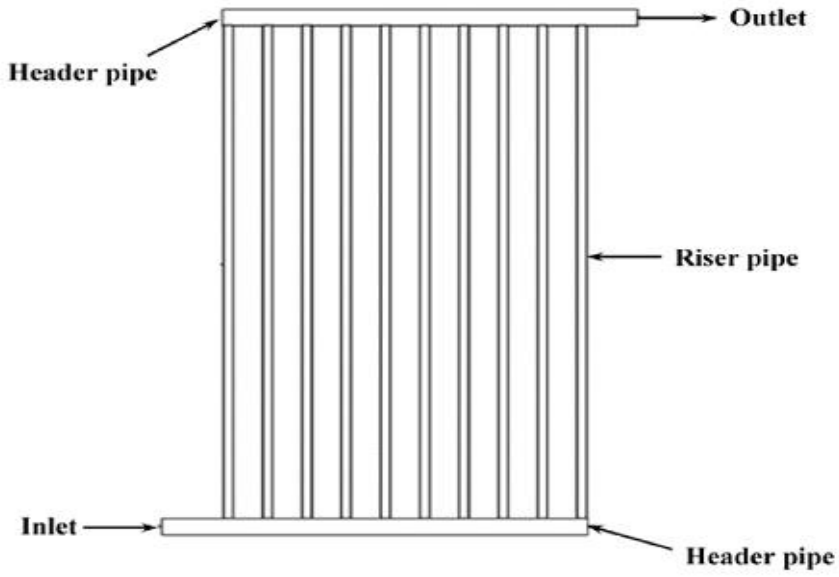

Figure 4.1: Schematic diagram of riser and header pipe (Robi et al., 2017)

The manufacturing specification of flat plate collector of SUNRAIN Company product for a model of FPC1200A is labeled on Table 4.1:

Table 4.1: Specification of solar collector

Description	Specification
Collector type	Sheet-and-tube solar collector
Length of collector (m)	2.005
Width of collector (m)	1.005
Length of the absorber plate (m)	1.9
Width of the absorber plate (m)	0.92
Overall area (m^2)	2.02
Absorber area (m^2)	1.745
Aperture area (m^2)	1.96
Housing	Aluminum-alloy
Surface	Aluminum-alloy
Back plate	Steel plate
Absorber plate	Cu/Al, oxide film
Thermal conductivity of absorber plate (W/mK)	386
Density of absorber plate (kg/m^3)	8954
Plate thickness (m)	0.001
Absorption (%)	94
Emittance of absorber plate	0.95
Ø manifold (mm)	Ø 22 x 0.75
Ø risers (mm)	Ø 10 x 0.5
Tube center to center distance (m)	0.092
Glass	Woven ultra-white toughened solar safety glass
Number of glass	1
Transmittance of glass (%)	≥91
Emittance of glass	0.86
Glass thickness (m)	0.003
Spacing between glass and absorber plat (m)	0.025
Insulation	Glass wool
Thermal conductivity of insulation material (W/mK)	0.044
Thickness of the insulation material (m)	0.05
Density of the insulation material (kg/m^3)	200
Max. stagnation temperature	250 °C under test conditions
Max. operating pressure	1.2 Mpa
Rated operating pressure	0.8 Mpa
Heat transfer medium	Water

4.2. Assumptions for Design

Different simplifying assumptions can be made to investigate a flat plate collector without obscuring the basic physical situation. These assumptions are as follows (Duffie and Beckman, 2013):

- Performance is steady state.
- Construction is of sheet and parallel tube type.
- The headers cover a small area of collector and can be neglected.
- The headers provide uniform flow to tubes.
- There is no absorption of solar energy by a cover insofar as it affects losses from the collector.
- Heat flow through a cover is one dimensional.
- There is a negligible temperature drop through a cover.
- The cover is opaque to infrared radiation.
- There is one-dimensional heat flow through back insulation.
- The sky can be considered as a blackbody for long-wavelength radiation at an equivalent sky temperature.
- Temperature gradients around tubes can be neglected.
- The temperature gradients in the direction of flow and between the tubes can be treated independently.
- Properties are independent of temperature.
- Loss through front and back are to the same ambient temperature.
- Dust and dirt on the collector are negligible.
- Shading of the collector absorber plate is negligible.

4.3. Governing Flat-Plate Collector Energy Balance Equation

The solar radiation absorbed by a collector per unit area of absorber (S) is equal to the difference between the incident solar radiation and the optical losses. The thermal energy lost from the collector to the surroundings by conduction, convection, and infrared radiation can be represented as the product of a heat transfer coefficient (U_L) times the difference between the mean absorber plate temperature T_{pm} and the ambient temperature T_a. In steady state the useful energy output of a collector of area A_c is the difference between the absorbed solar radiation and the thermal loss:

$$\dot{Q}_u = A_c[S - U_L(T_{pm} - T_a)] \quad \text{..... (4.1)}$$

Where, $S = \tau\alpha I_T$

τ, α, and I_T are the transmissivity of the glass cover, the absorptivity of the absorber and the incidence solar radiation on the collector respectively.

4.3.1. Incident Solar Radiation

Investigation of solar water heating system requires precise knowledge regarding the availability of global solar radiation and its components at the location of interests. Since the solar radiation reaching the earth's surface depends upon climatic conditions of the place, a study of solar radiation under local climatic conditions is essential. In previous section a model that represents a solar radiation incidence on a horizontal surface is developed. The solar radiation energy incident on the collector surface which is inclined at an angle of ($\beta = \varphi + 15^o$) to the horizontal surface is defined in terms of global, diffuse, beam and reflected radiation. Total solar radiation incident on a surface consists of beam, diffuse and reflected solar radiation from the ground and surrounding. Total radiation on a surface can be evaluated by arbitrary orientation from knowledge of beam, diffuse and global radiation on horizontal surface (Duffie and Beckman, 2013). The total incident radiation on the surface can be written as:

$$I_T = B_H R_b + D_H\left(\frac{1+cos\beta}{2}\right) + G_H\rho_g\left(\frac{1-cos\beta}{2}\right) \quad \text{..... (4.2)}$$

Where B_H, D_H, and G_H are the beam, diffused and global solar radiation incident on the horizontal surface and can be calculated from equation (3.40), (3.39), and (3.36) respectively, ρ_g is the ground reflectivity and R_b is beam radiation factor.

Beam radiation factor (R_b) is defined as the ratio of beam radiation incident on an inclined surface to that on a horizontal surface. Beam radiation factor (R_b) can be determined as:

$$R_b = \frac{\cos\theta_i}{\cos\theta_z} \quad \text{..... (4.3)}$$

Where, θ_i is angle of incidence

Angle of incidence is the angle between the beam radiation on a surface and the line normal to surface, and can be calculated as follows (Duffie and Beckman, 2013):

$$\cos\theta_i = (cos\varphi cos\beta + sin\varphi sin\beta)\, cos\delta cos\omega + sin\delta(sin\varphi cos\beta - sin\beta cos\varphi) \quad \text{..... (4.4)}$$

The latitude (φ) of a location is the angle made by the radial line joining the given location to the center of the earth with its projection on the equatorial plane. Adama is located on:

Latitude (φ) = 8.54^o due north.

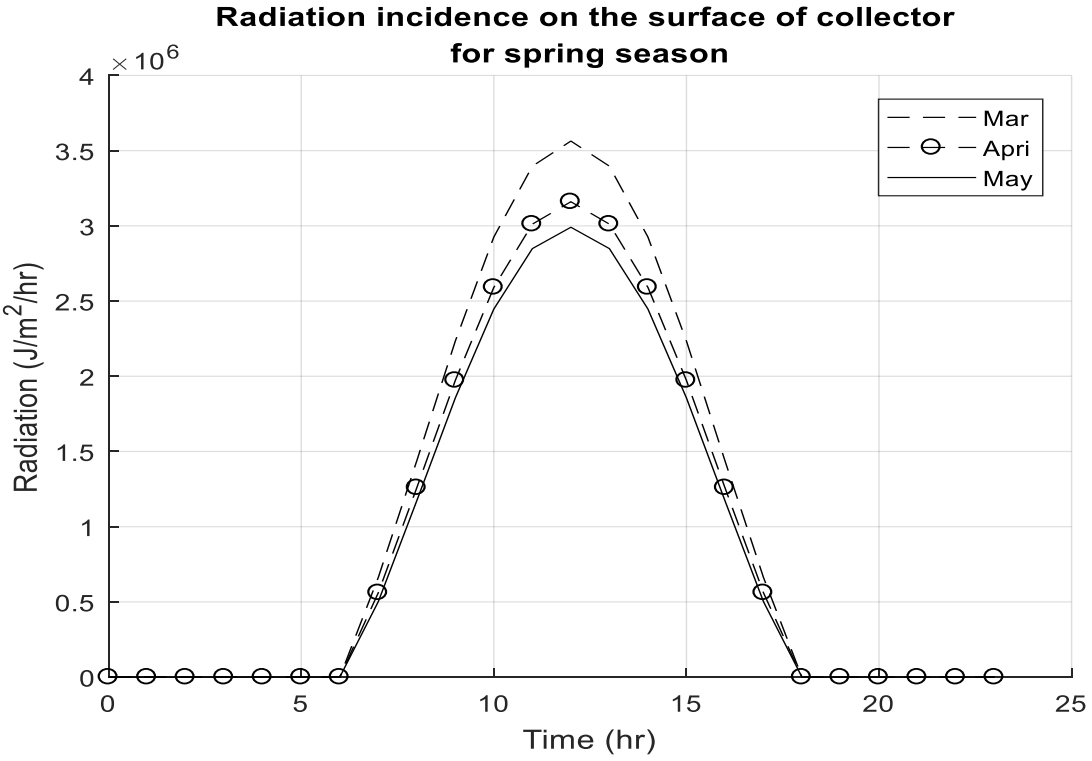

(a)

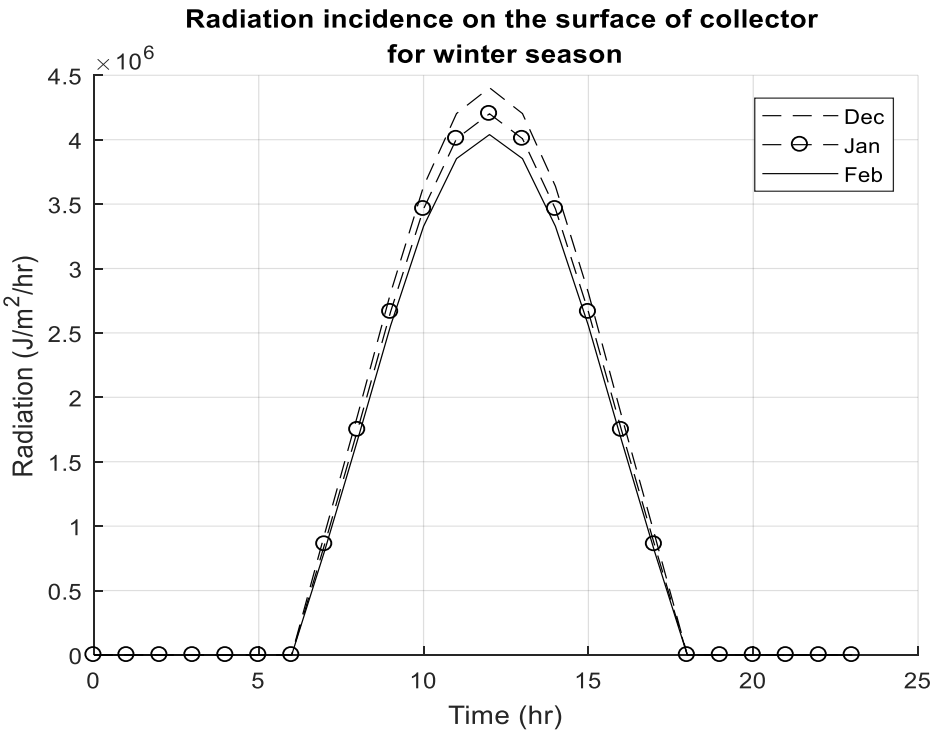
Radiation incidence on the surface of collector
for winter season
×10^6
4.5
4
3.5
3
2.5
2
1.5
1
0.5
0
Radiation (J/m^2/hr)
0
5
10
15
20
25
Time (hr)
Dec
Jan
Feb

(b)

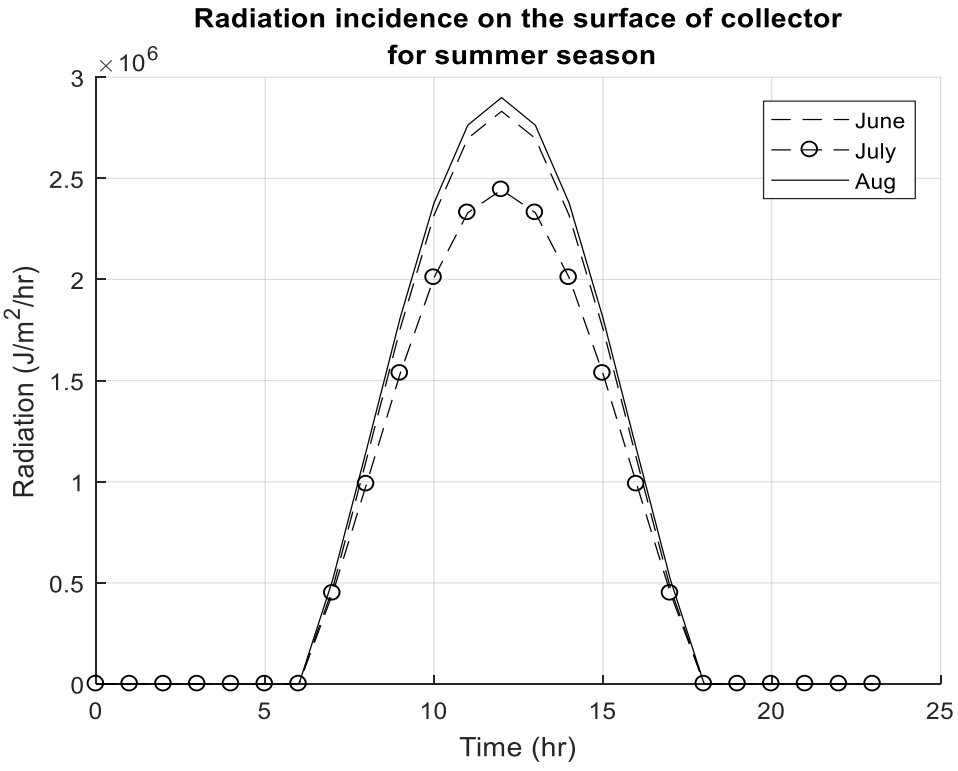
Radiation incidence on the surface of collector
for summer season
×10^6
3
2.5
2
1.5
1
0.5
0
Radiation (J/m^2/hr)
0
5
10
15
20
25
Time (hr)
June
July
Aug

(c)

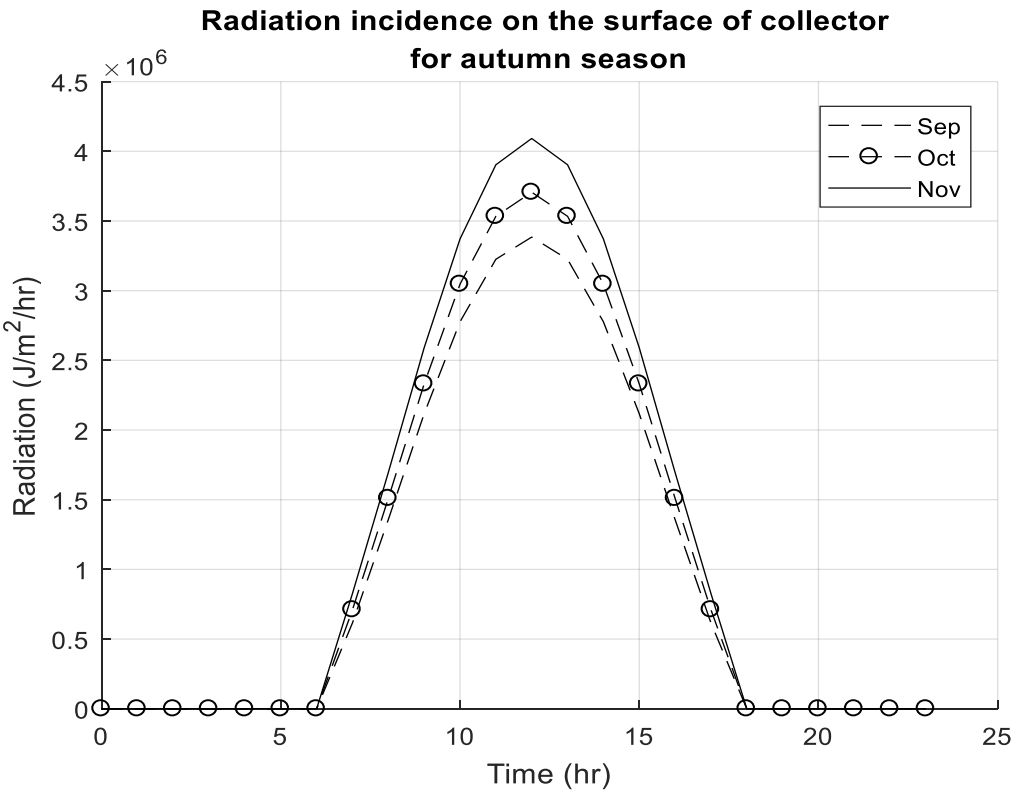

(d)

Figure 4.2: Monthly average hourly incidence solar radiation on a tilted surface for, (a) spring, (b) winter, (c) summer, and (d) autumn seasons

4.3.2. Collector Overall Heat Loss Coefficient

As the collector absorbs heat its temperature is getting higher than that of the surrounding and heat is lost to the atmosphere by convection and radiation. The rate of heat loss depends on the collector overall heat loss coefficient (U_L). The heat lost from the collector is the sum of the heat lost from the top, the bottom and the sides. Each of these loses is also expressed in terms of coefficients called the top loss coefficient, the bottom loss coefficient and the side loss coefficient and defined by the equations (Duffie and Beckman, 2013):

$$\dot{Q}_t = U_t A_c (T_{pm} - T_a) \quad \text{(4.5)}$$

$$\dot{Q}_b = U_b A_c (T_{pm} - T_a) \quad \text{(4.6)}$$

$$\dot{Q}_s = U_s A_c (T_{pm} - T_a) \quad \text{(4.7)}$$

Where, $\dot{Q}_t$, $\dot{Q}_b$ and $\dot{Q}_s$ are the top, bottom and side heat loss of the collector respectively, and U_t, U_b, and U_s are the top, bottom and top heat loss coefficient of the collector respectively.

The losses can also be pictured in terms of thermal resistance as shown below:

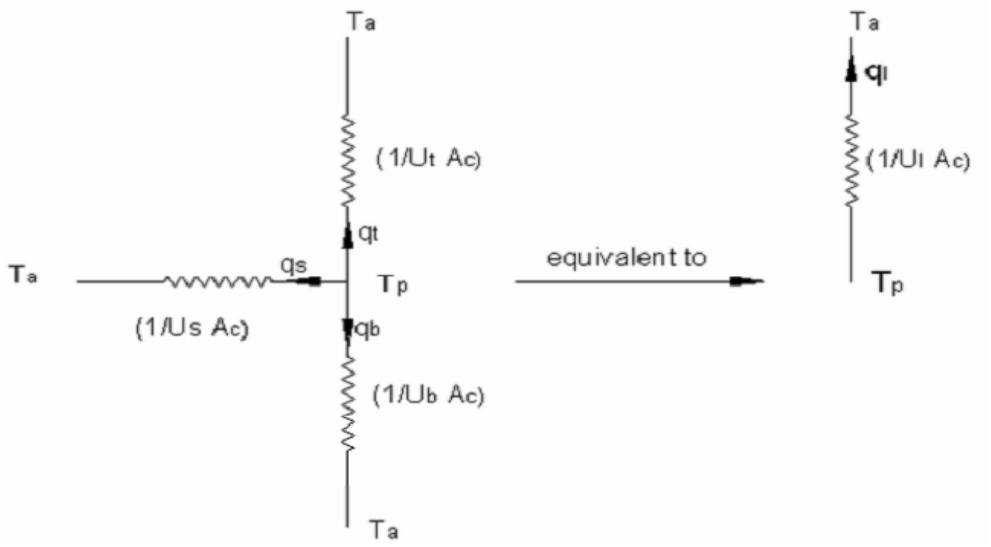

Figure 4.3: Thermal resistance network showing collector losses

4.3.2.1. Top Loss Coefficient

The top loss coefficient U_t is evaluated by considering convection and re-radiation losses from the absorber plate in the upward direction.

4.3.2.1.1. Convective Heat Transfer Coefficient

1) From the Plate to the Cover (h_{c1})

A heat transfer phenomenon from the plate to the cover is only due to free-convection (natural convection). Free-convection heat transfer data are usually correlated in terms of two or three dimensionless parameters: the Nusselt number Nu, the Rayleigh number Ra, and the Prandtl number Pr.

The Nusselt, Rayleigh, and Prandtl numbers are given by (Duffie and Beckman, 2013):

$$N_u = \frac{h_{c1}L}{k} \quad \text{(4.8)}$$

$$R_a = \frac{g\beta'\Delta T L^3}{\nu\alpha} \quad \text{(4.9)}$$

$$P_r = \frac{v}{\alpha} \quad \text{(4.10)}$$

Where: h_{c1} is the heat transfer coefficient of from the plate to the cover [W/m^{2}K], L is the plate spacing [m], k=thermal conductivity [W/m K]], g is the gravitational constant [m/s^2], β' is the volumetric coefficient of expansion (for an ideal gas, β' = 1/T)[1/K], ΔT is the temperature difference between plate and cover [K], v is the kinematic viscosity [m^2/s], and α is the thermal diffusivity [m^2/s].

Hollands et al., (1976) give the relationship between the Nusselt number and Rayleigh number for tilt angles from 0 to 75^o as (cited by, Duffie and Beckman, 2013):

$$N_u = 1 + 1.44\left[1 - \frac{1708(sin1.8\beta)^{1.6}}{R_a cos\beta}\right]\left[1 - \frac{1708}{R_a cos\beta}\right]^{+} + \left[\left(\frac{R_a cos\beta}{5830}\right)^{\frac{1}{3}} - 1\right]^{+} \quad \text{(4.11)}$$

Where, the meaning of the + exponent is that only positive values of the terms in the square brackets are to be used (i.e. use zero if the term is negative).

2) From the Glazing Cover to the Ambient Temperature (h_{c2})

The convective heat transfer coefficient (h_{c2}) at the glass cover is calculated from the following empirical correlation.

$$h_{c2} = 5.7 + 3.8u_{wind} \quad \text{(4.12)}$$

Where, h_{c2} is in W/m^{2}K, and u_{wind} is the wind speed in m/s.

4.3.2.1.2. Radiative Heat Transfer Coefficient

1) From the Plate to the Cover (h_{r1})

The radiative heat transfer coefficient from the plate to the glass cover is expressed as (Duffie and Beckman, 2013):

$$h_{r1} = \frac{\sigma(T_p^2 + T_g^2)(T_p + T_g)}{\frac{1}{\varepsilon_p} + \frac{1}{\varepsilon_g} - 1} \quad \text{(4.13)}$$

Where: T_p is the plate temperature [K], T_g is the glass temperature [K], σ is a Boltzman constant, ε_p and ε_g are the emissivity of plate and glass cover respectively.

2) From the Glazing Cover to the Ambient (h_{r2})

The radiative heat transfer coefficient from the glass cover to the ambient is expressed as (Duffie and Beckman, 2013):

$$h_{r2} = \varepsilon_g \sigma \left\{ \frac{T_g^4 - T_{sky}^4}{T_g - T_a} \right\} \quad \text{(4.14)}$$

Where, T_{sky} the equivalent sky temperature is evaluated according to Swinbank, (1963) correlation (cited by Hreiz et al., 2017):

$$T_{sky} = 0.0552 T_a^{1.5} \quad \text{(4.15)}$$

Note that temperatures values should be expressed in K.

The total heat transfer coefficient from collector plate to cover h_1 is expressed as (Duffie and Beckman, 2013):

$$h_1 = h_{r1} + h_{c1} \quad \text{(4.16)}$$

The total heat transfer coefficient from the cover to ambient h_2 is expressed as (Duffie and Beckman, 2013):

$$h_2 = h_{r2} + h_{c2} \quad \text{(4.17)}$$

The effective heat transfer coefficient from plate to ambient (i.e. the top loss coefficient) is given by (Duffie and Beckman, 2013):

$$U_t = \left[\frac{1}{h_1} + \frac{1}{h_2} \right]^{-1} \quad \text{(4.18)}$$

4.3.2.2. Bottom Loss Coefficient

The bottom loss coefficient (U_b) is evaluated by considering conduction and convection losses from the absorber plate in the downward direction through the bottom of the collector.

It will be assumed that the flow of heat is one dimensional and steady. In most cases, the thickness of insulation provided is such that the thermal resistance associated with conduction dominates. Thus, neglecting the convective resistance at the bottom surface of the collector casing, we have (Duffie and Beckman, 2013):

$$U_b = \frac{k_{ins}}{\delta_b} = \frac{0.044}{0.05} = 0.88 \ W/m^2K \quad \text{(4.19)}$$

Where: k_{ins} is the thermal conductivity of the insulation, and δ_b is the back insulation thickness.

4.3.2.3. Side Loss Coefficient

As in the case of the bottom loss coefficient, it will be assumed that the conduction resistance dominates and that the flow of heat is one-dimensional and steady. The one dimensional approximation can be justified on the grounds that the side loss coefficient is always much smaller than the top loss coefficient.

$$U_s = \frac{A_e}{A_c}\frac{k_{ins}}{\delta_e} = 0.1137\ W/m^2K \quad \text{(4.20)}$$

Where: $A_e = P * d_e$, P is the perimeter of the absorber plate, d_e is the height of the edge, and δ_e is the edge insulation thickness.

4.3.2.4. Overall Heat Loss Coefficient

The overall heat loss coefficient U_L is the sum of the top, bottom and edge loss coefficient. That is (Duffie and Beckman, 2013):

$$U_L = U_t + U_b + U_s \quad \text{(4.21)}$$

$$U_t = U_L - (U_b + U_s) = U_L - 0.9937\ W/m^2K \quad \text{(4.22)}$$

Apply energy balance between heat transfer from plate to cover and cover to ambient air and using the basic equation of top loss coefficient to find the heat transfer coefficient terms.

$$Q = A_c h_1 (T_P - T_g) = A_c h_2 (T_g - T_a) \quad \text{(4.23)}$$

$$h_1 (T_P - T_g) = h_2 (T_g - T_a) \quad \text{(4.24)}$$

And

$$U_t = [\frac{1}{h_1} + \frac{1}{h_2}]^{-1} = U_L - 0.9937 \quad \text{(4.25)}$$

Solve equation (4.24) and equation (4.25) simultaneously by try and error and came up with:

$$U_L = 8.38\ W/m^2K,\ U_t = 7.3863\ W/m^2K\ T_P = 367.15\ K,\quad T_g = 316.15\ K,$$

$$h_{1c} = 3.304\ W/m^2K,\quad h_{2c} = 16.72\ W/m^2K,\quad h_{1r} = 7.47\ W/m^2K,\quad h_{2r} = 6.75\ W/m^2K$$

Already, it is described in the above, in steady state the useful energy output of a collector of area Ac is the difference between the absorbed solar radiation and the thermal loss. The thermal

energy lost from the collector to the surroundings is a function of the mean absorber plate temperature T_{pm}. The problem with this expression is that the mean absorber plate temperature is difficult to calculate or measure since it is a function of the collector design, the incident solar radiation, and the entering fluid conditions. So that it is convenient to express the useful energy gain in terms of the inlet fluid temperature and a parameter called the collector heat removal factor.

4.3.3. Collector Heat Removal Factor (F_R)

It is convenient to define a quantity that relates the actual useful energy gain of a collector to the useful gain if the whole collector surface were at the fluid inlet temperature. This quantity is known as "the collector heat removal factor (F_R)"and is expressed as (Duffie and Beckman, 2013):

$$F_R = \frac{\dot{m}C_p(T_{fo}-T_{fi})}{A_c[S-U_L(T_{fi}-T_a)]} \quad \text{..... (4.26)}$$

Or

$$F_R = \frac{\dot{m}C_p}{A_cU_L}[1-\exp(-\frac{A_cU_LF'}{\dot{m}C_p})] \quad \text{..... (4.27)}$$

Where, F' is the collector efficiency factor.

4.3.4. Collector Efficiency Factor (F')

It is the ratio of the real energy output of the collector to the energy output in the case when the total absorber area was at the average fluid temperature with the same fluid quantity of flowing through the tube.

Consider the sheet-tube configuration shown below. The distance between the tubes is W, the tube diameter is D, and the sheet is thin with a thickness δ. Because the sheet material is a good conductor, the temperature gradient through the sheet is negligible.

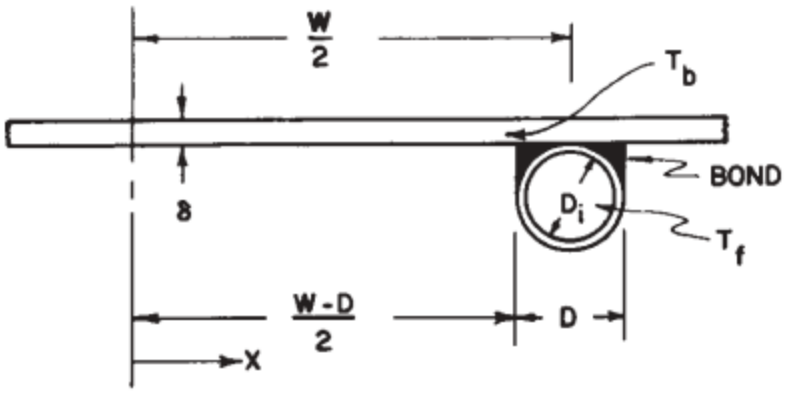

Figure 4.4: Sheet-tube configuration (Duffie and Beckman, 2013)

For a sheet-tube configuration, the collector efficiency factor can be expressed in equation form as (Duffie and Beckman, 2013):

$$F' = \frac{1/U_L}{\frac{1}{U_L[D+(W-D)]F}+\frac{1}{C_b}+\frac{1}{\pi D_i h_{fi}}} \quad \text{..... (4.28)}$$

The collector efficiency factor is essentially a constant for any collector design and fluid flow rate. The ratio of U_L to C_b, the ratio of U_L to h_{fi}, and the fin efficiency parameter F are the only variables appearing to formulate F', those may be functions of temperature. For most collector designs F is the most important of these variables in determining F'. The factor F is a function of U_L and h_{fi}, each of which has some temperature dependence, but it is not a strong function of temperature (Duffie and Beckman, 2013).

Where F is the fin efficiency, D_i is the inside tube diameter and h_{fi} is the heat transfer coefficient between the fluid and the tube wall. The bond conductance C_b can be estimated from knowledge of the bond thermal conductivity k_b, the average bond thickness γ, and the bond width b. On a per-unit-length basis:

$$C_b = \frac{k_b b}{\gamma} \quad \text{..... (4.29)}$$

The bond conductance can be very important in accurately describing collector performance. Simple wiring or clamping of the tubes to the sheet results in low bond conductance and significant loss of performance. It is necessary to have good metal-to-metal contact so that the bond conductance is greater than 30 W/m^{o}C (Duffie and Beckman, 2013). The value of internal heat transfer coefficient of a fluid is depending on the type of heat flow condition, either natural

convection or forced convection. The heat transfer coefficient inside the tube (h_{fi}) may be assumed:

- 300 W/m^2 ºC for natural convection (Thermosiphon heaters), and
- 1500 W/m^2 ºC for forced circulation.

In this study the working fluid circulates through the system, pressurized by external energy source, this lead to forced convection.

For a sheet-tube configuration the fin efficiency can be determined as:

$$F = \frac{\tanh[m(W-D)/2]}{m(W-D)/2} \quad \text{..... (4.30)}$$

Where $m = \sqrt{\frac{U_L}{k\delta}}$ ..... (4.31)

Where, δ is the sheet thickness and k is the thermal conductivity of absorber plate.

The outlet fluid temperature can be calculated by equation … and equation ….and can be expressed as:

$$T_{fo} = \frac{A_C F_R}{(\dot{m}C_P)}\left[S - U_L\left(T_{fi} - T_a\right)\right] + T_{fi} \quad \text{..... (4.32)}$$

The actual useful energy gain of a flat plate collector can be calculated as:

$$Q_u = A_c F_R[S - U_L(T_{fi} - T_a)] \quad \text{..... (4.33)}$$

The instantaneous thermal efficiency of flat plate collector is given by:

$$\eta_i = \frac{\dot{Q}_u}{A_c I_T(t)} = F_R\left[(\alpha\tau) - \frac{U_L(T_{fi}-T_a)}{I_T(t)}\right] \quad \text{..... (4.34)}$$

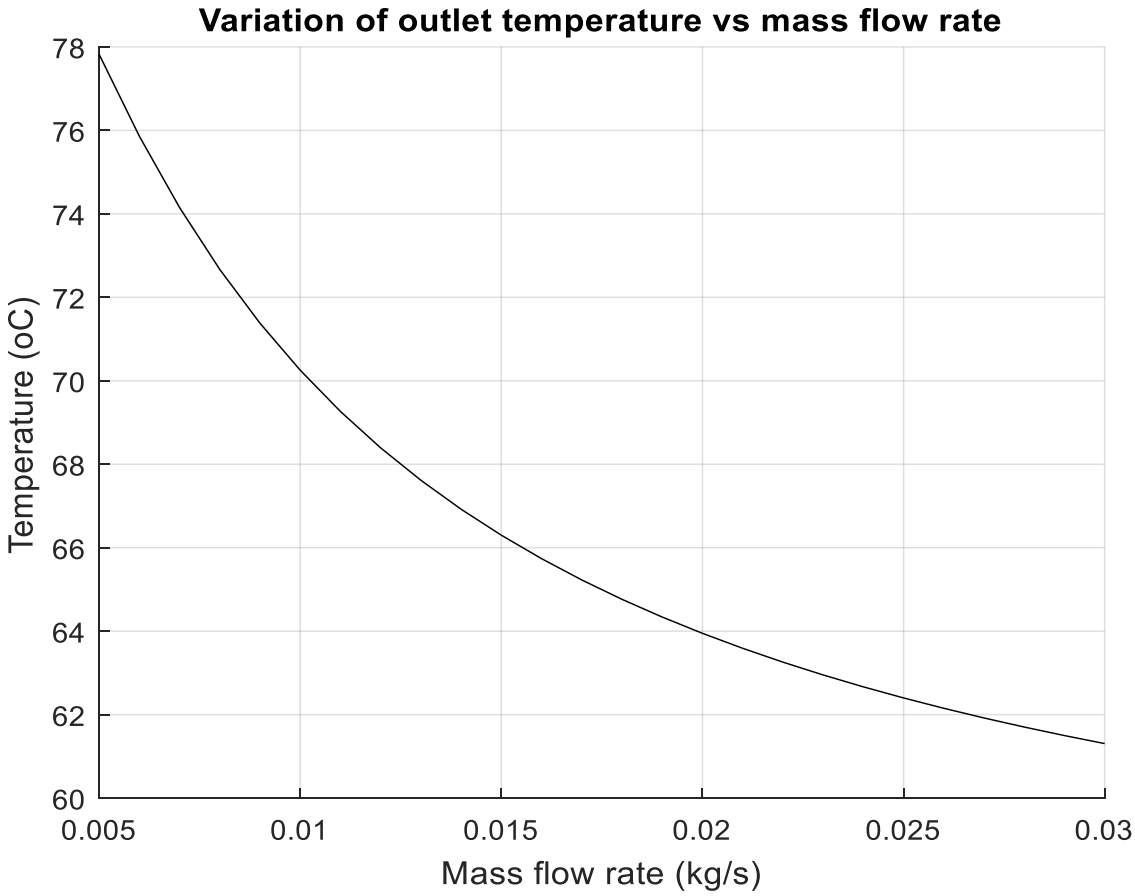

Figure 4.5: Variation of heat transfer fluid outlet temperature as a function of mass flow rate

As shown in the figure, as mass flow rate increases; heat transfer fluid outlet temperature decreases. The mass flow rate of heat transfer fluid is selected for the outlet heat transfer fluid temperature of 67 ^{o}C, based on these selection criteria the mass flow rate of heat transfer fluid is equal to 0.014 kg/s.

4.4. Transient Analysis of Flat Plate Solar Collector Using Finite Difference Method

In order to obtain the appropriate heat power for a particular installation of a flat plate solar collector, knowledge about the collector operating parameters is necessary. These parameters (e.g. the temperature of the working fluid at the collector outlet) depend on the level of sun exposure, and thus they are variable. The solar collector works under transient conditions.

In this section, the mathematical model used to simulate the dynamic behavior of liquid flat plate collectors is developed. The collector is divided in to five nodes (cover, air gap, absorber, fluid, and insulation) perpendicular to the flow direction. For each node, the equation describing the energy balance is derived. The derived differential equations are solved using the explicit finite-difference method. All the thermo-physical properties of the operating fluid, absorber, air gap, glass and insulation can be considered as constant.

The transient temperatures are evaluated iteratively, using relations derived for the equation of energy balance for each node.

i. Single Glass Cover

$$C_g\rho_g V_g \frac{dT_g}{dt} = \left[h_2\left(T_a - T_g\right) + h_{r1}\left(F\left(T_p\right) - T_g\right) + h_{c1}\left(T_{ag} - T_g\right) + \alpha I_T\right] W\Delta y \quad \text{(4.35)}$$

Where, $h_2 = h_{c2} + h_{r2}$

ii. Air Gap between Glass Cover and Absorber

$$C_{ag}\rho_{ag} V_{ag} \frac{dT_{ag}}{dt} = \left[h_{c1}\left(F\left(T_p\right) - T_{ag}\right) + h_{c1}\left(T_g - T_{ag}\right)\right] W\Delta y \quad \text{(4.36)}$$

iii. Absorber

$$C_p\rho_p V_p \frac{dT_P}{dt} = \left[h_{r1}\left(T_g - F\left(T_p\right)\right) + h_{c1}\left(T_{ag} - FT_P\right) + \alpha\tau I_T + \frac{k_{ins}}{\delta_{ins}}\left(T_{ins} - FT_P\right)\right] W\Delta y + \pi D_i h_{fi}\Delta y\left(T_f - FT_P\right) \quad \text{(4.37)}$$

iv. Working Fluid

$$C_f\rho_f A \frac{\partial T_f}{\partial t} = \pi D_i h_{fi}\left(F\left(T_P\right) - T_f\right) - \dot{m}_f C_f \frac{\partial T_f}{\partial y} \quad \text{(4.38)}$$

Where, $A = {\pi D_i}^2/_4$

v. Insulation

$$C_{ins}\rho_{ins} V_{ins} \frac{dT_{ins}}{dt} = \left[\frac{k_{ins}}{\delta_{ins}}\left(FT_P - T_{ins}\right) + h_{c2}\left(T_a - T_{ins}\right)\right] W\Delta y \quad \text{(4.39)}$$

The explicit finite-difference method is proposed to solve the system of equations. The time derivatives are replaced by a forward difference scheme, whereas the dimensional derivative is replaced by a backward difference scheme.

$$\frac{dT_g}{dt} = \frac{{T_{g,j}}^{t+\Delta t} - {T_{g,j}}^{t}}{\Delta t} \quad \text{(4.40)}$$

$$\frac{dT_{ag}}{dt} = \frac{{T_{ag,j}}^{t+\Delta t} - {T_{ag,j}}^{t}}{\Delta t} \quad \text{(4.41)}$$

$$\frac{dT_p}{dt} = \frac{{T_{p,j}}^{t+\Delta t} - {T_{p,j}}^{t}}{\Delta t} \quad \text{(4.42)}$$

$$\frac{dT_{ins}}{dt} = \frac{{T_{ins,j}}^{t+\Delta t} - {T_{ins,j}}^{t}}{\Delta t} \quad \text{(4.43)}$$

$$\frac{\partial T_f}{\partial t} = \frac{{T_{f,j}}^{t+\Delta t} - {T_{f,j}}^{t}}{\Delta t} \quad \text{(4.44)}$$

$$\frac{\partial T_f}{\partial y} = \frac{{T_{f,j}}^{t+\Delta t} - {T_{f,j-1}}^{t+\Delta t}}{\Delta y} \quad \text{(4.45)}$$

$$\frac{dT_a}{dt} = \frac{{T_{a,j}}^{t+\Delta t} - {T_{a,j}}^{t}}{\Delta t} \quad \text{(4.46)}$$

After some transformations, the following formulae were obtained:

For the glass cover,

$${T_{g,j}}^{t+\Delta t} = EE * \Delta t * {T_{g,j}}^{t} + BB * \Delta t * {T_{a,j}}^{t} + CC * F * \Delta t * {T_{p,j}}^{t} + DD * \Delta t * {T_{ag,j}}^{t} + GG * \Delta t * {I_T}^{t} \qquad j = 1, 2, 3, \ldots,N \quad \text{(4.47)}$$

For the air gap,

$${T_{ag,j}}^{t+\Delta t} = (1 - 2 * HH * \Delta t){T_{ag,j}}^{t} + HH * \Delta t * {T_{g,j}}^{t} + HH * F * \Delta t * {T_{p,j}}^{t},$$

$j = 1, 2, 3, \ldots,N$ (4.48)

For the plate (absorber),

$${T_{p,j}}^{t+\Delta t} = (1 - OO * F * \Delta t){T_{p,j}}^{t} + NN * \Delta t * {I_T}^{t} + JJ * \Delta t * {T_{g,j}}^{t} + KK * \Delta t * {T_{ag,j}}^{t} + LL * \Delta t * {T_{ins,j}}^{t} + MM * \Delta t * {T_{f,j}}^{t} \qquad j = 1, 2, 3, \ldots,N \quad \text{(4.49)}$$

For the working fluid,

$${T_{f,j}}^{t+\Delta t} = (1 - PP * \Delta t - \Delta y){T_{f,j}}^{t} + PP * F * \Delta t * {T_{p,j}}^{t} + \Delta y * {T_{f,j-1}}^{t},$$

$j = 1, 2, 3, \ldots,N$ (4.50)

For the insulation,

$$T_{ins,j}{}^{t+\Delta t} = (1 - SS * \Delta t)T_{ins,j}{}^{t} + QQ * F * \Delta t * T_{p,j}{}^{t} + RR * \Delta t * T_{a,j}{}^{t}, \quad j = 1, 2, \ldots, N \quad (4.51)$$

Where, T is for temperature, the abbreviations g,ag,p,f, and ins are for the glass, air gap, plate (absorber), working fluid and insulation respectively. D_i is for the internal diameter of the tube, F is for the fin efficiency of the absorber plate, t is the time, Δt is the time increment, C is for the specific heat capacity, ρ is for the density, k is for thermal conductivity, α is the thermal absorptivity of plate, τ is the thermal transmissivity of the glass, δ is for the thickness, $\dot{m}$ is for the mass flow rate, N is the number of nodes in the flow direction, and V is for the volume. Divide the length of riser tube in to 10 number points with the interval of 0.19 m length. This shows the riser have 11 nodes from inlet to the outlet.

In the above equations:

$$BB = \frac{h_2}{\rho_g C_g \delta_g} \quad (4.52)$$

$$CC = \frac{h_{r1}}{\rho_g C_g \delta_g} \quad (4.53)$$

$$DD = \frac{h_{c1}}{\rho_g C_g \delta_g} \quad (4.54)$$

$$EE = 1 - (BB + CC + DD) \quad (4.55)$$

$$GG = \frac{\alpha}{\rho_g C_g \delta_g} \quad (4.56)$$

$$HH = \frac{h_{c1}}{\rho_{ag} C_{ag} \delta_{ag}} \quad (4.57)$$

$$JJ = \frac{h_{r1}}{\rho_p C_p \delta_p} \quad (4.58)$$

$$KK = \frac{h_{c1}}{\rho_p C_p \delta_p} \quad (4.59)$$

$$LL = \frac{k_{ins}}{\rho_p C_p \delta_p \delta_{ins}} \quad (4.60)$$

$$MM = \frac{\pi D_i h_{fi}}{\rho_p C_p \delta_p W} \quad (4.61)$$

$$NN = \frac{\alpha\tau}{\rho_p C_p \delta_p} \quad (4.62)$$

$$OO = JJ + KK + LL + MM \quad (4.63)$$

$$PP = \frac{\pi D_i h_{fi}}{\rho_f C_f A} \quad \text{..... (4.64)}$$

$$QQ = \frac{k_{ins}}{\rho_{ins} C_{ins} \delta_{ins}{}^2} \quad \text{..... (4.65)}$$

$$RR = \frac{h_{c2}}{\rho_{ins} C_{ins} \delta_{ins}} \quad \text{..... (4.66)}$$

$$SS = QQ + RR \quad \text{..... (4.67)}$$

Initial conditions (At time equal to zero (at 12:00 PM)):

- The heat transfer fluid is at a temperature of 55 ^{o}C.

$$T_{fat\ j}(0) = 328.15\ K$$

- The glazing and insulation materials maintain an ambient temperature.

$$T_{fat\ j}(0) = 293.15\ K$$

- The plate temperature equals to ambient temperature plus ten degree Celsius.

$$T_{fat\ j}(0) = 303.15\ K$$

- The air gap temperature between plate and glazing equals average of plate and glazing temperature.

$$T_{fat\ j}(0) = 298.15\ K$$

Boundary conditions -Temperature of fluid at the inlet of riser tube is equal to the exit fluid temperature of biogas reactor.

$$T_{fat\ j=0}(t) = 328.15\ K$$

CHAPTER 5: Thermal Performance Analysis of Solar Thermal Energy Storage Device Packed With Phase Change Material

5.1. Introduction

The supply of solar energy is time-dependent, as such; a discrepancy may arise between solar energy supply and demand. Thermal energy storage (TES) systems may cater for this time-discrepancy by storing solar thermal energy during sunshine hours for use later. Thermal energy storage can be stored as a change in internal energy of a material as sensible heat, latent heat and thermochemical or combination of these. Amongst above thermal heat storage techniques, latent heat thermal energy storage is particularly attractive due to its ability to provide high-energy storage density and its characteristics to store heat at constant temperature corresponding to the phase transition temperature of phase change material (PCM).

Packed bed configurations have shown excellent heat transfer characteristics by providing a large surface area for heat exchange. The spherical geometry of encapsulation of PCM is preferred because it presents a larger area of the encapsulated PCM for heat transfer than other geometries of encapsulation. It also makes the storage tank to have a greater packing density.

A storage system operates in three modes as follows:

1. Charging mode:

The charging mode starts with circulation of the heat transfer fluid heated in the collection system at a temperature higher than the PCM melting temperature. This mode occurs during day time when solar energy collection takes place and terminates with complete melting of the PCM, charging of the store does not terminate with complete melting of the PCM if the inlet fluid temperature is above the melt temperature, charging of sensible heat continues.

2. Discharging mode

The discharging mode is started by circulation of the cold heat transfer fluid having inlet temperature lower than the PCM melting temperature. The heat transfer fluid exit temperature is time dependent because the rate of solidification of the PCM varies with time. This mode terminates with complete solidification of the PCM.

3. Standby mode

This mode occurs when there is no further storage of energy occurring because of decreasing heat transfer fluid temperature or the storage tank is completely charged or the energy is directly fed to the utility without using storage and/or no heating from the bed is required. This is the transition period between the charge and discharge modes.

In this study, a one dimensional heat transfer model for charging process is developed for either sensible or latent heat absorbing process by using the basic conservation of energy principle. The time dependent variables are discretized by using explicit finite difference scheme. And also for spatial variation a finite difference scheme is used to discretize for solving a charging mode.

5.2. Phase Change Material

Phase Change Material (PCM) is a substance with a high heat of fusion, which melts and solidifies at certain temperatures; is capable of storing or releasing large amounts of energy. Phase change materials are latent heat storage substance, in which energy is stored in the process of changing state, i.e. phase is changed from solid to liquid. When phase change materials attain the temperature at which phase change occur from solid to liquid, they absorb large amount of energy and release stored energy when phase change material solidifies (Patil and Karale, 2012).

Required properties for phase change material

i. Absorb and release large amounts of energy when melting and freezing; this requires the PCM to have a large latent heat of fusion and to be as dense as possible.

ii. Have a fixed and clearly determined phase change temperature (freeze/melt point); The PCM needs to change its phase over a small temperature range as possible. Many PCMs freeze or melt over a range of several degrees, and will often have a melting point that is slightly higher or lower than the freezing point. This phenomenon is known as hysteresis.

iii. Avoid excessive super cooling***;*** super cooling is observed with many eutectic solutions and salt hydrates. The PCM in its liquid state can be cooled below its freezing point whilst remaining a liquid.

iv. Remain stable and unchanged over many freeze/melt cycles; PCMs are usually used many times over, and often have an operational lifespan of many years in which they will be subjected to thousands of freeze/melt cycles. It is very important that the PCM is not

prone to chemical or physical degradation over time which will the energy storage capability of the PCM.

v. Non-hazardous

vi. Economical

Selection of PCM

In order to select the best qualified PCM as a storage media some criteria's are mentioned (Patil and Karale, 2012).

i. According to thermal properties, the melting point of the PCM must be lying in a practical range of operation.

ii. The latent heat should be as high as possible to minimize the physical size of the heat storage

iii. A high thermal conductivity would assist the charging and discharging of the energy storage.

iv. According to chemical properties, a suitable PCM should be non-toxic, non-flammable, non-dangerous, non-corrosive and long term chemically stable.

v. According to physical properties, it must have limited changes in density to avoid problems with the storage tank, low vapor pressure, and favorable phase equilibrium.

vi. Moreover PCM must be available in large quantities, cheap in order to make the system economically feasible.

The phase change material used in this study is a technical grade Paraffin n-Triacontane. It has a melting point of 65 – 66 ^{o}C. The thermo-physical properties of Paraffin n-Tricontane is presented on the Table 5.1 (Sharma et al., 2004 and Ukrainczyk et al., 2010):

Table 5. 1: Thermo-physical properties of phase change material (Paraffin n-Triacontane)

Melting point (^oC)	Latent heat of fusion (kJ/kg)	Density (kg/m^3)		Specific heat capacity (J/kgK)		Thermal conductivity (W/mK)		Thermal diffusivity 10^{-7} m^2/s
		Solid phase	Liquid phase	Solid phase	Liquid phase	Solid phase	Liquid phase	
65 - 66	252	910	765	1850	2384	0.21	0.15	1.02

5.3. Design Considerations

The major factors to be considered in the design of a storage unit containing a PCM include:

1. Temperature limits with in which the units is to operate.
2. The thermo-physical properties of the PCM.
3. The storage capacity of the tank.
4. The configurations of the transfer fluid.
5. The type of heat transfer fluid.

Design Assumption

Assumptions involved in the present study are:

1. The tank is perfectly insulated.
2. The flow in the tank is axial and incompressible.
3. The thermo-physical properties of the heat transfer fluid (HTF) are invariant with temperature.
4. Variation of temperature is only along the axial direction, i.e. the temperature is independent of radial position.

5. The tank of length H has been divided in to N elements of sufficiently small length H/N so that the element can be assumed to be at a single temperature.
6. The temperature of the HTF at the entry of storage tank is equal to the exit temperature of flat plate collector.
7. The thermal resistance of the encapsulation material is neglected.
8. Radiant heat transfer in the storage is neglected.
9. The PCM spheres are identical.
10. There is no internal heat generation in the bed.

5.4. Mathematical Model of Solar Thermal Energy Storage for Charging Mode

In this study a phase change material (Paraffin) is encapsulated by spherical capsules. Aluminum is used to as a capsule material. Encapsulated spherical phase change material spheres are identical and rectangular packed in storage tank with porosity (e), through which the heat transfer fluid flows. The heat transfer fluid and the phase changing material are assumed to be initially at the same temperature. The packed bed column is divided into N elements, each containing phase changing material capsules surrounded by heat transfer fluid. A schematic diagram of the packed bed LHTES system, consisting of a perfectly insulated vertical cylinder of length, H, diameter, D, (with length to diameter ratio of 1.5 (Regin et al., 2009)) with inlet and outlet manifolds at top and bottom ends, is shown in the figure below:

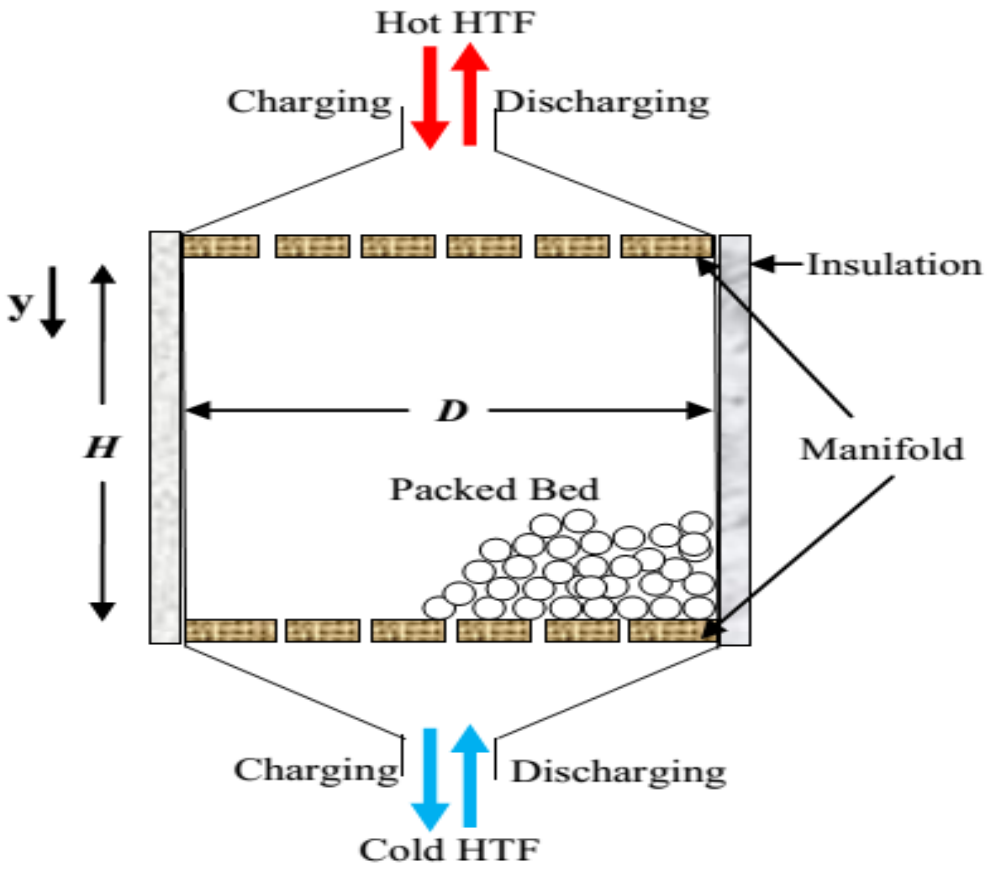

Figure 5. 1: Schematic diagram of the packed bed LHTES system (Regin et al., 2009)

The energy balance on an element of volume $A\Delta y$ having PCM at a temperature T_b and the heat transfer fluid flowing at the rate of $\dot{m}_f$ and entering at a temperature T_f can be written as (Regin et al., 2009):

$$(\dot{m}C_p)_f T_f - (\dot{m}C_p)_f \left[T_f + \frac{\partial T_f}{\partial y}\Delta y\right] =$$

$$U_v A\Delta y(T_f - T_b) + U_s \pi D\Delta y(T_f - T_\infty) + \rho_f (A\Delta y) e C_{P,f} \frac{\partial T_f}{\partial t} \quad \text{..... (5.1)}$$

The left hand side of the above equation represents heat flow by the movement of heat transfer fluid. The first and second terms on the right hand side represent the heat exchange between the capsule and heat transfer fluid and heat loss to the environment respectively. The last term represents the rate of stored energy of the heat transfer fluid in the control volume.

Where C_p represents the specific heat capacity, ρ_f is the density of the HTF, A the area of a storage tank, t is for time, T_∞ is the atmospheric temperature of the air and Δy is equal to the diameter of encapsulated phase changing material.

In case, the heat losses can be neglected (the storage tank is considered to be well insulated) and the energy stored in the heat transfer fluid is negligibly small, the energy balance at an instance of time becomes (Regin et al., 2009):

$$(\dot{m}C_p)_f T_f - \left(\dot{m}C_p\right)_f \left[T_f + \frac{\partial T_f}{\partial y}\Delta y\right] - U_v A \Delta y\left(T_f - T_b\right) = 0 \quad \text{..... (5.2)}$$

or

$$\frac{\partial T_f}{\partial y} = -\frac{U_v A}{\left(\dot{m}C_p\right)_f}(T_f - T_b) \quad \text{..... (5.3)}$$

On simplification,

$$\frac{\partial T_f}{\partial (y/H)} = -NTU(T_f - T_b) \quad \text{..... (5.4)}$$

Where $NTU = \frac{U_v A H}{\left(\dot{m}C_p\right)_f}$ is the number of transfer units.

Integration yields,

$$\frac{T_{fj+1} - T_{bj}}{T_{fj} - T_{bj}} = \exp\left(-\frac{NTU}{N}\right) \quad or \quad \frac{T_{fj} - T_{fj+1}}{T_{fj} - T_{bj}} = 1 - \exp\left(-\frac{NTU}{N}\right) \quad \text{..... (5.5)}$$

The outlet temperature of heat transfer fluid for jth element is (Regin et al., 2009):

$$T_{fj+1} = T_{fj} - [(T_{fj} - T_{bj})(1 - \exp\left(-\frac{NTU}{N}\right))] \quad \text{..... (5.6)}$$

Where T_{fj} is the heat transfer fluid temperature at inlet to the element, T_{fj+1} is the heat transfer fluid temperature at outlet from the element, T_{bi} represents the bed temperature of the element and $N = \frac{H}{\Delta y}$ is the number of elements in the packed bed. The above equation can be written for each control volume forming a system of N simultaneous equations. The NTU value and bed temperature of the element T_{bj} can be determined by knowing the volumetric heat transfer coefficient and the energy transferred into the PCM capsules. This can be explained as follows:

The volumetric heat transfer coefficient for thermal storage system can be written as (Regin et al., 2009):

$$U_v = \frac{6U_O(1-e)}{D_c} \quad \text{(5.7)}$$

Where: U_O is the overall heat transfer coefficient of capsule [W/m^{2}K], and D_c is diameter of the capsule [m].

For the capsule, the outer surface overall heat transfer coefficient, is a function of the mode (either charging or discharging), the state of the PCM capsule in the control volume (fully liquid, fully solid, or phase change processes) and the mechanism of heat transfer (conduction, convection or combined conduction and convection).

During the fully liquid or fully solid stages, the overall heat transfer coefficient can be calculated by using thermal resistance concept for each capsule as given below (Shobo et al., 2015):

$$U_O = \left(\frac{1}{A}\right)(R_{ext})^{-1} = \frac{2+1.1Re^{0.6}Pr^{1/3}}{D_c}k_f \quad \text{(5.8)}$$

Where, R_{ext} is the convective thermal resistance on the external surface of the capsule shell, $Re = \frac{\rho_{bm1}D_c eV_f}{\mu_f}$ is the Reynolds number, $Pr = \frac{C_f\mu_f}{k_f}$ is the Prandtl number, ρ_s is the density of the PCM, V_f is the velocity of the heat transfer fluid, μ_f is the dynamic viscosity of the fluid, C_f is the specific heat capacity of the fluid, and k_f is the thermal conductivity of the fluid.

During the phase change process the outer surface overall heat transfer coefficient can be calculated by using thermal resistance concept for each capsule as given below (Regin et al., 2009):

$$U_O = (\frac{1}{A})(R_{ext} + R_{in})^{-1} \quad \text{(5.9)}$$

Where, R_{in} is the resistance due to the solidified/melt PCM layer inside the capsule.

The internal resistance of the capsule R_{in} depends on the solid–liquid interface position which can be calculated by related to the effective thermal conductivity of a phase changing material.

For charging mode:

$$R_{in} = \frac{Dc}{k_{eff}A} \quad \text{(5.10)}$$

Where, k_{eff} the effective thermal conductivity of a phase change material, L the melt thickness and A is the surface area of capsule.

The effective thermal conductivity of a phase change material for charging mode can be calculated by (Gonzalez-Aguilar et al., 2015):

$$k_{eff} = k_{liq} C Ra^{m} \quad \text{(5.11)}$$

Where Ra the Rayleigh number, C is equal to 0.186 and m is equal to 0.18.

The Rayleigh number can be calculated by (Dzikevice et al., 2016):

$$Ra = \frac{g\beta' \Delta T R^3}{v\alpha} \quad \text{(5.12)}$$

The bed temperature is calculated by using the energy balance between the heat transfer fluid and the bed. The energy transferred to the bed, $U_v A \Delta y (T_f - T_b)$, results in raising the bed temperature at the rate of $\frac{\partial T_b}{\partial t}$ written as (Regin et al., 2009):

$$U_v A \Delta y (T_f - T_b) = \rho_b (A \Delta y)(1-e) C_{p,b} \frac{\partial T_b}{\partial t} \quad \text{(5.13)}$$

For simplification, multiply by $((AH)/(\dot{m}C_p)_f)$ on both sides

$$U_v (T_f - T_b) \left(\frac{AH}{(\dot{m}C_p)_f}\right) = \rho_b (1-e) C_{p,b} \frac{\partial T_b}{\partial t} \left(\frac{AH}{(\dot{m}C_p)_f}\right) \quad \text{(5.14)}$$

Since, $NTU = \frac{U_v AH}{(\dot{m}C_p)_f}$, the above equation can be written as:

$$\rho_b (1-e) C_{p,b} \frac{\partial T_b}{\partial t} \left(\frac{AH}{(\dot{m}C_p)_f}\right) = NTU(T_f - T_b) \quad \text{(5.15)}$$

The above equation can be discretized for 'jth' element by using simple explicit and first order finite difference formulation, and can be written as (Regin et al., 2009):

$$\frac{(\rho C_p)_b (1-e) AH}{(\dot{m}C_p)_f} \frac{(T_{bj}^{n+1} - T_{bj}^{n})}{\Delta t} = NTU({T_{fj}}^{n} - {T_{bj}}^{n}) \quad \text{(5.16)}$$

$$(\rho C_p)_b (1-e) AH (T_{bj}^{n+1} - T_{bj}^{n}) = (\dot{m}C_p)_f \Delta t NTU({T_{fj}}^{n} - {T_{bj}}^{n}) \quad \text{(5.17)}$$

This energy balance equation can be applicable only to the sensible heat storage materials and can be converted to enthalpy equation that can be applicable to the phase change storage bed material as:

$$\rho_b(1-e)AH\left(H_{bj}^{n+1}-H_{bj}^{n}\right)=\left(\dot{m}C_p\right)_f\Delta t\, NTU({T_{fj}}^n-{T_{bj}}^n)\ldots\ldots \quad (5.18)$$

$$H_{bj}^{n+1}=\frac{\left(\dot{m}C_p\right)_f\Delta t\, NTU({T_{fj}}^n-{T_{bj}}^n)}{(\rho)_b(1-e)AH}+H_{bj}^{n}\ldots\ldots \quad (5.19)$$

Using this equation, enthalpy of bed in the element at particular time can be determined by using the known enthalpy values in the previous time period. This equation is valid at all elements at a particular time.

The corresponding enthalpy–temperature (H–T) relations are (Regin et al., 2009):

(i) When PCM is in solid phase:

$$H = CpsT_b \quad T_b \leq T_{bm1}\ldots\ldots \quad (5.20)$$

ii. When PCM is in the solid–liquid phase:

This occurs in a temperature range T_{bm1} to T_{bm2}, the latent heat L_{fus} is similarly assumed to be supplied over this range and enthalpy is accordingly written as:

$$H = CpsT_b+\gamma' \mathrm{L_{fus}} \quad T_{bm1}\leq T_b\leq T_{bm2}\ldots\ldots \quad (5.21)$$

Where γ' is the melt fraction of the phase changing material, during phase changing process.

The melt fraction, γ', at each element of the PCM domain is given by (Bellan et al., 2017):

$$\gamma'=\begin{cases}0 & if\ T_b<T_{bm1}\\ \frac{T_b-T_{bm1}}{T_{bm2}-T_{bm1}} & if\ T_{bm1}\leq T_b\leq T_{bm2}\\ 0 & if\ T_{bm2}<T_b\end{cases}\ldots\ldots \quad (5.22)$$

iii. When PCM is in the liquid phase:

$$H = Cps(T_{bm1}-T_{initial})+Cpl(T_b-T_{bm2})+\mathrm{L_{fus}} \quad T_b\geq T_{bm2}\ldots\ldots \quad (5.23)$$

The phase change within the encapsulated PCM is accounted for by the apparent heat capacity method. The PCM undergoes three stages during charging and discharging, namely: solid stage, solid-liquid phase change and liquid stage.

a. During the solid stage, $T_b\leq T_{b_{m1}}$

$$C_b=C_{b_{m1}};\ \rho_b=\rho_{b_{m1}};\ k_b=k_{b_{m1}}\ldots\ldots \quad (5.24)$$

b. During solid-liquid phase change, $T_{b_{m1}}\leq T_b\leq T_{b_{m2}}$

$C_b = \frac{C_{b_{m1}} + C_{b_{m2}}}{2}$; $\rho_p = \frac{\rho_{b_{m1}} + \rho_{b_{m2}}}{2}$; $k_p = \frac{k_{b_{m1}} + k_{b_{m2}}}{2}$…….. (5.25)

c. c. During the liquid stage, $T_b \geq T_{b_{m2}}$

$C_b = C_{b_{m2}}; \rho_b = \rho_{b_{m2}}; k_b = k_{b_{m2}}$……... (5.26)

5.5. Initial and Boundary Conditions

At time t = 0, $T_f = T_b = T_{initial}$ for $0 \leq y \leq H$,

At time t > 0, $T_f(0,t) = T_{fi}$; $\frac{dT_b}{dy} = 0$ For y = 0

$\frac{dT_f}{dy} = 0$; $\frac{dT_b}{dy} = 0$ For y = H

5.6. Quantity of Heat Stored

The quantity of heat, Q, stored in an elemental volume of the PCM is calculated by (Shobo et al., 2015):

For the sensible heat from initial temperature ($T_{initial}$) to the commencement of phase change:

$Q_1 = \rho_{bm1} C_{bm1} (1 - e) V_{elem} (T_{m1} - T_{initial})$…… (5.27)

Where, V_{elem} [m^3] is the volume of the element of PCM at a height in the storage tank.

For the phase change:

$Q_2 = \rho_p (1 - e) V_{elem} L_{fus}$……... (5.28)

Where, L_{fus} [J/kg] is the latent heat of phase changing material.

For the sensible heating from end of phase change to final temperature (T_{final}) of the PCM in the element.

$Q_3 = \rho_{bm2} C_{bm2} (1 - e) V_{elem} (T_{final} - T_{m2})$…….. (5.29)

The total heat that can be stored in the thermal energy storage device can be calculated by summing the heat stored at different stages.

$Q = Q_1 + Q_2 + Q_3$…….. (5.30)

CHAPTER 6: Result and Discussion

6.1. Temperature Fluctuation of the Digestate

It is very important to calculate the temperature drop of the digester, to determine the energy requirement of digester that can operate at the desired temperature range. To analyze the daily energy requirement of digester, assume the digester without a heating device and analyze the temperature drop of the system. Digester temperature decrease due to heat is lost from the digester by two mechanisms. First, the inflow digestate enter in to digester at an ambient temperature, but outflow from the digester at the operating temperature of digester. Second, heat is lost through the boundaries of a digester. To determine the temperature drop of the digestate initially assume the digestete was at the desired temperature (328.15 K) at morning 6:00 AM. Below, the hourly average temperature drop of a digestate throughout the day for summer season is presented.

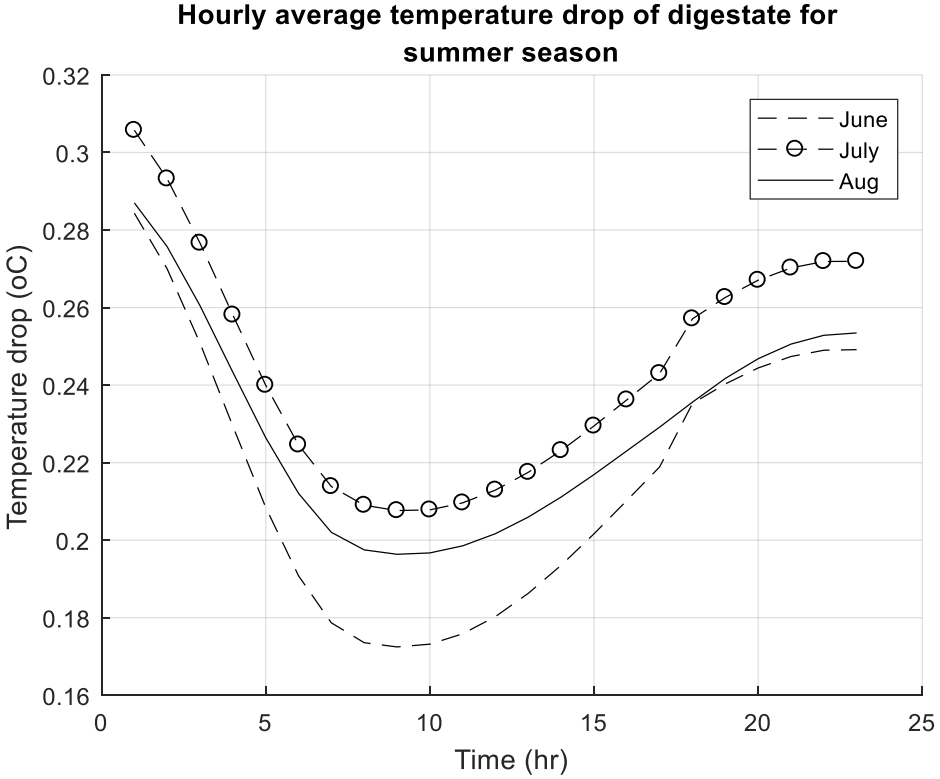

Figure 6.1: Hourly average temperature drop digestate for summer season

As shown in the Figure 6.1, hourly average temperature drop of a digestate decrease during day time and reach minimum around noon time. This temperature drop variation is due to the incidence solar radiation on the top surface of the digester.

Hourly average temperature drop of digestate throughout the day for other seasons are presented at APPENDIX (ANEXX A).

Hourly average temperature drop of digester cover throughout the day for summer season is presented below:

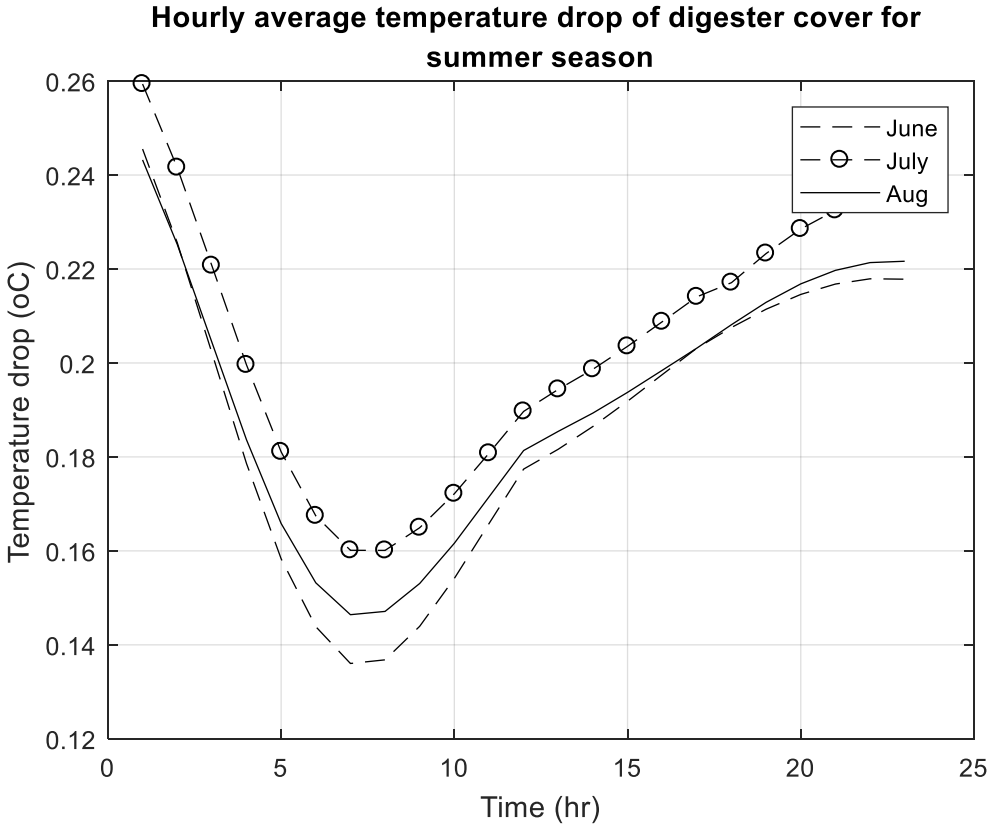

Figure 6.2: Hourly average temperature drop of digester cover for summer season

Similarly, the digester cover is exposed to atmosphere that has a temperature lower than the initial temperature of cover. In this case, it is expected, heat is lost from the digester to the atmosphere by either convection or radiation; this process drops the digester cover temperature.

Hourly average temperature drop of digester cover throughout the day for other seasons are presented at APPENDIX (ANNEX B).

Below the daily average temperature drop of a digestate for the representative days of months are presented. As shown on the Figure 6.3, the maximum temperature drop occurs on December and minimum temperature drop occur on May. This is due to, the monthly average atmospheric temperature reach minimum in December and maximum in May.

Similarly, the maximum average daily temperature drop of cover occurs on December and a minimum temperature drop occurs on May.

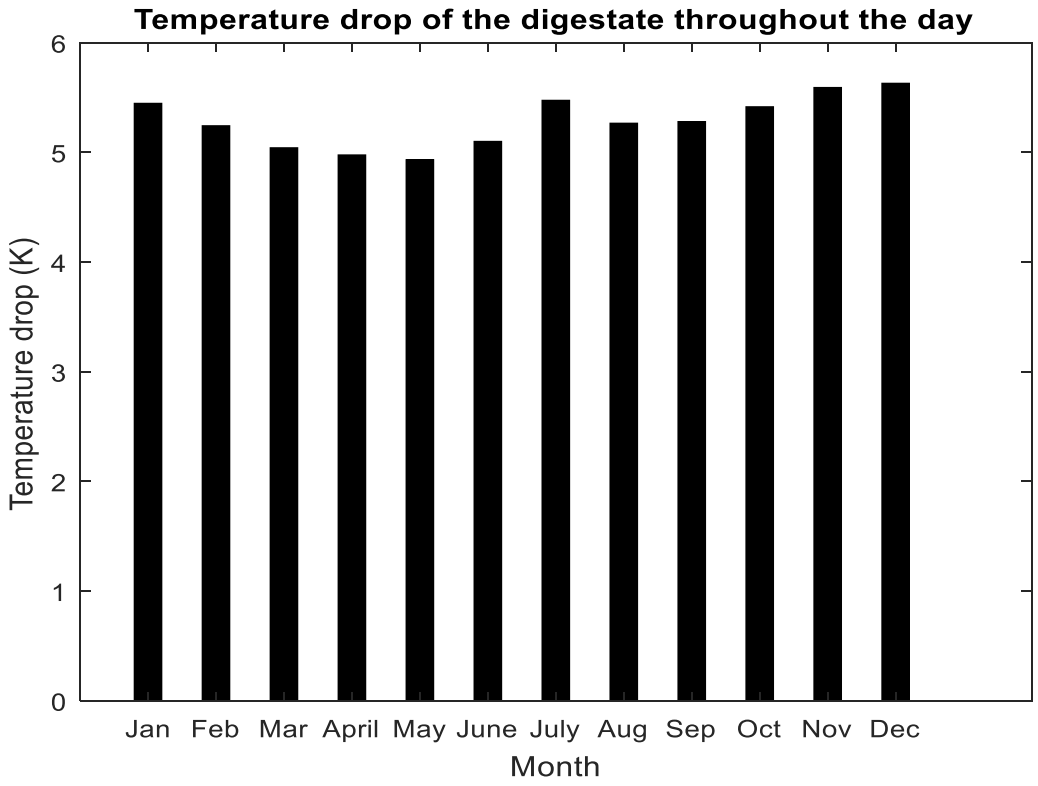

Figure 6.3: Daily average temperature drop of digestate for the representative day of each month

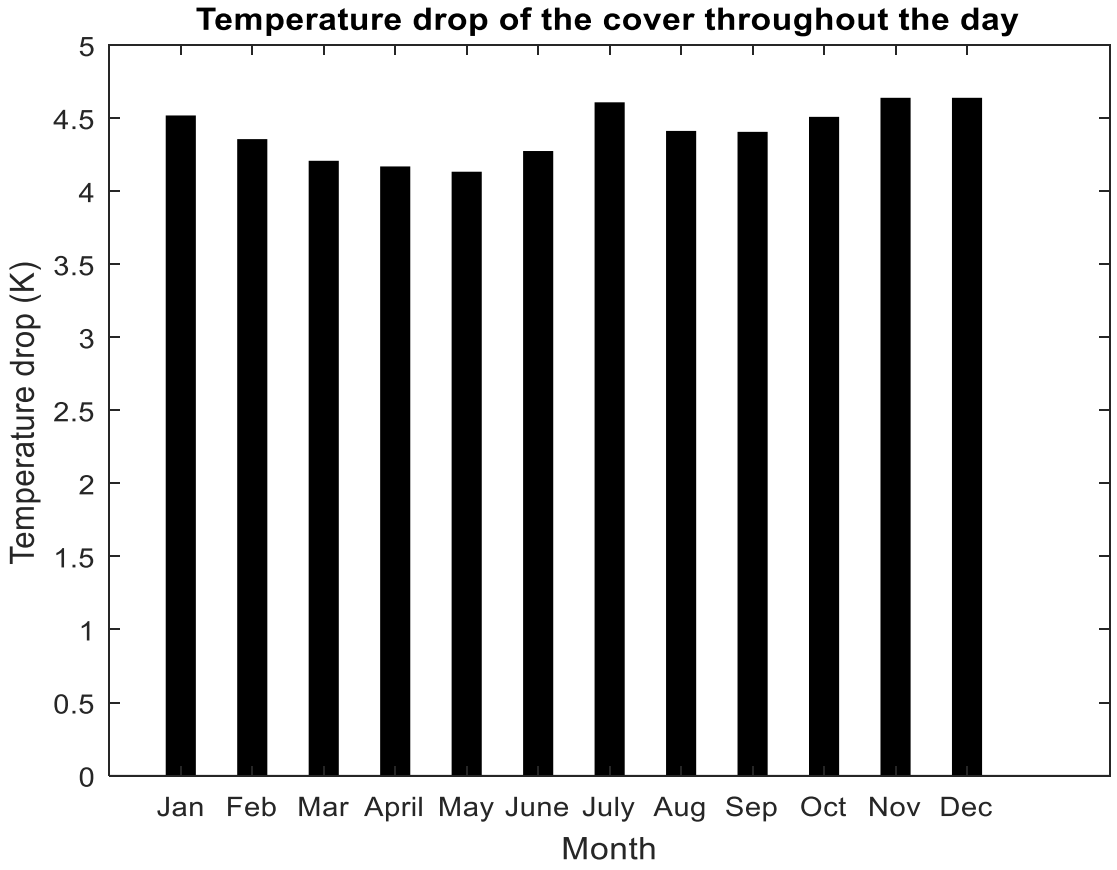

Figure 6.4: Daily average temperature drop of cover for the representative day of each month

As shown on the Figure 6.3 and 6.4 and, the digestate drops its temperature from 4.93 ^{o}C on May to 5.62 ^{o}C on December and digester cover drops its temperature from 4.12 ^{o}C on May to 4.63 ^{o}C on December, throughout the day.

6.2. Energy Requirement

i. Total Energy Requirement

Total energy loss from the digester can be calculated from the temperature drop of the digester. Below, monthly average daily total energy loss from the anaerobic digestion system through the representative day of each month is presented.

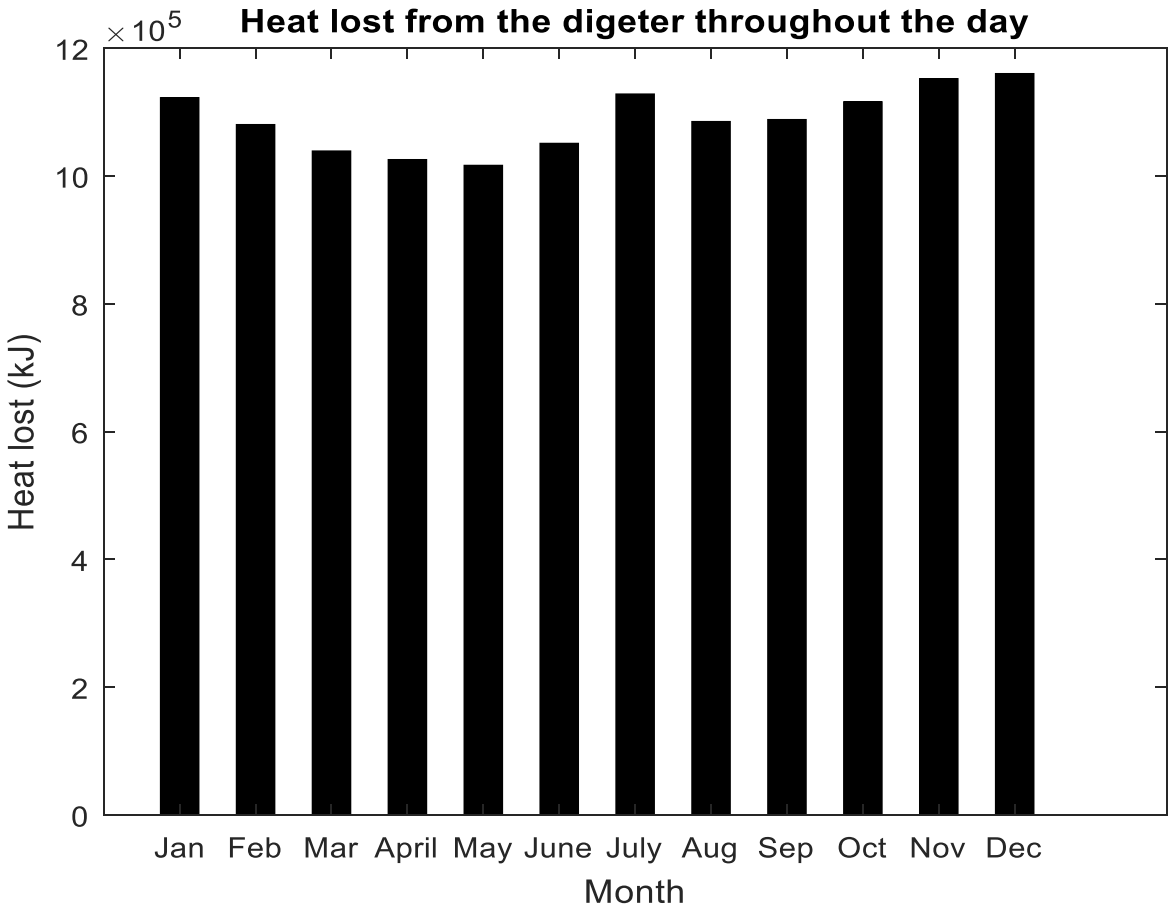

Figure 6.5: Total energy loss from the digester through the representative days of each month

As shown on the figure 6.5, the total amount of heat that required maintaining the desired temperature varies from $1.0166 * 10^6\ kJ/day$ on May to $1.1602 * 10^6\ kJ/day$ on December. The annual average daily heat requirement of digester calculated as $1.088775 * 10^6\ kJ/day$.

ii. Heat Energy Required to Compensating the Incoming Sludge

Heat energy required to compensating the incoming sludge can be calculated from the temperature drop of the digestate throughout the representative days of the months, by neglecting heat loss through the boundaries of the digester. A monthly average daily heat requirement of the digester to compensate the incoming sludge heat lost presented below.

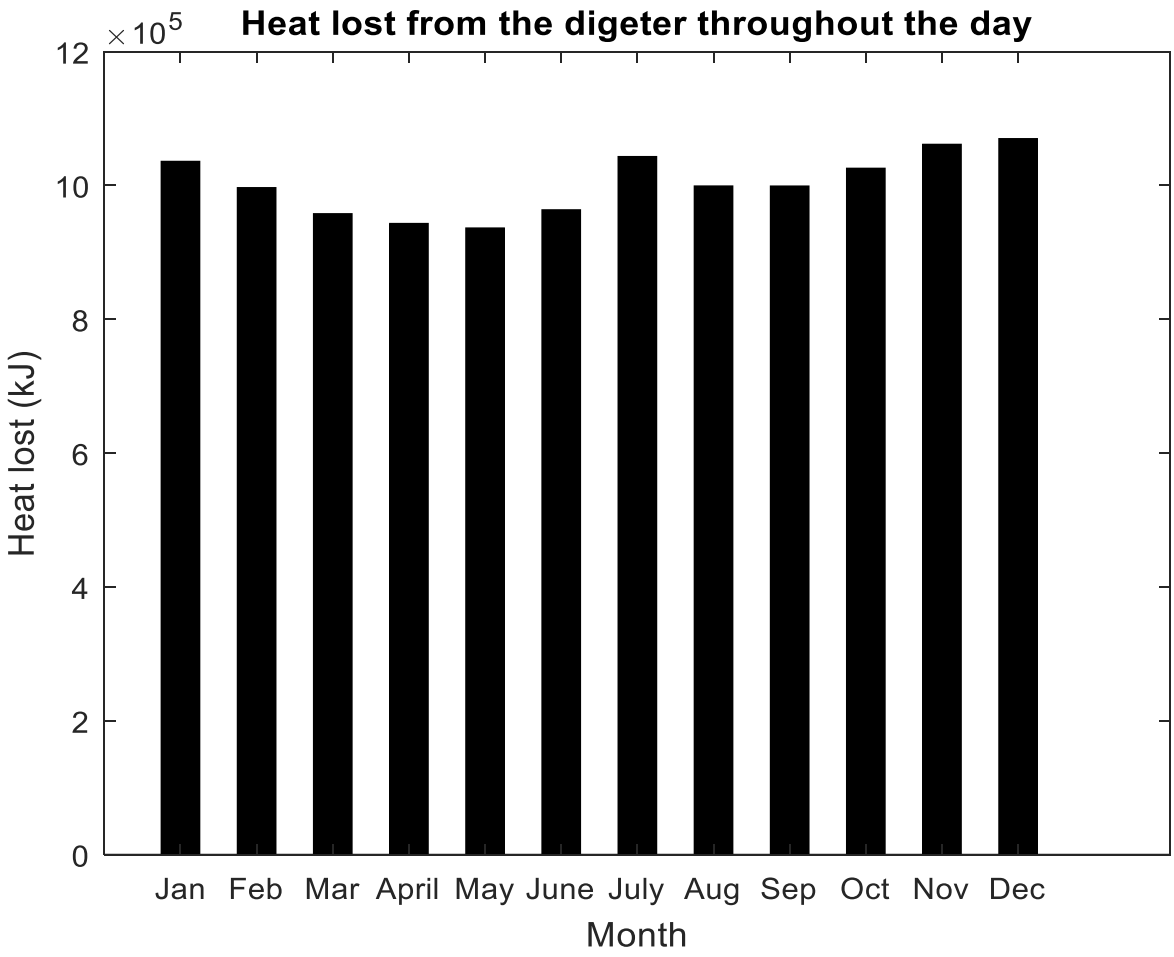

Figure 6.6: Energy loss from the digester throughout the representative day of each month without considering energy lossses through the boundaries of the digester

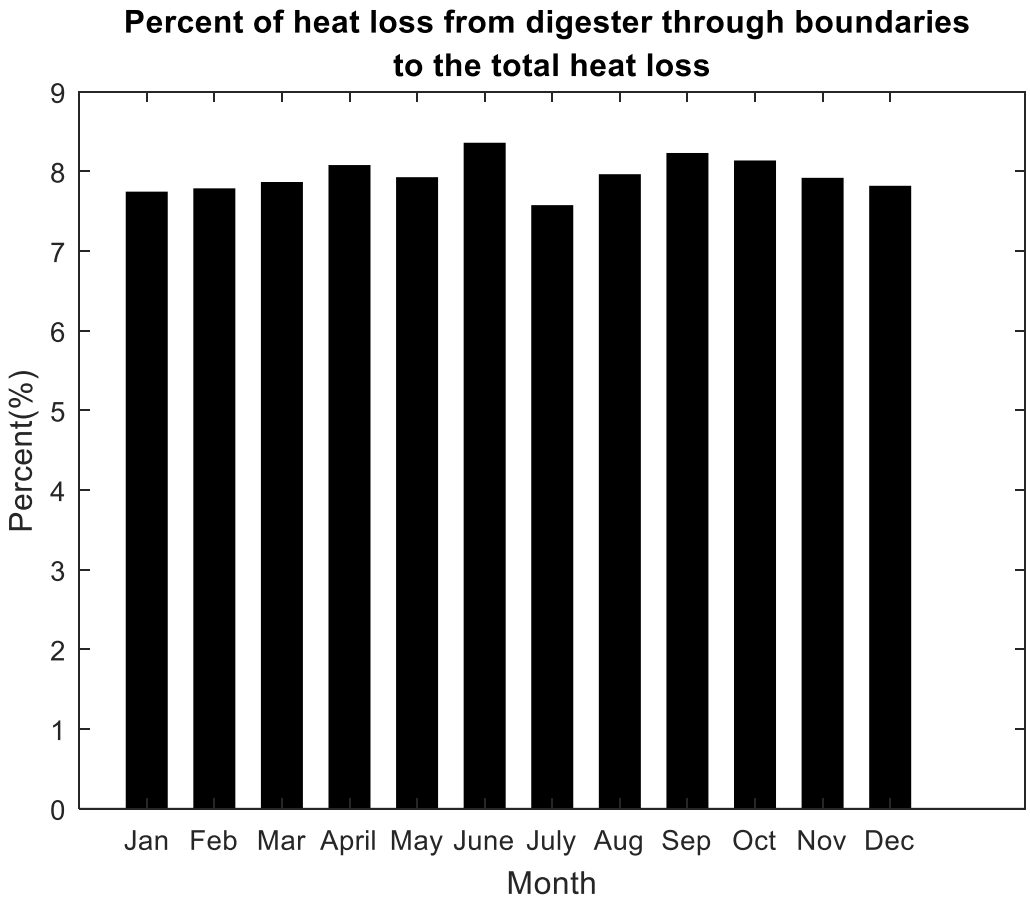

Figure 6.7: Percent of energy loss from the digester through boundaries to the total energy loss

From the result we can conclude that the major part of energy requirement is used to compensate the energy loss from the digester by incoming digestate. The energy losses through the walls of the digester are only account 7.73% to 8.22% of the total energy requirement of a digester.

iii. Validation

The result of this numerical simulation should validated by a similar experimental investigation result of Zupancic and Rose, (2003). Numerical and experimental results have a good agreement, except a small variation. This variation come due to, the two analyses performed for different locations, those have different weather conditions. The experimental results shows, heat losses of the digester through the boundaries make up only 2 – 8% of the heat requirements. Similarly, this numerical result show, the heat losses accounts for 7.73 – 8.22% of the total heat requirement of a digeste.

6.3. Heat Transfer Fluid Temperature Variation at the Outlet of Flat Plate Collector

The heat transfer fluid outlet temperature variation throughout the day for different seasons are calculated iteratively for each second time interval using Microsoft Excel, based on hourly average solar radiation incidence on the flat plate collector and average heat transfer coefficients. Below the result of simulation of outlet temperature variation for winter season is presented:

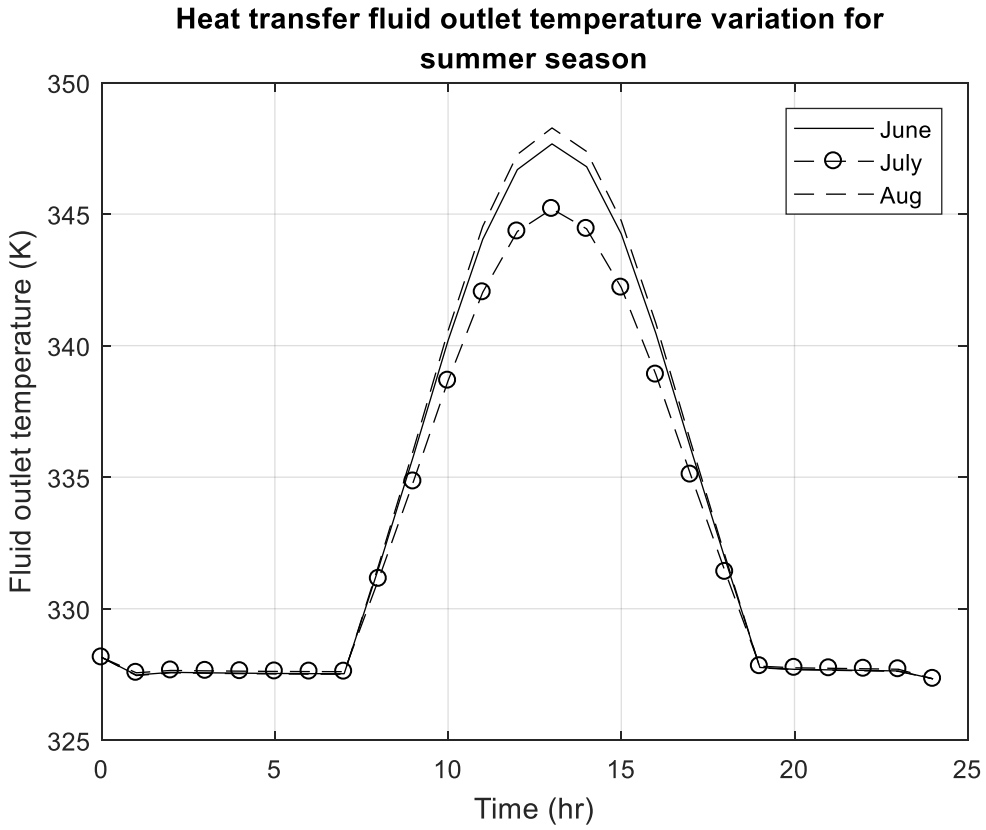

Figure 6.8: Heat transfer fluid outlet temperature fluctuation throughout the day for summer season

As shown on Figure 6.8, the heat transfer fluid temperature at the outlet of a flat plate collector at night time is lower than that of the inlet temperature of a fluid. This is due to, at night time there is no solar radiation and a flat plate collector is exposed to ambient air that have a temperature lower than the working fluid temperature due to that heat is lost from collector to atmospher. At day time the flat plate collector start to absorb solar radiation throughout the day start from

sunrise to sunset hours. The fluid temperature continuously rise from sunrise to noon time and reach maximum at noon, then decreases continuously up to sunset hour.

Heat transfer fluid temperature variations at the outlet of flat plate collector for other seasons are presented at APPENDIX (ANNEX C).

6.4. Temperature Fluctuation of Plate, Glass Cover, Air Gap and Insulation throughout the Day

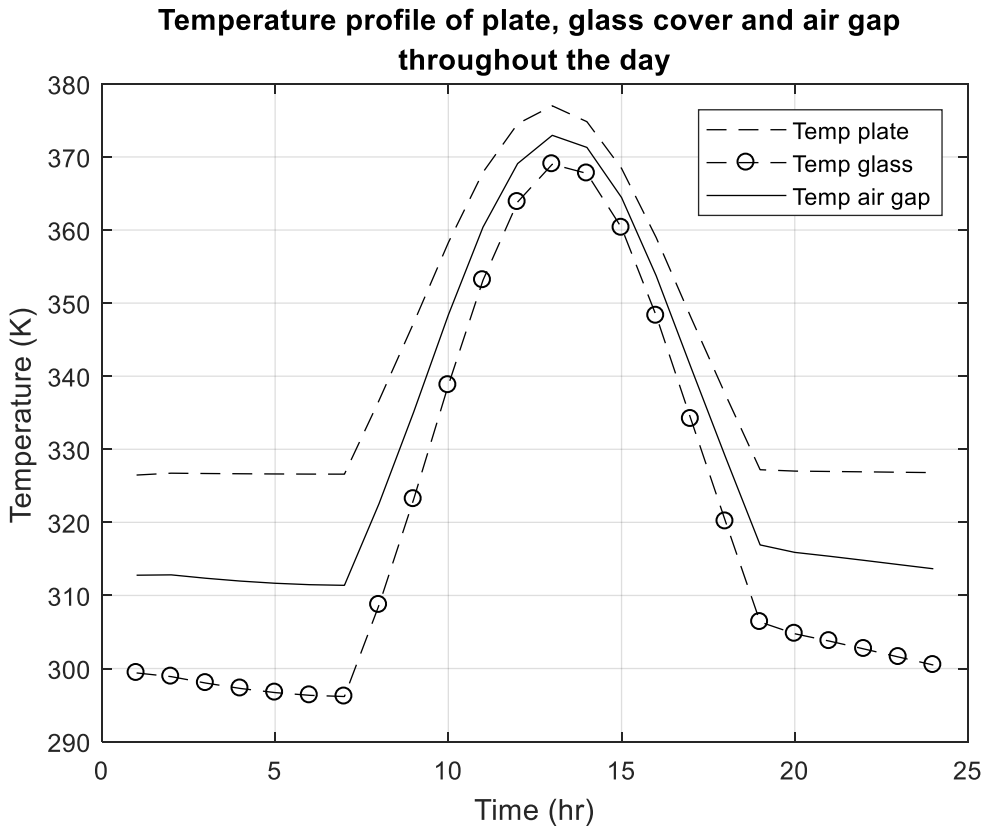

Figure 6.9: Temperature profile of plate, glass cover, air gap and insulation throughout the day for January 17

6.5. Hourly Average Useful Energy Collected by Unit Flat Plate Collector

A useful energy gained by a unit flat plate collector for each hour interval from sunrise to sunset is calculated from the result found from outlet fluid temperature variation of flat plate collector throughout the day, by multiplying temperature rise of the heat transfer fluid to its mass flow rate

and specific heat capacity of the fluid. Below, the hourly average useful energy gain of a unit flat plate collector of area 1.9 m^2 throughout the day for winter season is presented.

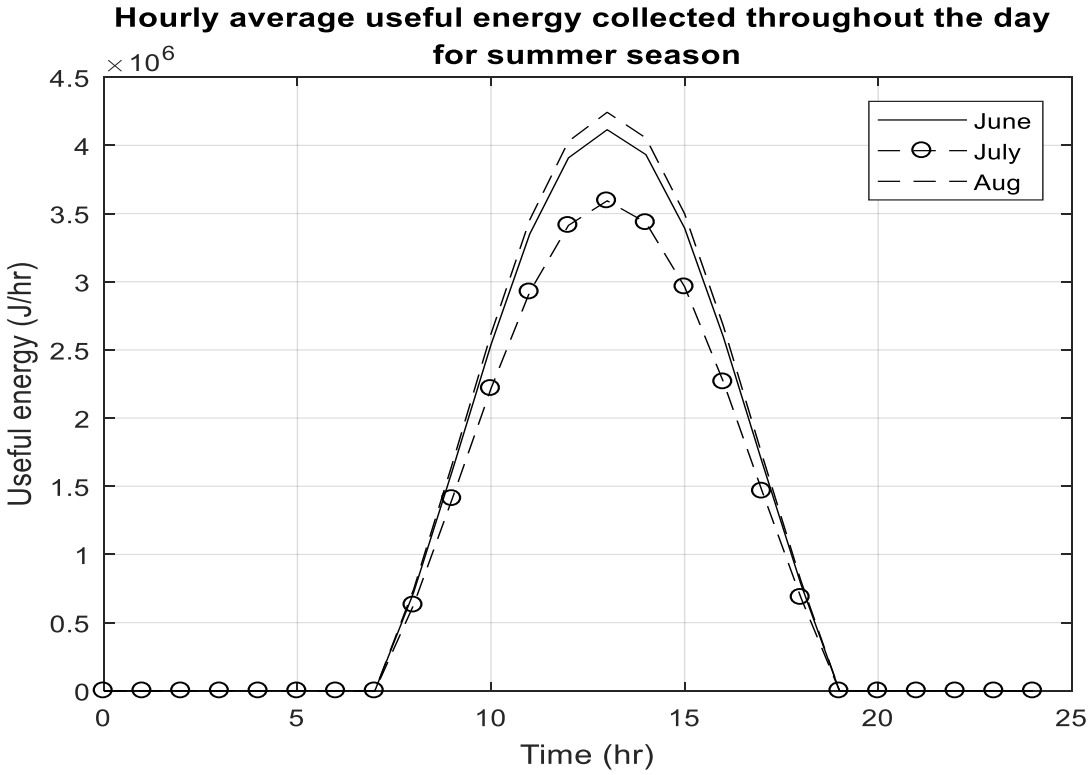

Figure 6.10: Hourly average useful energy collected from a unit flat plate collector throughout the day for summer season

From the result as shown on the Figure 6.10, the amount of energy collected by a flat plate collector continuously increases from sunrise hour up to noon time and reach a maximum amount at noon time, then decreases continuously up to sunset hour.

Hourly average useful energy collected by a unit flat plate collector for other seasons are presented on APPENDIX (ANNEX D).

6.6. Instantaneous Thermal Efficiency of Flat Plat Collector

The instantaneous thermal efficiency of a flat plate collector was analyzed from the instantaneous useful heat gained rate of a collector and the instantaneous total amount of solar radiation incidence on the collector surface. Instantaneous efficiency variation of a flat plate collector from sunrise to sunset for January 17 presented below.

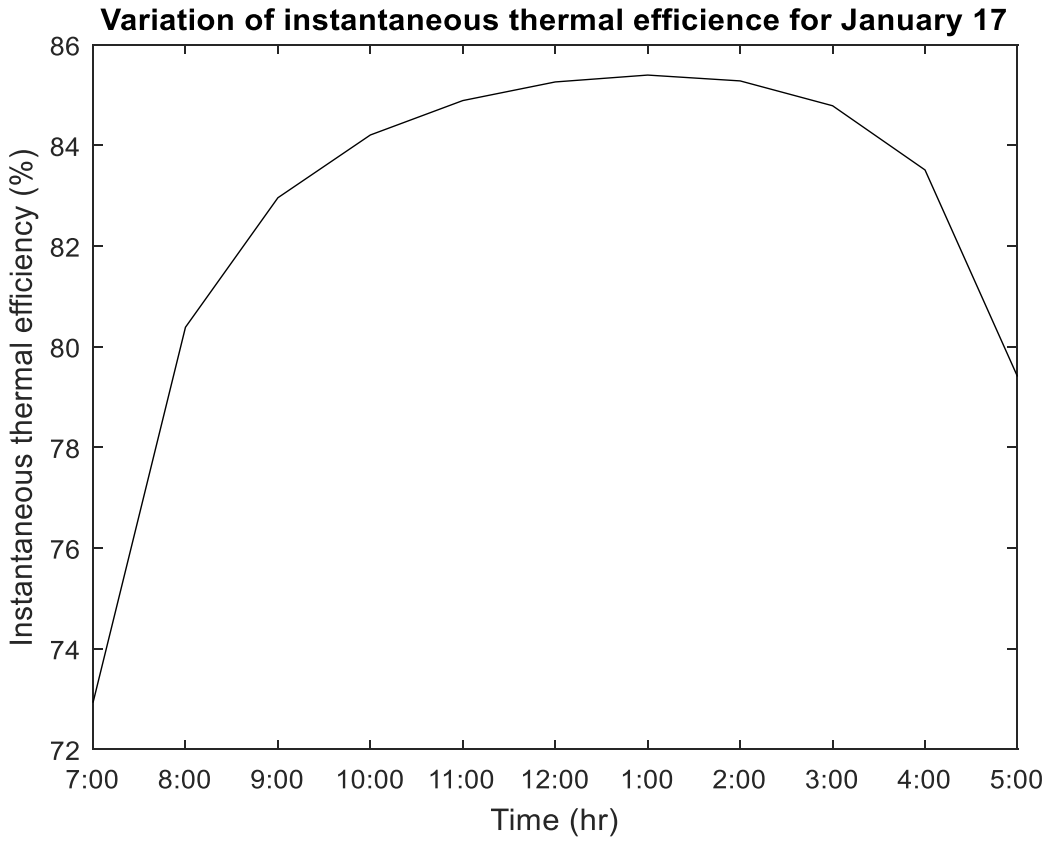

Figure 6.11: Instantaneous efficiency variation of a flat plate collector for January 17

The result shows, the lowest instantaneous efficiency of a flat plate collector occurs at the sunrise hours. This is due to; some percent of solar radiation incidence on the surface of collector were stored by cover, air gap, plate, and tube materials; then the rate of heat absorbed by system components decreased. The highest value of efficiency occurs around noon time, because the sun come to the overhead of the surface, due to this the major part of radiation is beam radiation.

6.7. Daily Average Useful Energy Collected by Unit Flat Plate Collector

The total amount of energy that can be collected by a unit flat plate collector throughout the day is analyzed for representative days of months. Below, the daily average useful energy collected by a unit flat plate collector for different months are presented.

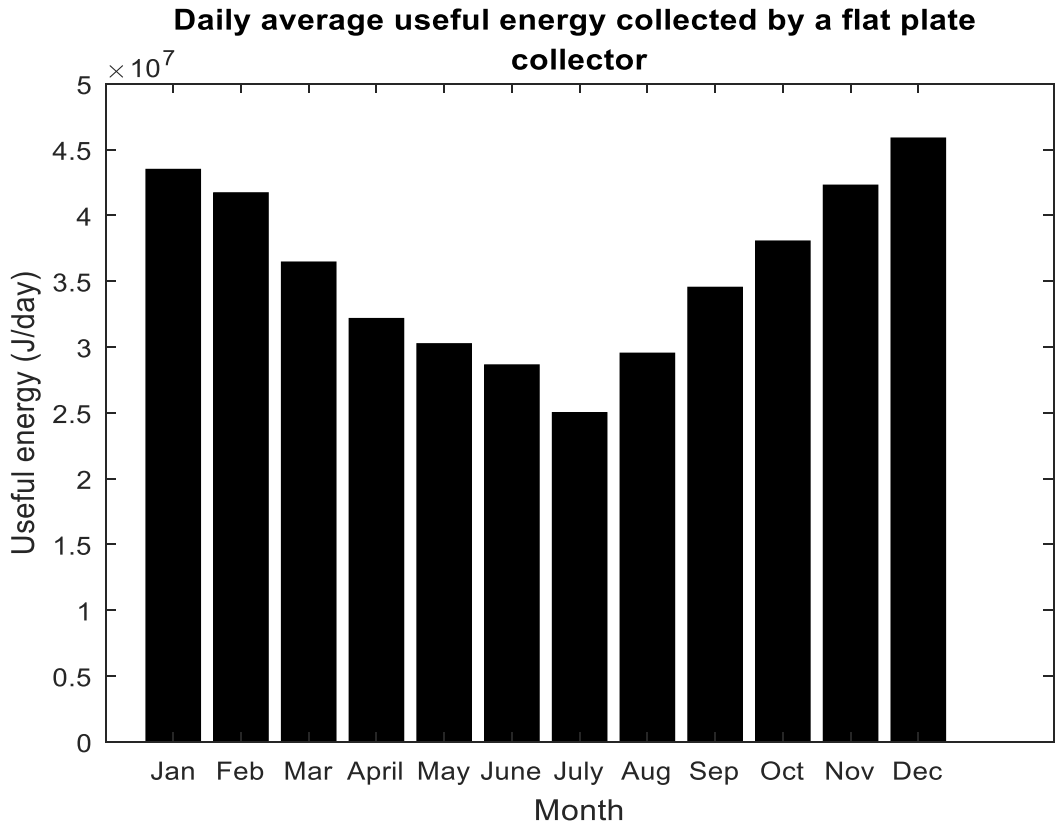

Figure 6.12: Monthly average daily average useful energy collected by a unit flat plate collector

From the result as shown Figure 6.12, the total amount of energy that can be collected by a unit flat plate collector per the day varies from $2.5 * 10^4\ kJ/day$ on July to $4.5867 * 10^4\ kJ/day$ on December. This shows, the average daily solar intensity on December is higher compared to the other months of the year and the solar intensity reaches the lowest value on July. And the annual average useful energy collected by a unit flat plate collector per day is $3.5659 * 10^4\ kJ/day$.

From the results as shown above, 31 units of flat plate collectors are required to fulfill the average daily energy requirement of digester. All are arranged in parallel. The total mass flow rate of heat transfer fluid is 0.434 kg/s.

6.8. Temperature Variation of Phase Changing Material on Charging Mode

Temperature variation of phase changing material on charging process has analyzed for fluctuating heat transfer fluid inlet temperature. Initial both the phase change material capsules

and the heat transfer fluid were at same temperature (55 ^{o}C). Charging process occurs for 9 hours' time duration, for the first 1.5 hours only a sensible heating process occurs. The phase changing process occurs within a narrow temperature range (1 ^{o}C). This process occurs for 6.5 hours' time duration. After the phase changing process completes, a sensible heating process continues for 1 hour.

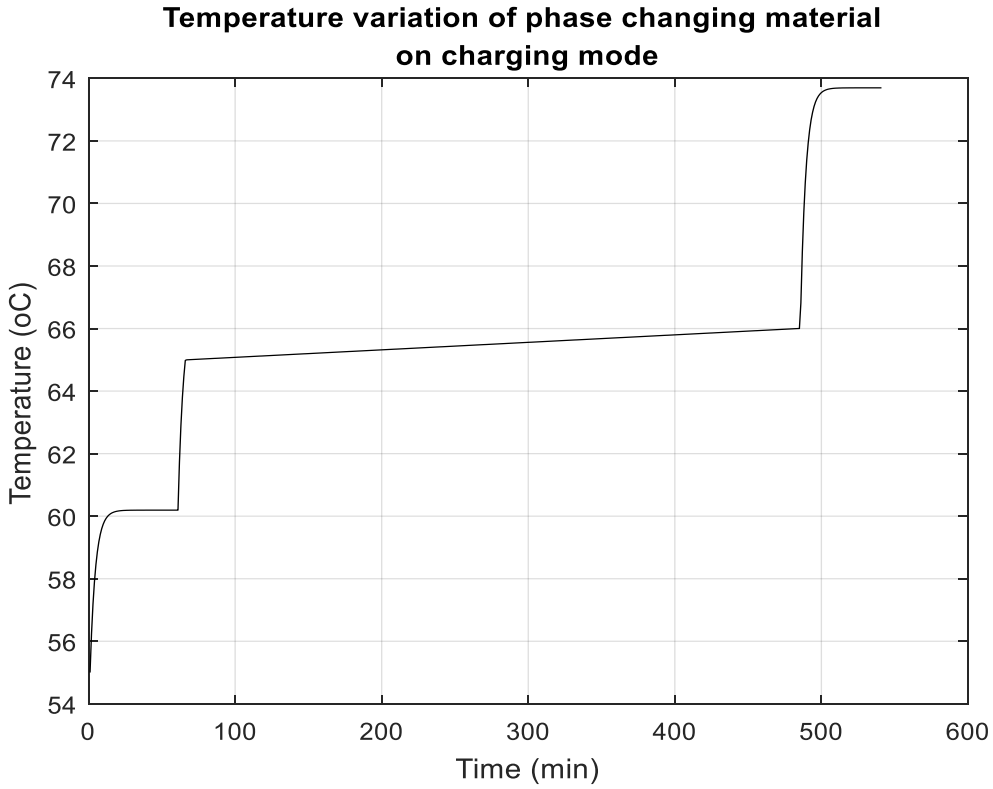

Figure 6.13: Charging process temperature variation of phase changing material for January 17

From the analysis, 3 m^3 of phase changing material (Paraffin) is required to store the energy consumption of digester for 15 hrs. Encapsulated spherical phase change material spheres are identical and have a diameter of 0.076 m and rectangular packed in storage tank of volume 5.73 m^3 with a porosity of 0.476, through which the heat transfer fluid flows. The total number of spherical capsules required to store the desire quantity of heat were 13,052.

Validation

The result of numerical simulation of phase changing material based thermal energy storage system for charging process were validated with a similar work of numerical investigation result of Shobo et al., (2015). The two numerical investigation result plots have similar shape but a

small variation in the melting time was seen. The size of spherical capsules and melting points of phase changing material used in the analysis are different, due to this their charging time and temperature limits are different.

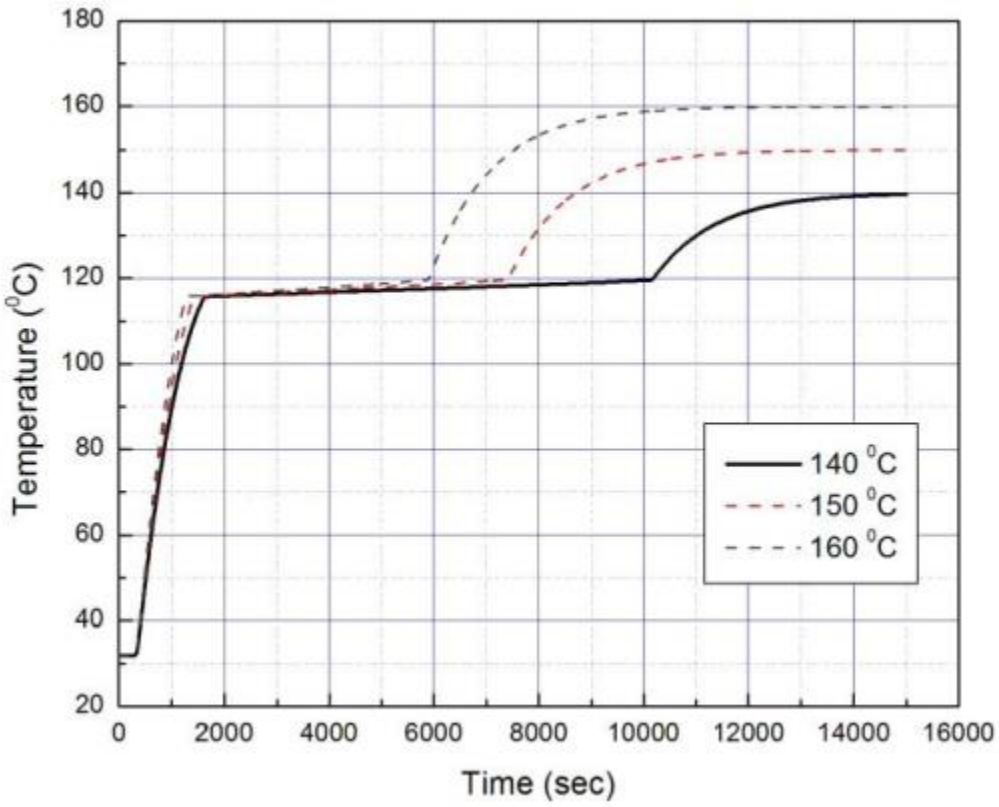

Figure 6.14: Phase change material temperature variation with charging time for different heat transfer inlet temperature (Shobo et al., 2015)

CHAPTER 7: Conclusion, Recommendation and Future Work

7.1. Conclusion

Temperature affects the production rate of biogas. Biogas yield rate increases with increasing the operating temperature of anaerobic digestion system. To increase the operating temperature of digester external source of energy is required. Solar energy for heating a biogas reactor could be a promising and environmentally friendly approach for anaerobic digester. The combination of solar energy and biogas production represents a kind of solar energy storage in the form of fuel gas. But contrary, incorporation of solar energy in the anaerobic digestion process may affect the process stability, which results from the daily fluctuations of the variable energy. Solar energy storage is a key issue to be addressed the intermittence of solar energy. Packed bed solar thermal energy storage with phase change material have a higher energy storage density and energy storage at constant temperature or with in small temperature range. Therefore, integrating a solar assisted anaerobic digestion system with packed bed solar thermal energy storage with phase change material have a higher advantage in biogas technology.

In this study, the thermal performance of a solar assisted anaerobic digestion system integrated with latent heat thermal energy storage was investigated. One dimensional heat transfer model was developed to characterize the behavior of a system. Iterative solving technique was used through finite difference scheme. Numerical results were validated by experimental investigation of other researchers.

To calculate the heat requirement of digestion system, assumes that initially the digester were at the desired temperature. The iterative solution shows that the digestate drops a temperature from 4.93 to 5.62 ^{o}C and digester cover drops a temperature from 4.12 to 4.63 ^{o}C per day. This temperature drop accounts for total heat losses of $1.0166\ x\ 10^{6}$ kJ/day on May to $1.1602\ x\ 10^{6}$ kJ/day on December. From which, the major part of heat requirement is used to compensate for the heat loss of digester to the incoming digestate. The heat loss through the walls of digester was only accounts for 7.73 to 8.22% of the total heat requirement of digestion system.

Similarly, the transient behavior of flat plate collector was numerically analyzed. The result shows, the total amount of energy that can be collected by a unit flat plate collector per day varies from $2.5\ x\ 10^{4}$ kJ/day on July to $4.5867\ x\ 10^{4}$ kJ/day on December with average thermal

efficiency of 82.6%. To satisfy the total energy requirement of digestion system, 31 units of flat plate collector with a total mass flow rate of heat transfer fluid of 0.434 kg/s.

And also, for charging mode of latent heat thermal energy storage system, the transient analysis was performed. The result shows, 3 m^3 of paraffin n-Triacontane is enough to store heat for 15 hours energy requirement of digestion system.

From which, we can conclude that 31 units of flat plate collectors with 3 m^3 of PCM can fulfill the energy requirement of digestion system that is responsible for producing biogas for the energy consumption of 100 peoples for their cooking purpose per day.

7.2. Recommendation

During summer season (June - August) heat collected by a flat plate solar collector is less than the heat requirement of anaerobic digestion system. To operate the anaerobic digestion system in the desired temperature auxiliary source of heat is used.

7.3. Future Work

The following points are recommended for future work

- Thermal distribution with in a digestion system varies with either radially or axially. In this study, assumes it is smoothly constant throughout the volume of digester. The same work can be done by considering the thermal distribution of a digestion system.
- Thermo-physical properties are a function of temperature, if they are taken as constant, can reduce the exactness of analysis. The same studies can be done by considering the variation of thermo-physical properties with temperature.
- The discharge mode of thermal energy storage system needs further investigation. The rate of solidification varies with time; this needs further investigation and detailed analysis, either numerical or experimental. For future researchers were recommended to investigate it as well.

References

1. A. Felix Regin, S.C. Solanki, J.S. Saini (2009). An analysis of a packed bed latent heat thermal energy storage system using PCM capsules: Numerical investigation. Renewable Energy 34, 1765–1773.
2. A.G. Hashimoto, V. H. Varel &, Y. R.Chen (1981). Ultimate methane yield from beef cattle manure: effect of temperature, ration constituents, antibiotics and manure age. Agrwuhural Wastes 3, 241-256.
3. Ahmad M. Salah. Modeling of flat-plate solar collector operation in transient states. Master's thesis, Purdue University, Fort Wayne, Indiana, May 2012.
4. Andreas Ch. Yiannopoulos, Ioannis D. Manariotis, Constantinos V. Chrysikopoulos (2008). Design and analysis of a solar reactor for anaerobic wastewater treatment. Bio resource Technology 99, 7742–7749.
5. Atul Sharma, V.V. Tyagi, C.R. Chen, D. Buddhi (2009). Review on thermal energy storage with phase change materials and applications. Renewable and Sustainable Energy Reviews 13, 318–345.
6. Baba Shehu, Umar Ibn, Abubakar and Nasir Ismail (2012). Anaerobic digestion of cow dung for biogas production. ARPN Journal of Engineering and Applied Sciences. vol. 7, no. 2.
7. D.G.Baker, D.C. Reicosky, L.J.Winkelman, and J.M.Baker (1989). Accuracy of hourly air temperatures calculated from daily minima and maxima. Agricultural and forest meteorology, 46, 193 – 209.
8. Deepanraj B, Sivasubramanian V. and Jayaraj S (2014). Biogas generation through anaerobic digestion process an overview. Res. J. Chem. Environ. Vol. 18(5).
9. G. Kocar and A. Eryasar (2007), An application of solar energy storage in the gas: Solar heated biogas plants, Energy Sources, Part A, 29:1513–1520.
10. G.D. Zupancˇic and M. Ros ˇ (2003). Heat and energy requirements in thermophilic anaerobic sludge digestion. Renewable Energy 28, 2255–2267.

11. George Otim, David Okaka and John Kayima (2010). Design of biogas plants for rural households in Uganda (Case study: Apac district). Second International Conference on Advances in Engineering and Technology, 544 – 550.

12. H. Varel, H. R. Isaacson and M. P. Bryant (1977). Thermophilic methane production from cattle waste. Applied and environmental microbiology, p. 298-307.

13. Hamed El-Mashad (2003). Solar theromphilic anaerobic reactor (STAR) for renewable energy production. Phd. Thesis Wageningen University, Wageningen, Netherland.

14. Hamed M. El-Mashad, Grietje Zeeman, Wilko K.P. van Loon, Gerard P.A. Bot, Gatze Lettinga (2004). Effect of temperature and temperature fluctuation on thermophilic anaerobic digestion of cattle manure. Bio resource Technology 95, 191–201.

15. Hamed M. El-Mashad, Wilko K.P. van Loon, Grietje Zeeman (2003). A Model of Solar Energy Utilization in the Anaerobic Digestion of Cattle Manure. Bio systems Engineering 84(2), 231–238.

16. Hamed M. El-Mashad, Wilko K.P. van Loon, Grietje Zeeman, Gerard P.A. Bot and Gatze Lettinga (2004). Design of a solar thermophilic anaerobic reactor for small farms. Bio Systems Engineering, 87(3), 345–353.

17. John A. Duffie, William A. Beckman. Solar engineering of thermal processes. Fourth Edition.

18. Linda Manon Kamp, Esteban Bermúdez Forn (2016). Ethiopia's emerging domestic biogas sector: Current status, bottlenecks and drivers. Renewable and Sustainable Energy Reviews 60, 475–488.

19. M.G. Mengistua, B. Simane, G. Eshete, T.S. Workneh (2015). A review on biogas technology and its contributions to sustainable rural livelihood in Ethiopia. Renewable and Sustainable Energy Reviews 48, 306–316.

20. Manuel Romero, Selvan Bellan, Jose Gonzalez-Aguilar, Muhammad M. Rahman, D. Yogi Goswami, and Elias K.Stefanakos (2015). Numerical investigation of PCM-based thermal energy storage system. Energy Procedia 69, 758 – 768.

21. Mikelis Dzikevice, Ance Ansone, and Dagnija Blumberga (2016). Modeling of phase

change in spheres for applications in solar thermal heat storage systems. Energy Procedia 95, 112 – 118.

22. N. Ukrainczyk, S. Kurajica, and J. Sipusiae (2010). Thermophysical comparison of five commercial paraffin waxes as latent heat storage materials. Chem. Biochem. Eng. Q. 24 (2) 129–137.

23. Nallusamy N, Sampath S, and Velraj R (2006). Study on performance of a packed bed latent heat thermal energy storage unit integrated with solar water heating system. J Zhejiang Univ SCIENCE A 7(8): 1422-1430

24. Nitin. D. Patil and S. R. Karale. Design and Analysis of Phase Change Material based thermal energy storage for active building cooling: a Review. International Journal of Engineering Science and Technology (IJEST).

25. Mugur Balan, Octavian Pop, and Lucian Fechete Tutunaru (2017). Numerical model for solidification and melting of PCM encapsulated in spherical shells. Energy Procedia 112, 336 – 343.

26. Ouhammou Badra, Aggour Mohammed, Frimane Azddini (2017). Feasibility study of integrating solar energy in to anaerobic digester reactor for improved performance using TRNSYS simulation: Application Kenitra Morocco. Energy procedia 136, 402-407.

27. P. Axaopoulos, P. Panagakis, A. Tsavdaris and D. Georgakakis (2001). Simulation and experimental performance of a solar heated anaerobic digester. Solar Energy Vol. 70, No. 2, pp. 155–164,.

28. P.S. Robi, Dawit Gudeta Gunjo, and Pinakeswar Mahanta (2017). CFD and experimental investigation of flat plate solar water heating system under steady state condition. Renewable Energy 106, 24 – 36.

29. Rainier Hreiz.B, Nouceiba Adouania, Yves Jannot, Marie-Noëlle Pons (2017). Modeling and simulation of heat transfer phenomena in a semi-buried anaerobic digester. Chemical engineering research and design 119, 101–116.

30. Selvan Bellan, Alice Cordiviola, Stefano Barberis, Alberto Traverso, José González-Aguilar, and Manuel Romero (2017). Numerical analysis of latent heat storage system with

encapsulated phase change material in spherical capsules. Renew Energy Environ Sustain.2, 3.

31. Shobo A. B and Mawire A (2015). Numerical investigation of a packed bed thermal energy storage system for solar cooking using encapsulated phase change material. Third Southern African Solar Energy Conference. 11 – 13.
32. Shripad Chopade, Sagar Kauthalkar, Pushpendra Kumar Sharma (2013). Solar heat energy storage in phase change materials. Engineering Research and Applications (IJERA) Vol. 3, Issue 4, pp. 471-473.
33. Su Yuan, Tian Rui, Yang Xiao Hong (2011). Research and analysis of solar heating biogas fermentation system. Procedia Environmental Sciences 11, 1386 – 1391.
34. T. M. Alkhamis, R. El-Khazali, M. M. Kablan and M. A. Alhusein (2000). Heating of a biogas reactor using a solar energy system with temperature control unit. Solar Energy Vol. 69, No. 3, pp. 239–247.
35. V. H. Varel, A. G. Hashimoto, and Y. R. Chen (1980). Effect of Temperature and Retention Time on Methane Production from Beef Cattle Waste. Applied and environmental microbiology, p. 217-222.
36. Yong Lu, Ye Tian, Haowei Lu, Lei Wu, Xianlin Li (2015). Study of solar heated biogas fermentation system with a phase change thermal storage device. Applied Thermal Engineering 88, 418-424.
37. Zhiguang Chen, Chaokui Qin (2014). Experiments and simulation of a solar-assisted household biogas system. Energy Procedia 61, 1760 –1763.

APPENDIX

ANNEX A: Hourly average temperature drop of Digestate

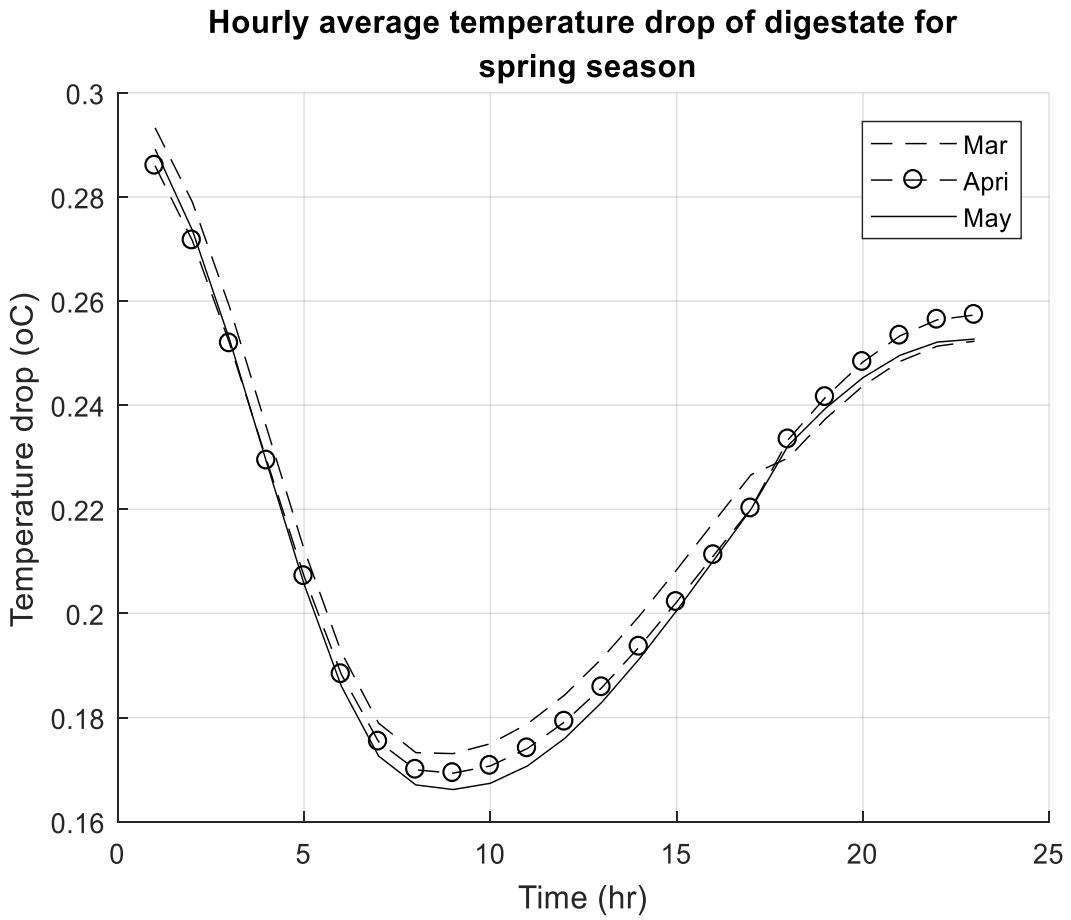

Figure A.1: Hourly average temperature drop of digestate for spring season

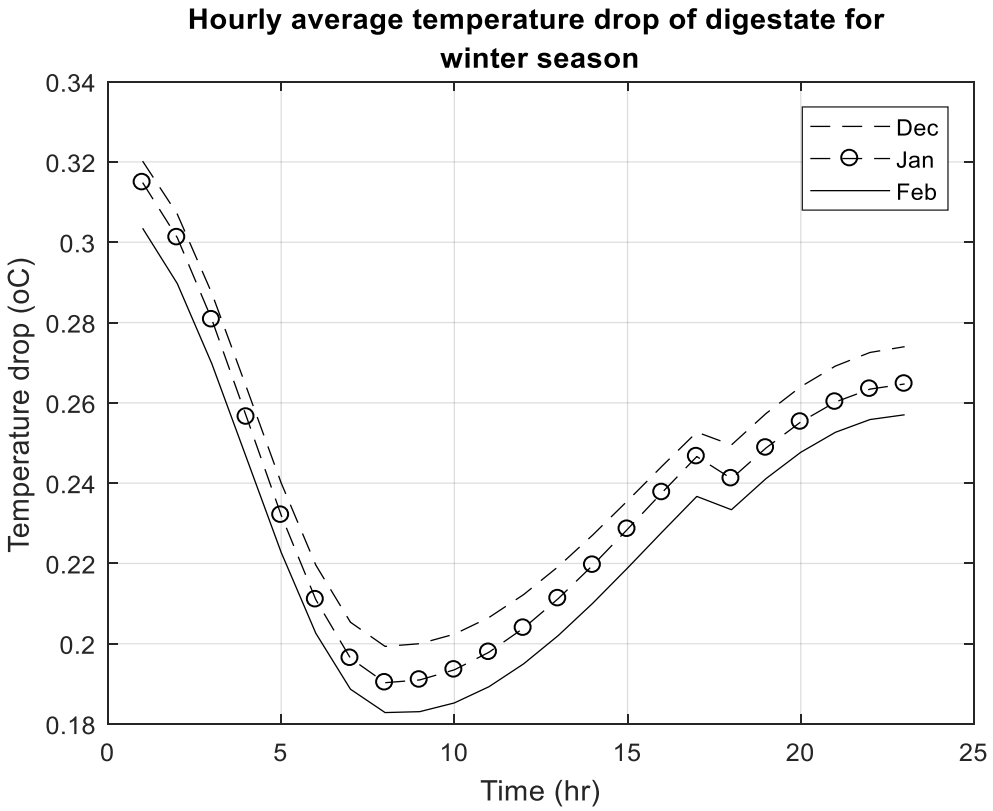

Figure A.2: Hourly average temperature drop of digestate for winter season

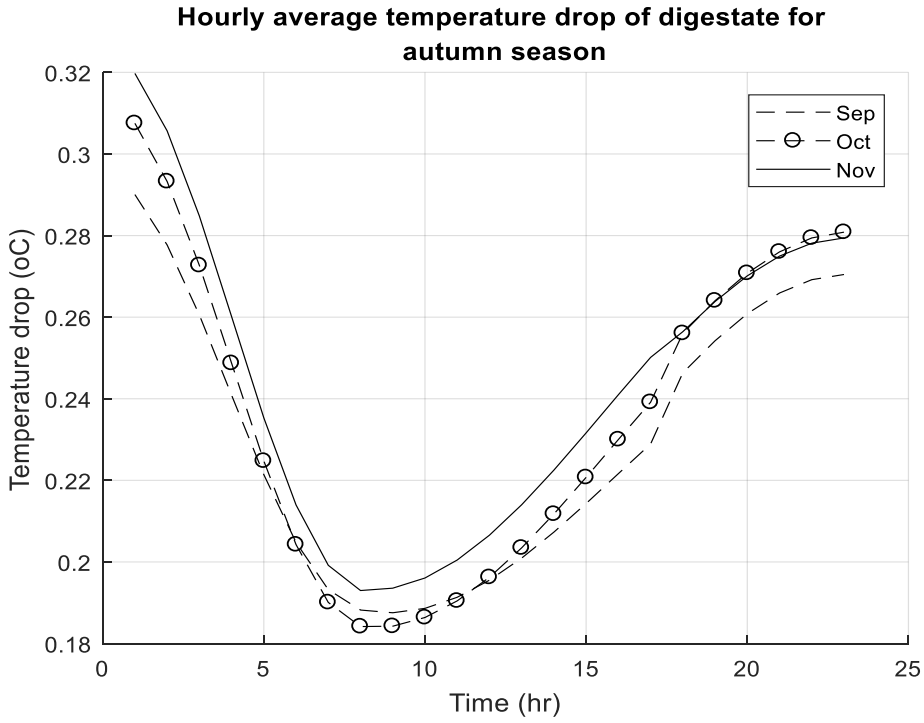

Figure A.3: Hourly average temperature drop of digestate for autumn season

ANNEX B: Temperature Fluctuation of Digester Cover

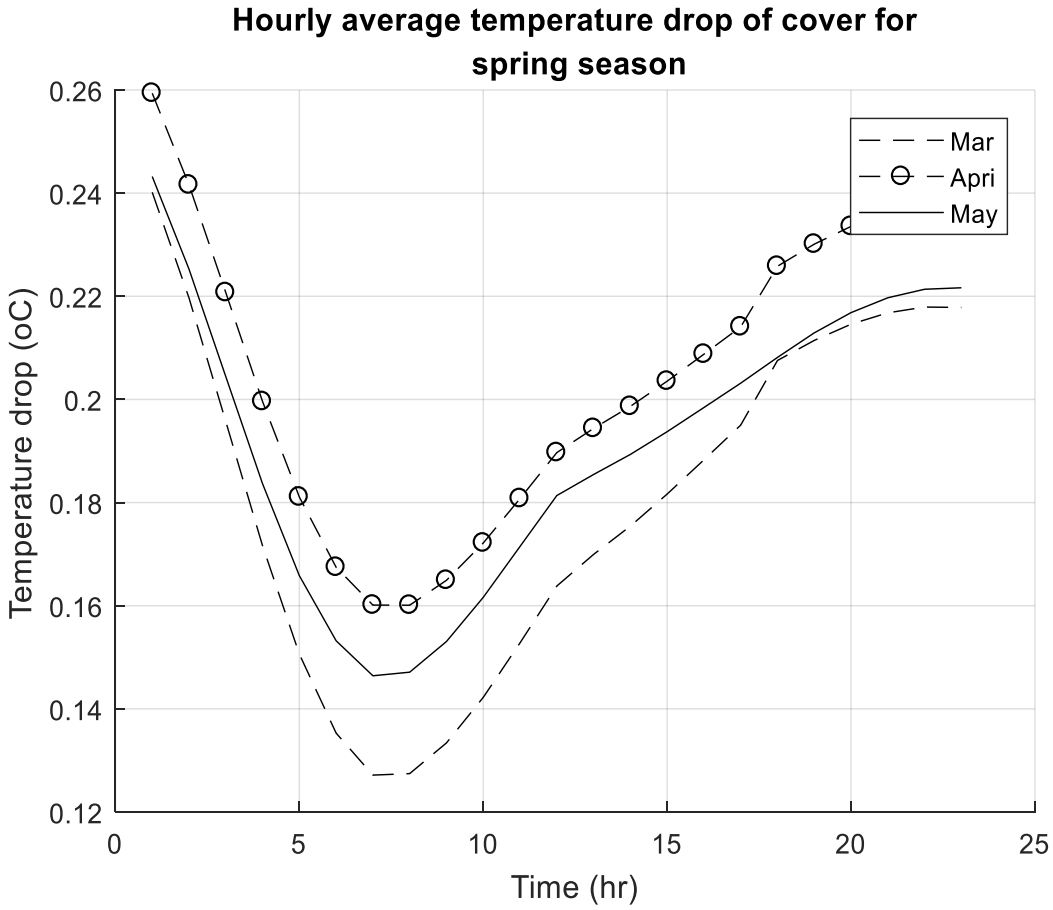

Figure B.1: Hourly average temperature drop of digester covers for spring season

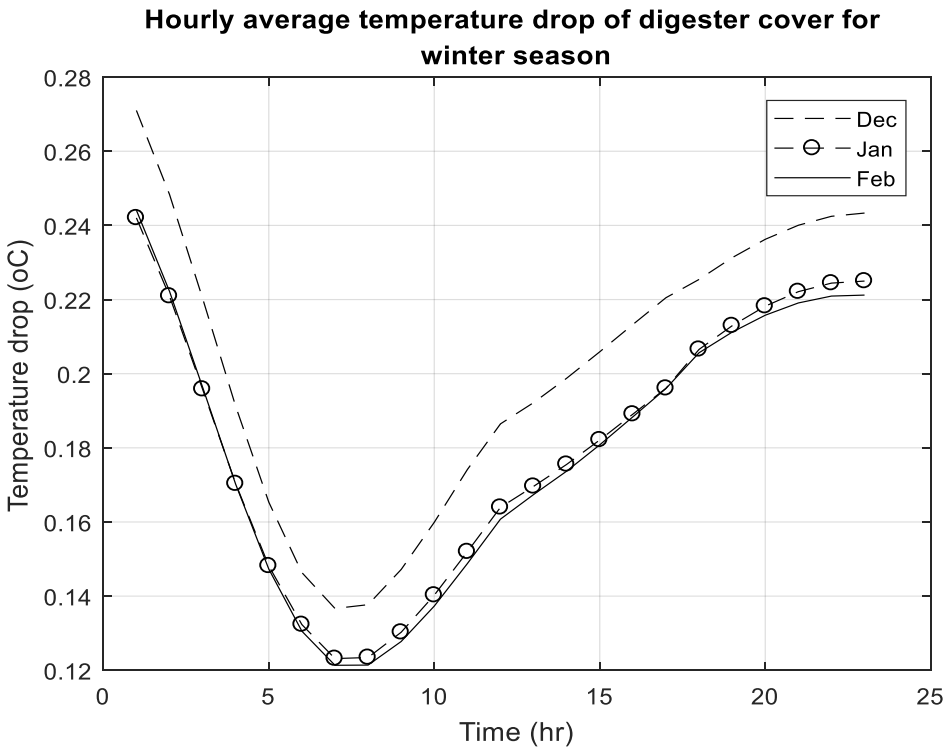

Figure B.2: Hourly average temperature drop of digester covers for winter season

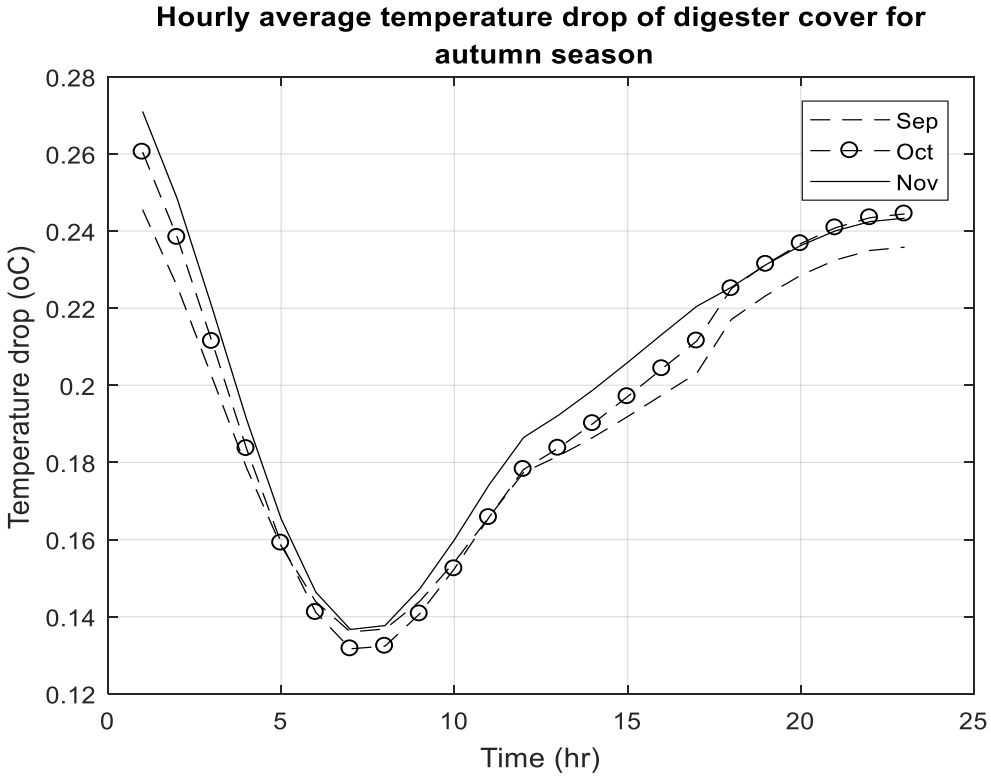

Figure B.3: Hourly average temperature drop of digester covers for autumn season

ANNEX C: Heat Transfer Fluid Outlet Temperature Fluctuation throughout the Day

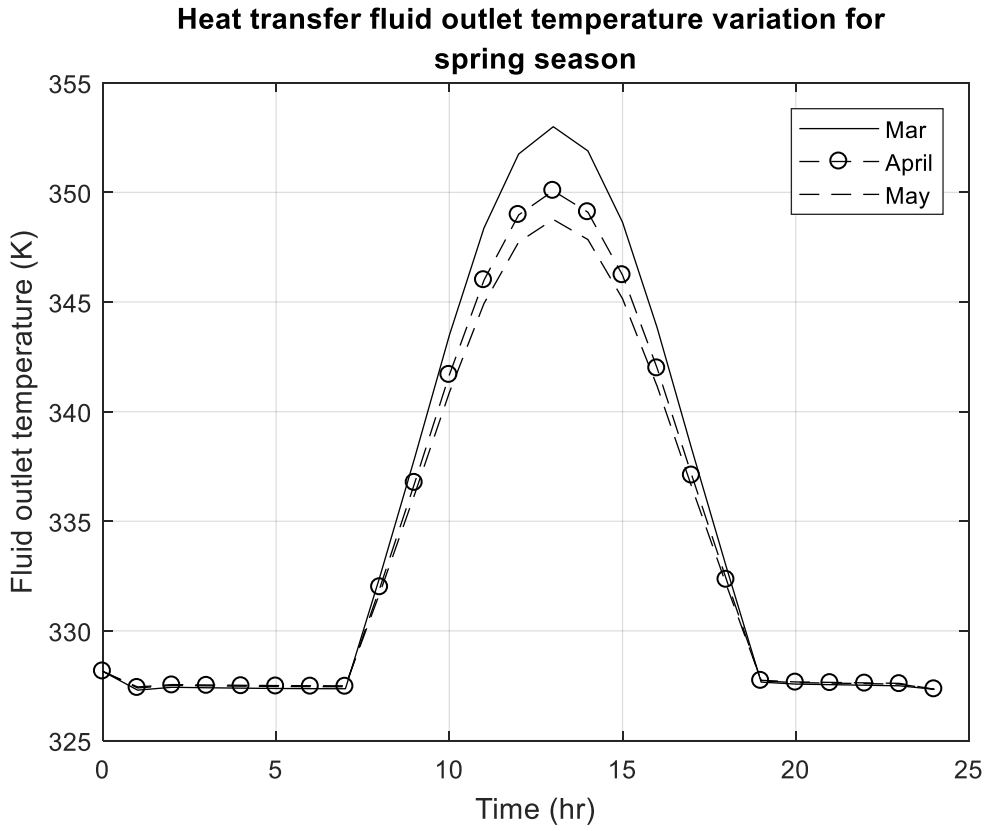

Figure C.1: Heat transfer fluid outlet temperature fluctuation throughout the day for spring season

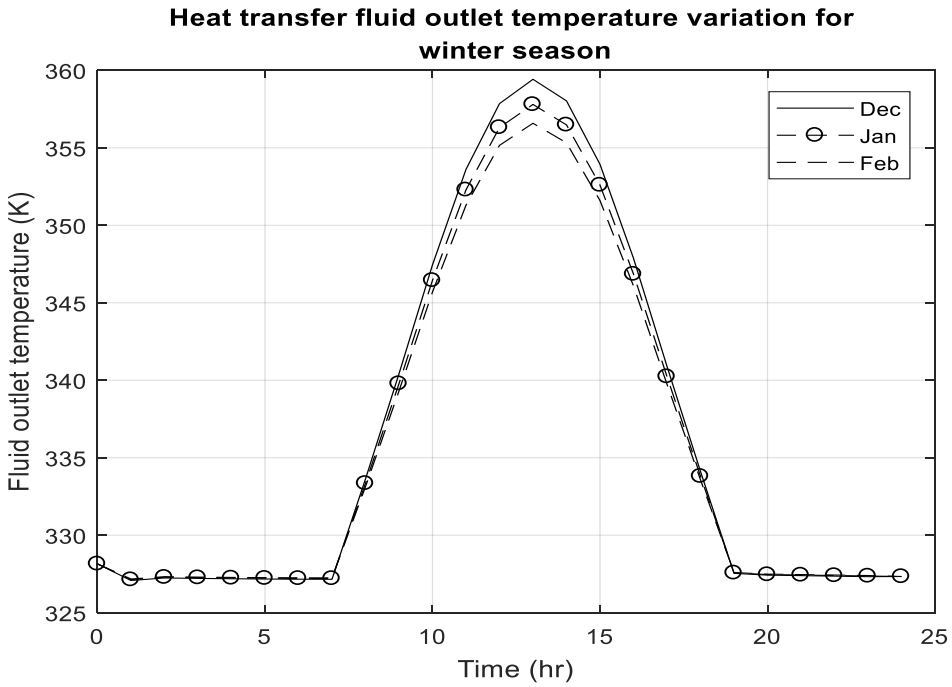

Figure C.2: Heat transfer fluid temperature variation at the outlet of flat plate collector for winter season

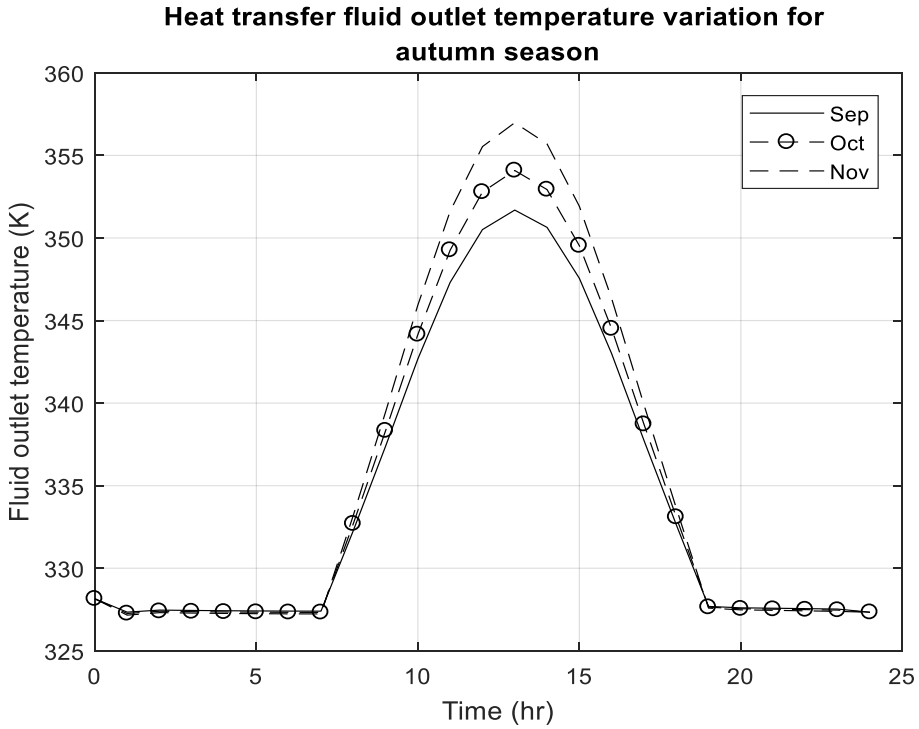

Figure C.3: Heat transfer fluid outlet temperature fluctuation throughout the day for autumn season

ANNEX D: Hourly Average Useful Energy Collected From a Unit Flat Plate Collector throughout the Day

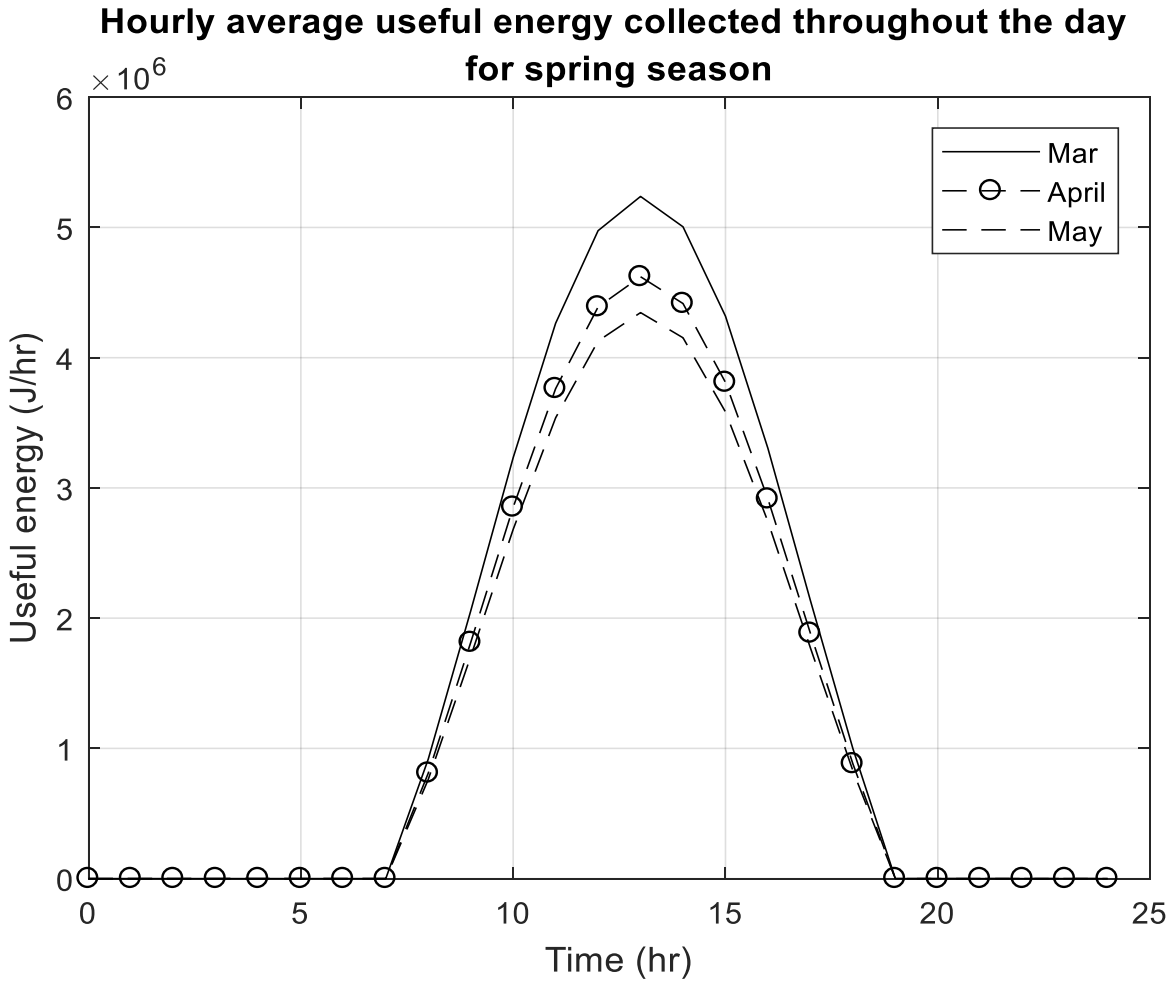

Figure D.1: Hourly average useful energy collected from a unit flat plate collector throughout the day for spring season

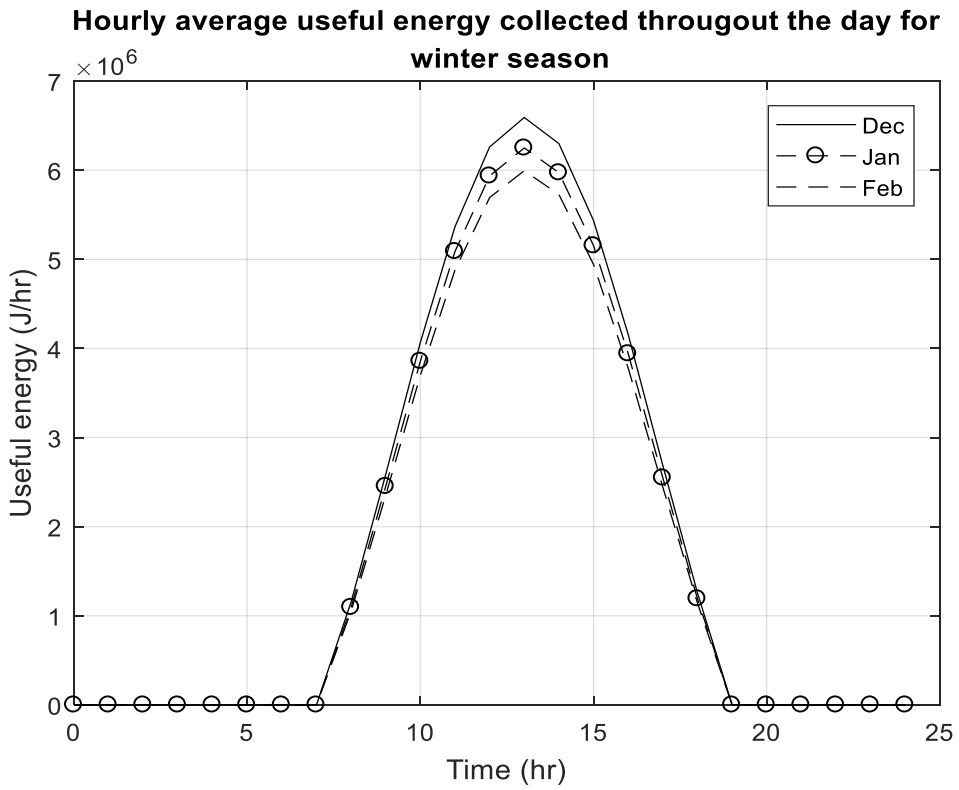

Figure D.2: Hourly average useful energy gain by a unit flat plate collector for winter season

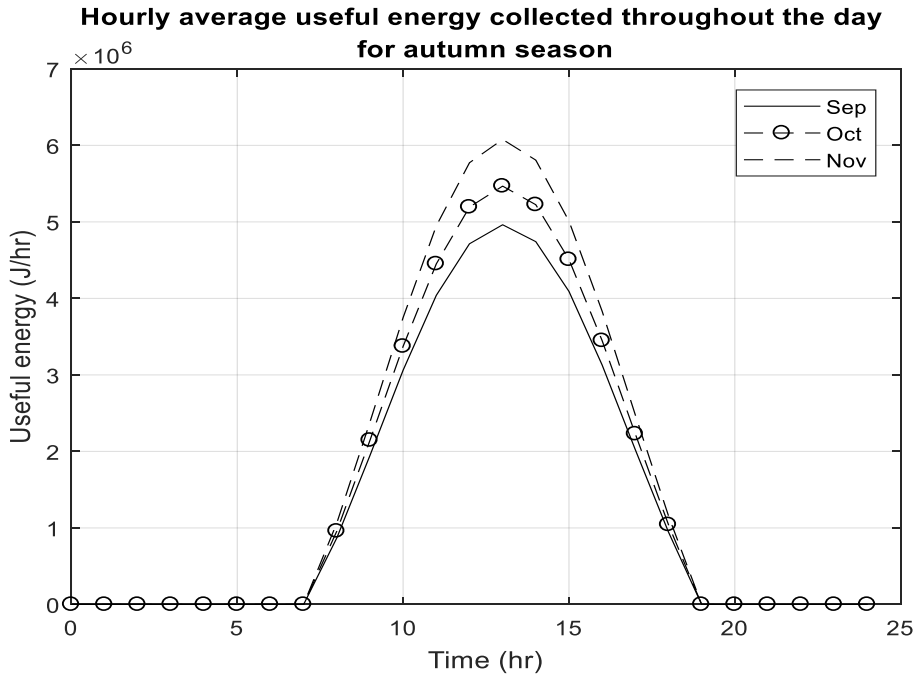

Figure D.3: Hourly average useful energy collected from a unit flat plate collector throughout the day for autumn season